PB-217 601

ATOMIZATION AND DROP SIZE OF NON-NEWTONIAN FLUID

K. H. Wang, et al

Syracuse University
Syracuse, New York

1969

DISTRIBUTED BY:

NTIS

National Technical Information Service
U. S. DEPARTMENT OF COMMERCE
5285 Port Royal Road, Springfield Va. 22151

WP-00867

PB 217 601

Final Report

ATOMIZATION AND DROP SIZE OF NON-NEWTONIAN FLUID

by

K.H. Wang, Yoshisuke Nakano

and

Chi Tien, Principal Investigator

Submitted to:

Federal Water Pollution Control Administration

Under Grant No. WP-00867

Details of illustrations in
this document may be better
studied on microfiche.

For the Period September 1, 1965 - May, 1969

LIBRARY
FWPCA, Ohio Basin Region
4676 Columbia Pkwy. Cinti, O. 45226

Reproduced by
NATIONAL TECHNICAL
INFORMATION SERVICE
U S Department of Commerce
Springfield VA 22151

SYRACUSE UNIVERSITY RESEARCH INSTITUTE

Department of Chemical Engineering and Metallurgy

SUMMARY

The object of this investigation is to study the effect of various physical parameters on the drop size distribution formed in an atomization process for liquid with non-Newtonian rheological behavior. This study was motivated by the potential application of the Atomization Suspension Technique in ultimate disposal and the observation that suspensions and slurries often behave like non-Newtonian fluid. The principal findings are:

(1) The freezing technique is an account method of determining liquid drop sizes.

(2) The drop size distribution of non-Newtonian liquid can be described in terms of square-root normal distribution.

(3) The drop size distribution in terms of mean values and standard deviation can be estimated within an accuracy of approximately ± 15% from the empirical correlations established in this work.

(4) A stochastic model was successfully developed for the breakup mechanism in pneumatic atomization.

It is recommended that further work in the following areas should be considered:

(1) The present study was restricted to polymer solutions such as CMC (Carboxymethylcellulose). These systems were chosen primarily because of their ease of handling, and, therefore, was more suitable for the initial study. With the perfection of experimental techniques, it becomes possible to consider systems such as slurries or suspensions (with various

concentrations) which approximate more closely to substances to be considered in ultimate disposal.

(2) A combustion and evaporation study of liquid droplet containing solids and suspended matter should also be considered. The effect of drop size distributions or the performance of a process employing an atomized suspension technique would be the center of emphasis of the study.

TABLE OF CONTENTS

Preface

I. Atomization and Drop Size Distribution of Non-Newtonian Fluid - An Experimental Study

II. Application of Branching Process For Liquid Atomization

I c

PREFACE

This report summarizes the research performed during the period of September, 1965 - May, 1969 at Syracuse University under the sponsorship of Federal Water Pollution Control Administration through Grant Nos. WP-00867-01, 02 and 03.

The major phase of this investigation is aimed at an experimental study of the drop size distribution of atomization processes for liquid systems with non-Newtonian rheological properties. A freezing technique was used to determine the liquid drop sizes and empirical correlations were obtained which predict the drop size distribution for the operating conditions as well as physical properties of liquid systems. This is described in Part I.

In Part II, a stochastic model was proposed which explains the liquid atomization processes. The theoretical model was found in agreement with earlier work on pneumatic atomization.

I D

PART I

ATOMIZATION AND DROP SIZE OF NON-NEWTONIAN FLUID

by

K.H. Wang and Chi Tien

TABLE OF CONTENTS

	Page
Acknowledgement	i
Table of Figures	iii
Table of Tables	iv
Section I - Introduction	1
Section II - Literature Survey of Existing Drop Size Correlations for Liquid Atomizations	3
Section III - Performance of Swirl-type Pressure Nozzles	11
Section IV - Theoretical Background	15
Section V - Experimental Method	36
Section VI - Selection of non-Newtonian Fluids and Their Rheological Measurements	45
Section VII - Experimental Results	48
Section VIII - Discussion	55
Section IX - Conclusions	63
Figures	65
Literature Cited	86
Nomenclature	90
Appendix I - Drop Size Distribution Data	94
Appendix II - Determination of Nozzle Performance	99
Appendix III - Boundary Layer Analysis	104
Biographical Data	

TABLE OF FIGURES

Figure		Page
1	Diagram of the Grooved-Core Swirl Nozzle	65
2	Coordinate System for Boundary-Layer Analysis	66
3	Diagram of the Spray Collector	67
4	Photograph of the Equipment	68
5	Photograph of the Sieve Shaker	69
6	Photograph of the Spray Drops	70
7	Correlation of C_{Qm}	71
8	Correlation of Z_m	72
9	Correlation of $\tan(\theta_m/2)$	73
10	Correlation of θ/θ_m for Glycerine Solution	74
11	Correlation of θ/θ_m for polymer solution	75
12	Rheological Diagram of Carbopol-934	76
13	Rheological Diagram of CMC-7L	77
14	Drop Size Distribution of CMC-7L, Nozzle 74-20	78
15	Drop Size Distribution of CMC-7L, Nozzle 58-21	79
16	Drop Size Distribution of CMC-7L, Nozzle 54-27	80
17	Correlation of Mean Drop Size with Physical Variables ...	81
18	Correlation of Mean Drop Size with Boundary-Layer Thickness	82
19	Correlation of Standard Deviation with Physical Variables	83
20	Correlation of Standard Deviation with Mean Drop Size ...	84
21	Boundary-Layer Thickness in the Swirl Chamber	85

TABLE OF TABLES

Table		Page
I	Orifice Inserts and Core Bodies	11
II	Experimental Drop Size Distributions	18
III	Water Soluble Polymers	46
IV	Physical Properties of Fluids	51
V	Drop Size Distribution for non-Newtonian Fluids	94
VI	Drop Size Distribution for Newtonian Fluids	96
VII	Experimental Values of C_{Qm}	99
VIII	Experimental Values of Z_m	100
IX	Comparison Between Predicted Values of Z_m	101
X	Spray Cone Angle at High Reynolds Numbers	102
XI	Shear Rate of Liquid at Orifice Based on Water Flow Rate	103
XII	Rheological Parameters of Polymer Solutions	109
XIII	Boundary Layer Calculations for non-Newtonian Fluids	110
XIV	Boundary Layer Calculations for Newtonian Fluids	112

SECTION I - INTRODUCTION

The atomization of liquids into fine drops constitutes the essential operations for many important engineering processes, such as spray drying, spray coating, and fuel injection. Information on the size distributions of the atomized liquid drops is of fundamental importance, because the mass transfer rate from and the heat transfer rate to these drops depend, to a very large extent, on the drop sizes and the drop size distribution. In the past three decades, tremendous amount of research work on liquid atomization has been performed, primarily with Newtonian fluids. Most of these researches were stimulated by the urgent need of understanding and improvement of the fuel combustions in internal or rocket engines.

Experimental results are very scarce, however, for the atomization of non-Newtonian fluids which are encountered more frequently than Newtonian fluids in many industrial processes, such as the spray drying of detergents and food products. This is probably because the development of rheological knowledge of non-Newtonian fluids is relatively recent. Since the advent of high polymers, polymer solutions which are invariably non-Newtonian fluids have been widely used in industrial operations and commercial products. For example, CMC and Carbopol have been used in coating fluids to suspend and deflocculate the pigments and to bind the coating more firmly to the surface. They have been used also in insecticides and paints to stabilize the emulsions. In view of the ever increasing importance of non-Newtonian fluids, we feel it is appropriate and useful to conduct an investigation on the atomization of these fluids. This investigation should provide us with, first of all, empirical distribution function of drop size in terms of the physical properties of the non-Newtonian fluids and the operating conditions of the atomizing process.

Secondly, we hope that the experimental results would bring us some understanding of the fluid flow through the nozzle and of the disintegration mechanism of the liquid jet. These are the objectives of the present research.

For the purpose that the experimental results could be of practical use, we have performed the experiments with aqueous solutions of commercial polymers and nozzles over a wide range of operating conditions. Also, we have devised a simple method of estimating the proper values of the apparent viscosities of the polymer solutions. The physical variables that we have used in the correlations of mean drop sizes and standard deviations are simply the pressure, the physical properties of the fluid, and the nozzle dimensions. Therefore, we believe that the correlations we have obtained are of general nature and are simple to use and that they should find immediate applications in design works.

In order that we can compare our correlations with those obtained by previous workers, we have included two Newtonian fluids in our experimental work. The results indicate that the agreement is consistent and that the final correlations which have incorporated some of the previous experimental results performed under comparable conditions are unifying.

As for the fluid flow through the nozzle and the disintegration mechanism of the liquid jet, we have provided some qualitative indications although the exact phenomenon still remains not well understood in a quantitative sense.

SECTION II - LITERATURE SURVEY OF EXISTING DROP SIZE CORRELATIONS FOR LIQUID ATOMIZATIONS

Drop size correlations for spray particles depend upon the type of atomizers. There are three basic types of liquid atomizers: the centrifugal atomizers, the pneumatic atomizers, and the pressure atomizers. An excellent description of the three types of atomizers can be found in the monograph by Marshall [M-2]. In the following, we intend to give a brief summary of the various drop size correlations which have been proposed in the past.

1. Centrifugal Atomizers

In a centrifugal atomizer, the liquid is fed to a fastly rotating disk through a central opening. The liquid is spun out from the edge of the disk by centrifugal force to form ligaments or films which quickly breaks up into fine drops. This type of atomizers is mostly used for spray drying. They are capable of handling slurries and suspensions. Two correlations for mean drop size were reported by Fraser, Eisenkalm and Dombrowski [F-1] and by Friedman, Gluckert and Marshall [F-3]. The second correlation was tested by Masters and Mohtadi [M-3] at high rotating speeds up to 24,000 RPM corresponding to a peripheral speed of 500 feet per second. The agreement was fair. A correlation for standard deviations was reported by Hatch and Choate [H-5].

2. Pneumatic Atomizers

In pneumatic atomization the liquid is discharged into a high velocity gas stream, either countercurrently or in an orthogonal direction. The thin liquid stream is then blasted by aerodynamic force into fine drops. This type of atomization is capable of producing very fine drops with a mean size down to one micron. It is used in aerosol generation, carburator atomization, and metal atomization. The power consumption for this type

of atomization is relatively high. The most important correlation for mean drop size was reported by Nukiyama and Tanasawa [N-3]. This well known correlation was tested by Lewis, Edwards, Golia, Rice and Smith [L-5] in the subsonic region and by Bitron [B-3] in the supersonic region with gas velocities up to Mach number II. In both cases good agreements with experimental results were obtained. The Nukiyama-Tanasawa distribution for spray drops was proposed in the same work. Correlations for mean drop size and standard deviation aimed at design purposes were reported by Gretzinger and Marshall [G-2]. Correlations based upon molten wax and alloys were reported by Wetzel [W-5], and Weiss and Worsham [W-4].

3. Pressure Atomizers

This type of atomizers uses pressure as the source energy for atomization. There are four kinds of pressure atomizers which have been investigated extensively:

(1) Jet-impact atomizers - A thin liquid jet emerging from a small orifice is directed to impact on a solid surface to achieve atomization. A correlation for mean drop size was published by Tanasawa, Sasaki, and Nagai [T-2].

(2) Fan-spray nozzles - The liquid flows out from the orifice as a fan-shaped sheet which breaks up into fine drops. This type of atomizers was extensively studied by British workers, most of whom were interested in the instabilities of liquid sheet. Mean drop size correlations were reported by Dorman [D-7], Fraser, Eisenkalm and Dombrowski [F-1], and Dombrowski and Hopper [D-5]. A correlation based on molten wax was reported by Hasson and Mizrahi [H-4]. All these correlations were restricted to operating pressures below 200 psi.

(3) Swirl-chamber nozzles - This type of atomizers is the same as grooved-core swirl nozzles except that no cores are used for guiding the liquid entering the swirl chamber. Atomization is the result of the break-up of the conical liquid sheet issuing from the orifice. Correlations for mean drop sizes were given by Golitzine, Sharp, and Badham [G-1], Joyce [J-2], Longwell [L-6], Pigford and Pyle [P-1], Tanasawa and Kobayasi [T-1], Turner and Moulton [T-8], and Watson [W-1].

(4) Grooved-core swirl nozzles - This is the type of nozzles used in the present work. These nozzles have been found very versatile in applications because they are able to produce fine drops with good space distributions at moderate pressures and they are simple to operate. Because of its direct relevance to the present work, a more detailed literature survey for this type of nozzles will be given as follows.

The first investigation was made by Turner and Moulton [T-8]. Molten naphthol and benzoic acid were sprayed into room temperatures, and the solidified particles were collected and classified by a microscopic technique. The corrected drop size distribution was found to approximate the log-normal distribution. The experimental correlations based on 36 runs with four nozzles were represented by the following equations:

$$\bar{x} = 16.56\, D_2^{1.52}\, W^{-0.44}\, \sigma^{0.71}\, \mu^{0.16} \qquad \text{(II-1)}$$

$$s = 0.173 + 0.126 \log_{10} D_2 \qquad \text{(II-2)}$$

where

$\bar{x}$ = mean drop diameter (microns)

s = log-normal standard deviation (log of microns)

D_2 = orifice diameter (mm)

W = mass flow rate (g/sec.)

σ = surface tension (dynes/cm)

μ = viscosity (centipoises)

The ranges of the physical variables covered in the above correlations were rather restricted. The pressure was varied from 33 to 125 psi, orifice diameter from 0.723 to 2.03 mm, mass flow rate from 1.81 to 28 g/sec., surface tension from 27.3 to 37.2 dynes/cm, and viscosity from 0.81 to 2.02 centipoises.

The second investigation was made by Tate and Marshall [T-3] on the atomization of water. Sprayed particles formed by dyed water were collected in an immiscible fluid contained in a small sample cell. Drop size distributions determined by photographic method were found to approximate the square-root normal distribution. The correlation for the Sauter mean drop size was given by the following equation:

$$\bar{x}_{32} = 286(D_2 + 0.17) \exp\left(\frac{13}{V_{ax}} - 0.0094\ V_t\right) \qquad \text{(II-3)}$$

where

$\bar{x}_{32}$ = Sauter mean drop diameter (micron), which is defined as the ratio of total volume to total surface for the entire spray drops.

D_2 = orifice diameter (in.)

V_{ax} = average axial velocity based on orifice area (ft./sec.)

V_t = average tangential velocity based on entry flow area (ft./sec.)

The particular functional form of Equation (II-3) was used in an attempt to determine the relative importance of V_{ax} and V_t in atomization. This correlation should be considered as qualitative, since it was determined from only twelve experimental runs. The pressure was varied from 60 to 891 psi and orifice from 0.0135 to 0.040 inches. The nozzle

cores that were used were Nos. 16, 17, and 27.

The third group of investigations were made by Darnell [D-1] and McIrvine [M-7]. They made comprehensive studies on the performance of grooved-core nozzles, and measured the air core diameters by photographing water flow in transparent plastic nozzles. Darnell determined drop size distributions by collecting water spray drops in an immiscible fluid, followed by photography. The sampling devices were placed at two different levels in the spray. The drop sizes at five inches below the nozzle were found to be finer than those at ten inches below. He believed the drop sizes measured at the ten inch level were more accurate and his correlation for mean drop size was based upon the ten inch level measurements. The correlation was given by the following equation:

$$\bar{x}_{32} = \exp [5.45 - 0.0054\ V] \qquad \text{(II-4)}$$

where

$\bar{x}_{32}$ = Sauter mean drop diameter (micron)

V = average total velocity based on liquid film thickness (ft./sec.)

Darnell also found that the drop size distribution can be approximated by the square-root normal distribution.

In an attempt to eliminate the time-consuming process of measuring each individual drop size from the photographic pictures, Choudhury [C-2] introduced the liquid nitrogen freezing method. Sample liquids were sprayed directly into liquid nitrogen and the frozen particles were sieve-screened in a cold room to obtain drop size distribution. However, his experimental results were not published, nor quoted by others.

The fifth and the most comprehensive investigation was made by Nelson and Stevens [N-1, N-2]. The sample liquids were sprayed into a cold chamber which was maintained at very low temperatures with flowing

liquid nitrogen. The frozen particles were collected in a set of sieves and screened in an insulated box. The results from sieve analysis supported the use of square-root normal distribution. The mean drop size and the standard deviation were related to the physical variables by dimensional analysis.

$$\frac{\bar{x}}{D_2} = f\left(\frac{D_2 V_{ax} \rho}{\mu}, \frac{V_{ax}^2 D_2 \rho}{\sigma}, \tan\frac{\theta}{2}\right) = f\left(Re, We, \tan\frac{\theta}{2}\right) \qquad \text{(II-5)}$$

$$\frac{\bar{s}}{D_2} = g\left(\frac{D_2 V_{ax} \rho}{\mu}, \frac{V_{ax}^2 D_2 \rho}{\sigma}, \tan\frac{\theta}{2}\right) = g\left(Re, We, \tan\frac{\theta}{2}\right) \qquad \text{(II-6)}$$

where

V_{ax} = average axial velocity at orifice, based on liquid film thickness (cm/sec.)

θ = spray cone angle (degree)

and the film thickness and the spray cone angle were based on Darnell's work. Water and six organic fluids were used to cover a wide range of physical variables. The viscosity ranged from 0.879 to 8.29 centipoises, density from 0.774 to 2.95 g/cm^3, surface tension from 24.5 to 72.0 dynes/cm, and pressure from 100 to 1500 psi. The orifice inserts and the core bodies were the same as listed in Table I.

The experimental volumetric mean drop sizes for the six organic fluids, as determined from 97 runs with 9 nozzles, were correlated by the following equation:

$$Y = 0.0811\, X^2 + 0.124\, X - 0.186 \qquad \text{(II-7)}$$

where

$$Y = \log_{10}\left[\bar{x}/D_2\right]$$

$$X = \log_{10}\left[Re^{0.45}\, We^{0.55}\, (\tan\tfrac{\theta}{2})^{1.2}\right]$$

The experimental mean drop sizes for water, as determined from 13 runs with 3 nozzles were found to be distinctly larger than those for organic fluids, but in agreement with Darnell's data for water, as determined from 27 runs. The combined results from the totality of the 40 runs were then shown to be correlated by the following equation:

$$Y = -0.114\ X^2 + 0.72\ X - 1.26 \qquad \text{(II-8)}$$

where

$$Y = \log_{10} [\bar{x}/D_2]$$

$$X = \log_{10} \left[Re^{0.80}\ We^{0.20}\ (\tan \tfrac{\theta}{2})^{1.2} \right]$$

However, the square-root standard deviations for both organic fluids and water were found to agree with each other, and were correlated by one equation as written below.

$$Y = 0.150\ X^2 - 0.359\ X + 0.686 \qquad \text{(II-9)}$$

where

$$Y = \log_{10} \left[\frac{s}{(D_2)^{1/2}}\ We \right]$$

$$X = \log_{10} [Re^{-0.50}\ We]$$

In summarizing the five investigations, we first notice that the correlations obtained by Turner and Moulton covered very narrow ranges of surface tension and viscosity. Therefore, the correlations could reflect only the effects of orifice diameter and flow rate. However, the fact that the mean drop sizes could be correlated with the flow rates indicated that they could be correlated also with the operating pressures, provided that an additional parameter pertaining to the nozzle dimensions was included.

The correlation of Tate and Marshall was based on a rather small number of experimental runs. Besides, the axial velocities and the tangential velocities used in their correlations (Equation II-3) were evaluated at two different locations in the nozzle. This is hardly justifiable if the authors' attempt was to determine the relative importance of axial and tangential velocities in atomization. However, the observation by the authors that the drop size distribution approximated the square-root normal distribution proved to be useful.

Darnell [D-1] and McIrvine [M-7] demonstrated clearly the existence of air core in swirl nozzles and made quantitative measurements of the air core diameters. However, the correlation given by Darnell did not appear to be very useful. Besides, the drop sizes, and hence the correlation, were found to depend upon the sampling locations.

Choudhury did not publish his experimental results, but the liquid-nitrogen freezing process which he introduced proved to be a practical method of determining drop size distribution.

The investigation made by Nelson and Stevens covered extensive ranges of physical variables. This was perhaps the best organized experimental work which had been done on liquid atomization with grooved-core nozzles. However, the observation that the mean drop sizes of water were larger than those of organic liquids by about 30 to 50% did not appear to have any obvious justifications, if the possibility that vaporizations of the more volatile organic liquids had happened was ruled out. The pooling of water data obtained by Nelson and Stevens with those of Darnell was questionable because they were obtained in different experimental conditions.

SECTION III - PERFORMANCE OF SWIRL-TYPE PRESSURE NOZZLES

The atomization nozzles chosen for the present work are the grooved-core SPRAYDRY nozzles manufactured by the Spraying System Company, Bellwood, Illinois. This class of nozzles has been widely used in industries and by many researchers in the past. They are generally used in fuel injection, spray drying, vessel coating, gas scrubbing, fire protection, and many other applications. Drop size distribution of non-Newtonian fluids obtained from tnese nozzles should find immediate applications and can be compared with the existing drop size distribution data of Newtonian fluids.

The nozzle consists of two essential parts, the orifice insert and the core body. For a given fluid and pressure, the degree of atomization and the flow rate are controlled by orifice diameter and the flow area of the entry slots which are grooved on the front edge of the core body. We have selected six orifice inserts and six core bodies. They can be interchangeably combined to form a single nozzle. The orifice diameters and the flow areas of the core bodies are listed in Table I.

TABLE I - ORIFICE INSERTS AND CORE BODIES

Orifice Insert		Core Body	
No.	Orifice Dia.(cm)	No.	Flow Area (cm^2)
80	0.0343	10	0.00232
74	0.0571	16	0.00496
67	0.0812	20	0.00800
58	0.1066	17	0.00993
54	0.1396	21	0.01808
46	0.2060	27	0.03100

For purpose of clarity, a diagrammatic drawing of the nozzle is shown in Figure 1. A liquid under high pressure enters through the slant slots into the conical swirl chamber, acquiring both a radial and a tangential velocity. As a consequence, the liquid in the swirl chamber pursues a helical path toward the orifice exit where it emerges into

atmospheric pressure to form a liquid jet. The form of the liquid jet depends upon the Reynolds number which is defined as $D_2\sqrt{P\rho/\mu}$, where D_2 is the orifice diameter, P the total pressure, ρ the density of the liquid, and μ the viscosity of the liquid. At low Reynolds numbers the jet is cylindrical. As the Reynolds number increases beyond a certain limit, there is an air core generated in the orifice and through the center of the swirl chamber. This happens when the swirling velocity head plus the friction loss from the wall to the center of the swirl chamber totally compensates the pressure head. When the air core appears, the liquid jet begins to assume the form of a conical sheet which eventually breaks into fine drops. The formation of a conical sheet is a desirable condition for atomization since the conical sheet jet breaks up more readily and produces finer drops than a cylindrical jet. This is because that in the conical sheet jet, more surface area per unit volume of the liquid is exposed to aerodynamic forces. At very high Reynolds numbers the liquid sheet breaks up very near to the orifice, making itself hardly visible.

Besides the drop size distribution, there are three measurable quantities that characterize the performance of a nozzle. They are the discharge coefficient (C_Q), the air core to orifice diameter ratio (Z), and the spray cone angle (θ). The discharge coefficient is defined as follows:

$$C_Q = \frac{\text{Volumetric flow rate}}{(\text{Orifice area})(\text{Total pressure head})}$$

$$= \frac{Q}{\frac{\pi}{4} D_2^2 [2P/\rho]^{1/2}} \qquad \text{(III-1)}$$

where

D_2 = orifice diameter

ρ = liquid density

P = inlet pressure

For a specific nozzle, C_Q, Z, and θ all depend on Reynolds number, but approach to their respective asymptotic values at high Reynolds numbers. Let these values be C_{Qm}, Z_m, and θ_m, respectively. Since these asymptotic values are independent of Reynolds numbers, they could be functions of nozzle dimensions only. The geometries of the nozzles are identical save that the orifice diameter and flow area of the slots vary from one nozzle to the other. Based upon experimental observations made with water and several polymer solutions we have found that C_{Qm}, Z_m, and $\tan(\theta_m/2)$ can be correlated by a single parameter A defined as the ratio of the orifice area over the flow area of the slots. These correlations are shown in Figures 7, 8, and 9, respectively. The values of C_{Qm}, Z_m, and θ_m are determined as described below.

The values of C_{Qm} are calculated from the measured water flow rates. For large nozzles the measured flow rates are in good agreement with the data supplied by the nozzle manufacturer. For small nozzles the measured flow rates are slightly higher. The limiting value of C_{Qm} as A approaches zero can be taken to be 0.64 corresponding to the discharge coefficient of a sharp-edged circular orifice at high Reynolds numbers. The correlation for C_{Qm} over the experimental range can be represented by the following equation:

$$C_{Qm} = 0.220\ A^{-0.455} \qquad \text{(III-2)}$$

The values of θ_m have been determined by taking pictures of the conical sprays at different pressures and with different fluids. For a

given nozzle the values of θ_m obtained with different fluids are the same within experimental error. The correlation of θ_m versus A is based on the results obtained with water which agree well with manufacturer's data [S-3]. The growth of the spray cone angle with increasing Reynolds numbers has been observed by using a glycerine solution which has a viscosity of 24 centipoises at a room temperature of 74°F. A unique correlation has been obtained for all nozzles by plotting the ratio of θ/θ_m versus Reynolds number as shown in Figure 10. In low Reynolds number region, the spray cone gradually diminishes into non-existence. By observing the transitions from conical sheet into cylindrical jet, the critical Reynolds number for spray cone formation has been estimated at about 450 for the nozzles under consideration.

The correlation of Z_m versus A is derived from Darnell's data who determined the variation of Z_m with nozzle sizes by photographing the air cores generated in transparent plastic nozzles. His experimental results have been quoted in a graphic form in a monograph by Marshall [M-2].

The complete calculations for determining C_{Qm}, θ_m, and Z_m are summarized in Appendix II.

SECTION IV - THEORETICAL BACKGROUND

1. Mathematical Representation of Drop Size Distribution

The statistical distribution of a given quantity in a sample population is equivalent to a probability problem. In our case of drop-size distributions, the sample population is the collection of the entire spray particles, and the given quantity is the drop-size variable which can be defined, for the time being, as the drop diameter. Let this size variable be denoted by x. The distribution of the size variable in the entire spray particles is specified by the probability density function f(x) which can be defined most conveniently in two ways:

$$(1) \quad f_n(x) = \frac{1}{N} \frac{dn}{dx} \tag{IV-1}$$

$$(2) \quad f_v(x) = \frac{1}{V} \frac{dv}{dx} \tag{IV-2}$$

where n and v are the number and the volume of the particles, and N and V are the total number and volume of the entire spray particles.

Using the density function $f_n(x)$ defined by Equation (IV-1), various kinds of mean drop sizes can be defined:

(1) Length mean:

$$\bar{x}_{10} = \int_a^b x f(x)\, dx \tag{IV-3}$$

(2) Surface mean:

$$\bar{x}^2_{20} = \int_a^b x^2 f(x)\, dx \tag{IV-4}$$

(3) Volume mean:

$$\bar{x}^3_{30} = \int_a^b x^3 f(x)\, dx \tag{IV-5}$$

(4) Volume-surface of Sauter mean:

$$\bar{x}_{32} = \frac{\int_a^b x^3 f(x)\, dx}{\int_a^b x^2 f(x)\, dx} = \frac{\bar{x}_{30}^3}{\bar{x}_{20}^2} \qquad \text{(IV-6)}$$

(5) In General:

$$(\bar{x}_{pq})^{p-q} = \frac{\int_a^b x^p f(x)\, dx}{\int_a^b x^q f(x)\, dx} = \frac{\bar{x}_{p0}^p}{\bar{x}_{q0}^q} \qquad \text{(IV-7)}$$

(6) Hypergeometric mean:

$$\log \bar{x}_{pp} = \frac{\int_a^b x^p (\log x) f(x)\, dx}{\int_a^b x^p f(x)\, dx} \qquad \text{(IV-8)}$$

(7) Geometric mean:

$$\log \bar{x}_g = \int_a^b \log(x) f(x)\, dx \qquad \text{(IV-9)}$$

where the integration limits a and b in Equations (IV-3) through (IV-9) are the smallest and the largest drop sizes in a sample population.

The usefulness of a particular form of the mean drop size depends upon the physical phenomenon, since each of these mean values as defined above has its own physical significance.

If it is desired to acquire the information about the density function $f_n(x)$ directly from the experimental results, it is necessary to measure the individual drop sizes for a large number of drops. For experimental results obtained from sieve analysis, it is more practical to use the volumetric density function $f_v(x)$ as defined by Equation (IV-2). By numerical calculations made on the results of accurate sieve analysis, the various mean drop sizes as defined by Equations (IV-3) through (IV-9) can be obtained also. In order to define the mean drop size when $f_v(x)$ is

used as the density function, the distribution function $F_v(y)$ should be defined first:

$$F_v(y) = \int_a^y f_v(x)\, dx \qquad \text{(IV-10)}$$

Clearly, $F_v(y)$ is the decimal fraction of the total volume which contains all the drops whose sizes are small than or equal to y. The mean drop diameter ($\bar{x}$), which is the mean drop size used in the present work and which is also frequently called the mass median diameter, is defined by the following equation:

$$F_v(\bar{x}) = 0.50 \qquad \text{(IV-11)}$$

The functional form of the density function can be derived mathematically, if the exact mechanism of the liquid disintegration could be known and formulated analytically. Otherwise, it has to be determined by curve-fitting the experimental results, as is usually the case. The simplest distribution function which can be used to fit the experimental results is the Gaussian normal distribution which is completely determined by two distribution parameters: the mean value ($\bar{x}$) and the standard deviation (s). The Gaussian distribution is symmetrical about the mean value. The histograms of drop-size distributions obtained from liquid atomizations exhibit, however, some degree of skewness, if the size variable is defined simply as the drop diameter. It is then necessary either to define the size variable differently in order to apply the normal distribution or to devise empirical distributions in order to fit the histograms. If one chooses to use the drop diameter as the size variable, the required degree of skewness of the histogram can be achieved by writing $f(x)$ as $g(x)e^{-h(x)}$ where $g(x)$ and $h(x)$ are polynomial expressions of x, each containing one or two distribution parameters. The density

function f(x) must satisfy two conditions.

(1) $f(x) \to 0$ as $x \to a$ and as $x \to b$

(2) $\int_a^b f(x)\,dx = 1$

where a and b are the lower and the upper limits of the size variable.

Along this line several empirical distributions or modified normal distributions have been suggested by various authors for the representation of drop size distribution in atomization process. A summary is given in Table II.

TABLE II - EXPERIMENTAL DROP SIZE DISTRIBUTIONS

Distribution Name	Density Function	Size Variable*	Distribution Parameters	Lower and Upper Limits of Variable
Rosin-Rammler	$\frac{\delta x^{\delta-1}}{\bar{x}} e^{-(x/\bar{x})^{\delta}}$	$x = d$	$\bar{x}$, δ	0, ∞
Nukiyama-Tanasawa	$\frac{b^{6/\delta}}{\Gamma(6/\delta)} x^5 e^{-bx^{\delta}}$	$x = d$	b, δ	0, ∞
Log-normal	$\frac{1}{s\sqrt{2\pi}} e^{\frac{-(x-\bar{x})^2}{2s^2}}$	$x=\log(d)$	$\bar{x}$, s	$-\infty$, ∞
Log-normal with upper limit (Mugele-Evans)	$\frac{1}{s\sqrt{2\pi}} e^{\frac{-(x-\bar{x})^2}{2s^2}}$	$x=\log(\frac{d}{m-d})$	x, s, m	$-\infty$, ∞
Square-root normal (Tate-Marshall)	$\frac{1}{s\sqrt{2\pi}} e^{\frac{-(x-\bar{x})^2}{2s^2}}$	$x=(d)^{1/2}$	$\bar{x}$, s	0, ∞

*In column 3, d = drop diameter, and m = maximum drop diameter

It is clear from the definitions of the drop size variables that more weights have been given to the smaller drops in the three modified normal distributions. This may result in more symmetrical distributions about the mean sizes. Detailed discussions of these distributions can be found in

the papers by Epstein [E-1], Kottler [K-3], Mugele and Evans [M-11], and Tate and Marshall [T-3]. A general treatise on the subject of small particle statistics has been given by Herdan [H-6].

2. Liquid Disintegration Mechanism

When a liquid or a liquid stream, which has an extended free surface, is subjected to an internal or external cause of disturbance, the liquid surface could be ruptured if the disturbance develops and becomes sufficiently large. The result is the disintegration of the liquid into small elements. The mechanism of a liquid disintegration is generally very complex and the process very fast. In the past forty years, a great number of experimental investigations have been performed by using high speed photography in order to capture the sequence of the disintegration process. These investigations have been very useful in furnishing evidences to theoretical analyses and in bringing out the physical pictures of the disintegration phenomena. To list but a few of them, we mention the work of Scheubel [S-1] on carburator atomization, Taylor [T-4] on the deformation of liquid globules, Lane [L-3] on the shatter of drops in gas streams, Hinze and Milborn [H-9] on rotating disk atomization, Wetzel and Marshall [W-6] on pneumatic atomization, Dombrowski and Fraser [D-3] on the break of liquid sheets, Magarvey and Taylor [M-1] on free falling drops, and Christiansen and Hixson [C-3] on the break up of a liquid jet.

However, mathematical analyses must be made, in addition to the experimental investigations, in order to understand the hydrodynamical nature of liquid disintegration. Numerous theoretical studies pioneered by the earlier work of Lord Rayleigh [R-1] and Lamb [L-2] have been made by many authors over a span of almost a century. The mathematical methods used in these works, however, are very similar. Most of them are based upon the

assumption of either an inviscid fluid or small disturbances, or both, so that the problem can be solved by using the potential functions and the linearized Navier-Stokes equations. These assumptions contribute, in most cases, to the discrepancies between theoretical and experimental results. The second factor which must be considered in order to account for the discrepancies is that a liquid disintegration could be a multistage process, and hence a single analysis may not suffice. Despite of these imperfections and simplifications, theoretical analyses have led to, at least, some basic understandings and qualitative descriptions of liquid disintegration mechanisms.

Before we present the results of some of the representative theoretical analyses, it would be helpful to list below the causes of liquid disintegration and their resistances.

External Causes of Disintegration

(i) Unbalanced pressure exerted on the liquid surface.

(ii) Viscous drag exerted on the liquid surface.

(iii) Fluctuation of pressure on the liquid surface.

Internal Causes of Disintegration

(i) Inertial force.

(ii) Inherited vibration or oscillation.

(iii) Inherited turbulence.

Resistances to Disintegration

(i) Surface force.

(ii) Viscous force.

(iii) Elastic force.

It can be seen from the preceding list that there will appear three-dimensionless parameters in the mathematical analysis for a general problem of liquid disintegration.

(i) Reynolds number (Re) = $\frac{\text{Inertial force}}{\text{Viscous force}}$

(ii) Weber number (We) = $\frac{\text{Inertial force}}{\text{Surface force}}$

(iii) Elastic force parameter = $\frac{\text{Inertial force}}{\text{Elastic force}}$

The proper definitions of these dimensionless parameters depend upon the specific problem. The disruptive action in liquid disintegration is always associated with the inertial force of either the liquid itself or the surrounding fluid, and is always opposed by the three resistant forces. Therefore, an optimum disintegration of the liquid would be such that the action of the disruptive inertial force is a maximum with respect to the resistant forces.

For our purpose of understanding the basic nature of liquid disintegration phenomena, it suffices to examine the mathematical analyses of four cases of liquid disintegration: the breakup of a cylindrical jet of low velocity, the breakup of a spherical liquid drop when suddenly exposed to a gas stream of uniform velocity, the breakup of a liquid sheet, and the surface erroding of a liquid by a high velocity gas stream. The representation is itemized in the following:

(1) <u>The Breakup of a Cylindrical Jet of Low Velocity</u>

This was one of the earliest problems of liquid instability, first attacked by Lord Rayleigh [R-1] who considered the breakup as a result of the growth of some disturbance waves initially imposed on the jet surface. He showed that, among the disturbance waves of different wave lengths, only one of them could grow in amplitude at maximum rate. This wave would have dominating influence on the breakup of the jet. His analysis was based upon a consideration of

the kinetic and potential energy of the jet. Levich [L-4] has discussed this problem in a more general manner.

By assuming the amplitude of a disturbance wave is proportional to $e^{\beta t}$, Lord Rayleigh [R-1] obtained the following equation governing the wave-growth rate (β) for an inviscid jet:

$$\beta^2 = \frac{\sigma k}{\rho a^2} (1 - k^2 a^2) \frac{I_1(ka)}{I_o(ka)} \qquad \text{(IV-12)}$$

where k is the wave number, a is the jet radius, and I_o and I_1 are the modified Bessel functions of the first kind.

Equation (IV-12) can be written in the dimensionless form

$$\frac{\rho \beta^2 a^2}{\sigma k} = (1 - k^2 a^2) \frac{I_1(ka)}{I_o(ka)} \qquad \text{(IV-13)}$$

where the dimensionless group, $\rho\sigma^2 a^2/\sigma k$, can be identified as the Weber number of the wave motion on the jet surface.

By differentiation of Equation (IV-13) with respect to ka, we find that the maximum value of the Weber number, namely, the maximum ratio of inertial force to the surface force, occurs at

$$(ka)_{max} = 0.679 \qquad \text{(IV-14)}$$

and the corresponding wave length is

$$\lambda_{max} = \frac{2\pi}{k_{max}} = 9.02(a) \qquad \text{(IV-15)}$$

Needless to say, that λ_{max} maximizes also the growth rate of the disturbance wave. Assuming the jet breaks up into fragments of lengths λ_{max}, the mean drop size ($\bar{x}$) can be calculated by the mass balance

$$\frac{\pi}{6} (\bar{x})^3 = \frac{\pi}{4} (2a)^2 (\lambda_{max}) \qquad \text{(IV-16)}$$

and, therefore,

$$\bar{x} = 1.89(2a) \qquad \text{(IV-17)}$$

From this result we conclude that the breakup of a low velocity jet produces drops with a mean drop size as large as twice the jet diameters. This result has been thoroughly verified by Tyler [T-9] for liquid-air systems, and by Christiansen and Hixson [C-3] for liquid-liquid systems.

Since λ_{max} is independent of σ, it follows that a change in surface tension has no effect on the mean drop size. This has been confirmed also by Christiansen and Hixson [C-3]. However, the degree of instability as represented by the growth rate (β) is dependent on σ. It can be seen from Equation (IV-12) that an increase in the ratio of σ/ρ will result in a greater growth rate, and hence a shorter breakup length of the jet. The breakup length of the jet is defined as the continuous portion of the jet up to the breakup point.

The effect of liquid viscosity on the jet breakup was considered in a later paper by Lord Rayleigh [R-2]. The result showed that the values of λ_{max} were shifted to the long wave region with the increase of viscosity. This result is understandable because disturbance waves of short wave lengths are quickly damped out by viscous dissipation. Consequently, viscous liquids produce larger drops.

In Lord Rayleigh's first analysis the existence of the ambient fluid were entirely neglected. The influence of the ambient fluid were treated in great detail by Weber [W-2] and Tomotika [T-7). We briefly mention some of their results with which we are concerned. Weber considered the effect of surface loading due to ambient pressure. His analysis also led to the conclusion that for viscous fluids, λ_{max}

would be very large. Tomotika investigated the breakup of a cylindrical thread of a viscous liquid in the atmosphere of another viscous liquid. His analysis resulted in a functional relation between λ_{max} and the ratio μ/μ', where μ and μ' were the viscosities of the jet and the surrounding liquid, respectively. Numerical calculations revealed that λ_{max} became indefinitely large as the ratio of μ/μ' became either very large or very small and that λ_{max} assumed a minimum value when μ and μ' were nearly equal. This result demonstrates the fact that the breakup of liquid thread or jet in the presence of another fluid is an interfacial problem. When the viscosity of either fluid is very large, λ_{max} will shift to the long wave region because of the viscous damping of the short waves of disturbance.

The instability of a jet can be varied by imposing secondary motion on the jet or by varying the ambient conditions. Ponstein [P-2] has considered the instability of a rotating jet. Miesse [M-10] and Dityakin and Yagodkin [D-2] have discussed the effect of oscillations of ambient pressure and velocity on jet instability. Miesse [M-9] has also conducted investigations on the effect of vaporization using liquid nitrogen. Holdroyd [H-11] postulated that the major cause of jet breakup was due to turbulence. Lychesvsky [L-7] and Vereshchagin, Semerchan and Sekoyan [V-1] have furnished experimental evidences of the turbulence effect on jet instability.

(2) <u>The Breakup of a Spherical Liquid Drop When Suddenly Exposed to a Gas Stream of Uniform Velocity</u>

When a liquid drop is suddenly exposed to a gas stream, its spherical shape is deformed by the action of the dynamic pressure of the gas stream, and this deformation may result in the breakup of the drop. This type of liquid disintegration occurs in pneumatic

atomization with relatively low velocities of the gas stream, and also in the breakup of a freely falling drop in open air.

Hinze [H-7] considered this problem and performed an analysis for the axisymmetric deformation of a spherical drop of radius a when suddenly exposed to a gas stream of uniform velocity V_a. By relating the surface displacement (δ) to the pressure distribution around the sphere, he obtained the following expression for the maximum surface displacement at the stagnation point under the assumption that $\mu^2/\sigma\rho a << 1$.

$$\left(\frac{\delta}{a}\right)_{max} = - 0.17 \frac{\rho_a V_a^2 a}{\sigma} \qquad \text{(IV-18)}$$

A similar analysis for freely falling drops yielded

$$\left(\frac{\delta}{a}\right)_{max} = - 0.095 \frac{\rho_a V_t^2 a}{\sigma} \qquad \text{(IV-19)}$$

where V_t is the terminal velocity of the drop.

In Equations (IV-18) and (IV-19) we recognize that the dimensionless group $\rho_a V_a^2 a/\sigma$ is the proper definition of Weber number for the system. Thus the analysis results in a relation between the Weber number and the maximum displacement possible for a given velocity of the gas stream. The validity of these two equations can be tested by experimental results obtained with the water-air system which certainly satisfies the condition that $\mu^2/\sigma\rho a$ is much less unity even for a drop as small as 0.5 mm in diameter.

The experimental results obtained for the freely falling liquid drops and the shatter of liquid drops by air blast all indicate the existence of a critical Weber number at which a drop loses its identity and disintegrates into smaller drops. Based upon the experimental data of Merrington and Richardson [M-6] on freely falling

drops, the critical Weber number calculated by Hinze [H-7] has a mean value of about 10, and hence $(\delta/a)_{critical} \simeq 1$ according to Equation (IV-20). This shows that at the moment of drop breakup, the displacement of a liquid particle in the drop is as large as the drop radius. In fact, high speed photographs reveal that, just before the time of breakup, the drop has been blown into a bag-shaped film. Therefore, the actual maximum displacement of the liquid drop at the stagnation point is even larger than the radius.

Using this value of $(\delta/a)_{critical} \simeq 1$, it follows from Equation (IV-19) that the critical Weber number of liquid drops when suddenly exposed to air blast is 6.0. This agrees well with the experimental value of 5.3 as determined by Lane [L-3], $5.3 \sim 7.0$ as published by Volynski [V-2], and $6.7 \sim 7.2$ obtained by Masugi [M-4].

(3) The Breakup of a Liquid Sheet

This type of liquid disintegration is of great importance in atomization since it is involved in two of the most useful atomization devices: the swirl-type and the fan-spray nozzle. This problem has been treated by Lamb [L-2], Squire [S-4], York, Stubbs and Tek [Y-1], Hagerty and Shea [H-2], and Dombrowski and Johns [D-6]. As in the case of liquid jet, the instability of the liquid sheet has been considered as the result of disturbance growth.

Hagerty and Shea [H-2] considered the wave growth on a liquid sheet of thickness 2a which travels with a uniform velocity V. The ambient gas is moving parallel to the sheet with a velocity V_a. Under the assumption that the wave lengths are relatively large, the analysis yields the following expressions for the maximum rate of wave growth and the corresponding wave length:

$$\frac{a\beta_{max}}{V} = \frac{1}{2We'} \frac{(We' - 1)^2}{We' + 1} \frac{\rho_a}{\rho} \qquad \text{(IV-20)}$$

$$\lambda_{max} = \frac{2\pi}{We} (2a) \qquad \text{(IV-21)}$$

where

$$We' = \frac{a\rho V^2}{\sigma} \quad \text{and} \quad We = \frac{a\rho_a V^2}{\sigma} \ .$$

The validity of the results has been tested by the same authors. They determined the maximum growth rate of artificially generated waves of long wave lengths which were imposed on the liquid sheet. The results were in good agreement with Equation (IV-21). The analyses made by Squire [S-4], and York, Stubbs and Tek [Y-1] yielded essentially the same result as represented by Equation (IV-20).

Theoretically, the action of the unstable wave growth results in the tearing apart of the liquid sheet at the breakup point, producing long ligaments which further breaks up into small drops as a result of Rayleigh instability. This mechanism of drop production from a liquid sheet has strong support from the experimental evidences obtained by Dombrowski and Fraser [D-3]. Based on this mechanism, a correlation formula for the mean drop size has been worked out for fan-spray nozzles by the joint effort of Fraser, Eisenkalm, Dombrowski and Hasson [F-2],

$$\bar{x} = 7.56 \left(\frac{\rho}{\rho_a}\right)^{1/6} \left[\frac{k_o \sigma}{\rho V^2}\right]^{1/3} \qquad \text{(IV-22)}$$

$$= 0.035 \left[\frac{k_o \sigma}{C_Q^2 P}\right]^{1/3} \left(\frac{\rho}{\rho_a}\right)^{1/6} \quad \text{(centimeters)} \qquad \text{(IV-23)}$$

where k_o is a parameter related to the sheet thickness. [The quoted

authors did not calculate the numerical coefficient in Equation (IV-23).]

Dombrowski and Hooper [D-5] made an extensive comparison of Equation (IV-24] with experimental results obtained by various authors with liquids of low viscosities and at low pressures. They found that the numerical coefficient in Equation (IV-23) varied from 0.022 to 0.036. The agreement should be considered as very good.

Despite the success, it should be noted that the particular form of the dependence of $\bar{x}$ on the operating variables as represented by Equation (IV-23) is restricted to the long wave region of the disturbances, and hence to region of low injection pressures where the sheet extends to a relatively long distance from the orifice. As the operating conditions of the nozzle is varied considerably, the dependence of $\bar{x}$ on the operating variable could be different from Equation (IV-23). This has been discussed in great length by Dombrowski and Hooper [D-5].

Using an approach similar to the above analysis, Dombrowski and Jones [D-6] analyzed the breakup of a viscous liquid sheet also produced by fan-spray nozzles by taking into account the viscous dissipation along the liquid sheet. The derived equation for correlating the mean drop diameter was in a reasonable degree of agreement with the experimental equation of Hasson and Mizrahi [H-4] obtained for molten waxes.

As a conclusion, it can be stated that the breakup of a liquid sheet produced at low pressures follows a two-stage process. First, the ligaments are formed due to unstable wave growth and then the ligaments break up into drops according to Rayleigh instability.

(4) The Surface Erroding of a Liquid by a high velocity gas Stream

When a gas stream of high velocity is blowing over a liquid surface, disturbance waves of varying wave lengths are generated on the surface. This phenomenon is commonly called the wave generation by wind. The interaction between the gas and the liquid results in some work being done on the liquid by the normal pressure of the gas over the liquid surface. As a consequence, a wide spectrum of waves can be maintained in propagation and growth. This has been suggested by Jeffreys [J-1], and Levich [L-4] has given a clear explanation of the phenomenon.

When the amplitude of a wave has grown to a height comparable to its wave length, the wave crest can be erroded as ligaments which immediately breaks down into small drops. This type of liquid disintegration possibly occurs whenever there is a high relative velocity between a gaseous and a liquid phase, as in the cases of pneumatic atomization and the breakup of a liquid stream traveling at a high velocity in a quiescent gaseous medium.

The following equation governing the growth rate of the wave amplitude on deep water was first derived by Lamb [L-2].

$$\frac{d\beta}{dt} = \left[\frac{\gamma \rho_a (V_a - c)^2}{2c\rho} k - \frac{2\mu}{\rho} k^2 \right] \beta \qquad \text{(IV-24)}$$

where γ is the sheltering coefficient and c is the wave velocity. Based upon this equation, Mayer [M-5] performed an analysis and obtained the following correlation for the mean drop size.

$$\bar{x} = 9\pi \, (16)^{1/3} \, B \left[\frac{\mu}{\rho_a V_a^2} \left(\frac{\sigma}{\rho}\right)^{1/2} \right]^{2/3} \qquad \text{(IV-25)}$$

where B is a constant coefficient.

Although this equation is derived for fluid with large depth, it can be used also for a liquid with finite dimensions provided the waves are much smaller than the depth of the liquid. In this case, it can be transformed into the following form:

$$\frac{\bar{x}}{D} = 9\pi\ (16)^{1/3}\ B\ Re^{-2/3}\ We^{-1/3} \qquad \text{(IV-26)}$$

where

D = a characteristic dimension of the liquid

$$Re = \frac{DV_a\rho_a}{\mu} \qquad We = \frac{D\rho V_a^2}{\sigma}$$

For the purpose of comparison, Equation (IV-26) can be written in the form,

$$\bar{x} \sim V_a^{-4/3}\ \sigma^{1/3}\ \mu^{2/3} \qquad \text{(IV-27)}$$

This can be compared with the experimental results obtained by Weiss and Worsham [W-4] for pneumatic atomization of molten wax (Equation IV-28), by Nukiyama and Tanasawa [N-3] for pneumatic atomization of alcohol and glycerine mixtures at high ratio of gas to liquid flow rate (Equation IV-29), by Wetzel and Marshall [W-6] for pneumatic atomization of molten wax and metals (Equation IV-30), and by Hanson, Domick, and Adams [H-3] for shatter of drops in a shock tube (Equation IV-31).

$$\bar{x} \sim V_a^{-4/3}\ \sigma^{1/4}\ \mu^{1/3} \qquad \text{(IV-28)}$$

$$\bar{x} \sim V_a^{-1}\ \sigma^{1/2} \qquad \text{(IV-29)}$$

$$\bar{x} \sim V_a^{-1.11} \sim -1.68 \qquad \text{(IV-30)}$$

$$\bar{x} \sim V_a^{-1.50} \sim -1.70 \qquad \text{(IV-31)}$$

where V_a in the last four equations is the velocity of the gas phase relative to the liquid phase.

From the above comparison, it appears that the surface erroding mechanism is a possible explanation of the liquid disintegration under the action of a high velocity gas stream.

(5) Conclusions on Liquid Disintegration Mechanism

From the preceding analyses and their comparisons with experimental observations, it can be stated that the primary cause of liquid disintegration is, in most cases, due to the amplitude growth of some initial waves of disturbances. The wave growth can be greatly amplified by the action of an ambient fluid.

In the case of a cylindrical jet, the breakup is certainly due to Rayleigh instability when the jet velocity is low. The produced drop size is, therefore, large but uniform. As the jet velocity is increased, the influence of the ambient fluid through the action of aerodynamic pressures gradually becomes significant. As a result, surface waves of different wave lengths can be excited on the surface, and the produced drop sizes will be no longer uniform. At very high velocities, the breakup is probably dominated by the aerodynamic pressures, and surface erroding may become the basic mode of disintegration. The surface erroding of a high-velocity jet was first suggested by Castleman [C-1]. However, the existence of the ligaments as the intermediate stage of atomization has not been confirmed by experiments, probably because the life time of a ligament is very short. Haenlein [H-1] has given a detailed discussion on the breakup of a liquid jet at different velocities.

The breakup of a liquid drop moving in another gaseous fluid

strongly depend upon the Weber number defined as $\rho_a V_a^2 a/\sigma$. At low Weber numbers, the drop may become flattened, but it does not disintegrate. As the Weber number is increased to a critical value, the drop is deformed into a hollow 'bag' which disintegrates readily into small drops. At very high Weber numbers, the disintegration of drop is probably governed by surface erroding. The transition in the breakup mechanism from the 'bag' formation type to the surface-wave type as the Weber number is increased has been clearly observed by Lane [L-3] in the experiments of shattering liquid drops by air blast. The related phenomenon of liquid drop dispersion in another liquid has been discussed by various authors including Taylor [T-4], Hinze [H-8], and Klinter [K-2].

The disintegration of a liquid sheet is very similar to that of a cylindrical jet. At low velocity, the sheet breaks up according to the mechanism as we have described before. At high velocities, surface erroding may become important. The importance of the aerodynamic forces exerted by the ambient fluid can be realized by observing the breakup of a liquid sheet in high vacuum. An experiment in this respect has been performed by Fraser, Eisenkalm, Dombrowski and Hasson [F-2]. According to their observations, the stability of a liquid sheet can be considerably increased by diminishing the ambient gas densities. In these conditions, the breakup of the liquid sheet follows a pattern quite different from that under atmospheric pressures. This shows that in the presence of an ambient gas, the instability of a liquid jet is primarily of aerodynamic nature in the region of high velocities.

3. Dimensional Analysis

In the discussions of liquid disintegration mechanism we have seen

that the results of theoretical considerations are in good agreement with experimental observations obtained from some simple systems, for which the assumptions of inviscid flow and small disturbances are generally valid. In other cases, the agreement is only qualitative. From a practical viewpoint, the most expedient approach to correlate drop size distributions is to use dimensional analysis.

Before we can perform a dimensional analysis, we have to know how many parameters are required to characterize the drop size distributions for swirl-type pressure nozzles. In the absence of theoretical guidance, this information can be obtained only by curve-fitting the experimental data as we have described in part 1 of this section. For Newtonian fluids and swirl nozzles, Tate and Marshall [T-3] and Nelson [N-1] have been successful in fitting experimental results with the square-root normal distribution. It is possible that this distribution law can be used for non-Newtonian fluids, since the disintegration mechanisms may be similar for both fluids. By this assumption, the drop size distribution of a non-Newtonian fluid is characterized also by two parameters: the mean drop size ($\bar{x}$) and the standard deviation (s).

The most important thing in dimensional analysis is the selection of relevant physical variables. In the case of several alternative choices, the decision is usually dictated by the convenience of data manipulation. For the present situation, it is reasonable to decide that the physical variables which determine the drop size distribution should be the inlet pressure, the physical properties of the fluid, and the nozzle dimensions.

We have seen in Section III that the performance of a swirl nozzle depends upon the Reynolds number and the dimensionless parameter A. In view of this, it can be assumed that the effect of the nozzle dimensions

on drop size distribution can be accounted for adequately by the orifice diameter (D_2) and the parameter A.

The viscosity of a non-Newtonian fluid is a function of shear rate, its specification requires at least two parameters as in the simplest case of power law model for the shear stress and shear rate relation. However, for the present case of liquid atomization, we suspect that the disintegration of the liquid occurs within a certain range of shear rates, and it may be possible to simplify our problem by using an average value of the apparent viscosity. The proper range of the shear rates in which atomizations take place remains to be investigated.

Now we can write the following equations for the mean drop size ($\bar{x}$) and the standard deviation (s).

$$\bar{x} = f(P,\rho,\sigma,\mu,D_2,A) \qquad \text{(IV-32)}$$

$$s = g(P,\rho,\sigma,\mu,D_2,A) \qquad \text{(IV-33)}$$

where

ρ = density of fluid

σ = surface tension of fluid

μ = average apparent viscosity of fluid

By the requirement of dimensional homogeneity, these two equations can be readily transformed into dimensionless forms.

$$\frac{\bar{x}}{D_2} = f\left(\frac{D_2\sqrt{P\rho}}{\mu}, \frac{D_2P}{\sigma}, A\right) \qquad \text{(IV-34)}$$

$$\frac{s}{D_2} = g\left(\frac{D_2\sqrt{P\rho}}{\mu}, \frac{D_2P}{\sigma}, A\right) \qquad \text{(IV-35)}$$

where the two-dimensionless groups, $D_2\sqrt{P\rho}/\mu$ and D_2P/σ are the Reynolds number and the Weber number.

Correlations based upon the above equations have the salient feature

that once the operating conditions of the nozzle and the physical properties of the fluid and the nozzle size are specified, the mean drop size and the standard deviation are determined. No physical quantities which demand cross reference or additional measurements are included in the correlations.

SECTION V - EXPERIMENTAL METHOD

1. The Selection for Freezing Process

There are three basic methods of determining the size distribution of liquid drops produced by a spray nozzle.

(1) Photographic Method - Pictures are taken of the liquid drops which are collected on sample plates or in a non-mixing fluid. Drop sizes are measured from enlarged pictures or by examining the pictures under a microscope. The procedures are very tedious. Besides, the distortion of the drop when deposited on sample plates, evaporation of the liquid drops, and the difficulties associated with obtaining representative samples tend to yield inaccurate results.

(2) Electronic Scanning - The labor of measuring drop sizes from photographs is taken over by an electronic computer. A description of the basic principles of the scanning device can be found in a paper by Adler and cc-workers [A-1]. The Spraying System Company claims to have developed an electronic scanning computer which observes a selected portion of a projected spray for intervals on one-millionth second, records the number and measures the diameters of all the spray particles, and classifies them into given size ranges. However, the cost of this instrument forbids its use in most laboratories.

(3) Freezing Method - The liquid spray particles are introduced into a cooling medium where they become solidified. Sieve analysis of the frozen drops yields size distributions directly. The frozen drops must be kept from melting by sufficient and continuous cooling during the time of screening and weighing. The

method of using molten waxes to simulate ordinary fluids belongs, in principle, to this category.

In addition to these methods, Ranz [R-3] has attempted the impact method, and Cohen [C-4] has made use of light scattering techniques in determining the size distribution of spray drops. General references to the determination of fine particle sizes can be found in the treatises by Orr and Dallavalle [O-2] and by Herdan [H-6].

The freezing process has been chosen as our method of determining the size distributions. This choice was made based on three considerations. First, in this method all the particles produced in a spray are collected and processed. The problem of partial sampling is eliminated, and hence the experimental results are believed to be closer to the true distribution. Second, coalescence and secondary atomization of the spray particles can be minimized by using a cooling agent of sufficiently low temperature for fast freezing. And third, the operation is relatively simple and rapid.

Choudhury [C-2] appears to be the first person who used liquid nitrogen as the freezing medium for spray particles. In his work, the sample fluids were sprayed directly into liquid nitrogen and the screenings of the frozen particles were accomplished in a cold room maintained at low temperatures by refrigeration. Nelson [N-1] made extensive studies on the atomization of Newtonian fluids using a similar but much simplified method. He eliminated the necessity of a cold room by screening the frozen particles within an insulated sieve-container mounted on a giant shaker. Liquid nitrogen was poured intermittently over the container to keep the particles from melting. The experimental method of the present work is essentially based upon the one described by Nelson.

2. Experimental Equipment

The equipment consists of five main units: a pressurizing system, a swirl nozzle, a collecting unit for spray drops, a sieve shaker, and a weighing box.

The pressurizing system includes a stainless high-pressure vessel and a stainless pipe line. The vessel is an inspected cylinder having a working pressure of 1,800 psi and a capacity of one and a half gallons. It was constructed by welding two thick head pieces of stainless steel to an 18 inch cut of schedule 80 stainless pipe of six inch nominal diameter. The pipe line is made of half inch stainless tubing and Ferulok fittings. The flow in the pipe line is controlled by a normally closed solenoid valve. The system is pressurized with compressed nitrogen from a commercial cylinder. The system pressure is controlled by a high pressure regulator which is equipped with a mechanism that releases the system pressure slowly without producing shock noise.

The collecting unit is composed of an upper and a lower section. A sketch of the collecting unit is shown in Figure 3. The upper section is a cyclone-like cold chamber made of galvanized iron sheet and fiber glass. It is 20 inches in I.D. and in height. Liquid nitrogen can be introduced into the chamber and distributed uniformly over the wall surface by means of two copper rings which are situated at the top of the collecting chamber and are connected individually to two commercial liquid nitrogen tanks, each of which is 160 liters in capacity. The chamber has a thick insulated cover made of galvanized iron sheet and fiber glass which can be locked tightly to it. A neoprene foam gasket is used between the cover the chamber for sealing. There is an 8 inch opening at the center of the cover through which a sample fluid is sprayed from

the nozzle into the chamber. Covering the opening is a stainless housing for a sliding cut-off drawer which is operated manually to control the spray time. The spray time is recorded on an electric timer triggered by the motion of the drawer. The spray nozzle is placed in the drawer housing facing the 8 inch opening.

The lower chamber of the collecting unit is a cylindrical one of similar construction, 14 inches in I.D. and 20 inches in depth. It is spring loaded on a rolling platform so that it can be adjusted to fit with the upper chamber or removed from it readily. A piece of silicon rubber serves as a gasket between the two chambers when aligned. Inside the lower chamber there is a removable and perforated plate on which the sieves are placed.

The sieve shaker is virtually a reproduction of the one used by Nelson and perhaps also by Choudhury. A photo picture of the shaker is shown in Figure 5. The frame in the center which carries the insulated sieve container is motorized to swing back and forth through the actions of a large flying wheel and an eccentric cam. The motion of the frame is stopped on both sides by metal blocks to generate shocking impacts and vibrations. The deafening noise can be minimized considerably by wrapping the metal blocks with tough leathers. Before we built the present siever shaker, we had tried a gyratory type of sieve shaker designed for testing soil particles. The shaker had been modified slightly in order to generate an increased intensity of vertical tapping. However, due to the added weight of the insulated sieve container, the shaker was not able to give satisfactory screening results.

The weighing box is a large insulated chest designed for weighing the sieves and storaging some dry ice to maintain low temperatures. The weighing

balance is placed on the top of the box and the weighing pan is suspended inside the box by a nylon cord through a small opening on the box.

3. Operation Requirements and Test Runs

For best results which can be expected from the present method, the following requirements of operation must be fulfilled.

(1) Room temperature should be maintained at the vicinity of the nozzle orifice so that the spray particles are produced in conditions comparable to those in other processes.

(2) Fast freezing should be achieved to minimize the coalescence or shattering of liquid drops.

(3) Material loss of spray drops due to incomplete recovery or vaporization should be prevented.

(4) Effective screening must be provided to give satisfactory sieve analysis.

To satisfy the first requirement, dry nitrogen is continuously injected into the small enclosure surrounding the spray nozzle to keep the cold atmosphere which prevails in the collecting chamber from reaching the nozzle. To meet the second requirement the collecting chamber is designed to operate with a film of liquid nitrogen running down the wall surface. With this arrangement, the bulk of the chamber would be filled with a nitrogen vapor at the equilibrium temperature of liquid nitrogen at essentially atmospheric pressure, which is -195°C. The liquid drops which travel through this cold atmosphere should become solidified in a very short time. Material loss due to deposition of spray particles on the wall surface of the collecting chamber is greatly reduced when the wall is covered by the running film of liquid nitrogen. Loss due to evaporation is negligible when the sieve container and the weighing box are kept at sufficiently low

temperature. From the calibrated flow rate and the recorded spray time a calculation on material recovery can be readily made.

Based upon these considerations, a series of test runs with water and polymer solutions were made. It started with the initial equipment which differed from the existing equipment described in the previous pages. The main difference was the replacement of the gyratory sieve shaker by the one shown in Figure 5. It took about sixty test runs before the system was improved to a working condition capable of producing consistent and reproducible results.

Each test run began with the filling of a sample fluid into the pressure vessel. Then the system was pressurized, dry nitrogen was injected to surround the spray nozzle, and the liquid nitrogen was allowed to flow into the collecting chamber to generate a cold atmosphere and to form a liquid film on the wall surface. With one tank supplying liquid nitrogen, the highest flow rate into the chamber was about three to four liters per minute at the maximum delivery pressure of 25 psig. At this maximum flow rate the wall temperature was brought down rapidly to that of liquid nitrogen in about one and a half minutes, as was indicated by thermocouple measurements. In order to make sure that the wall surface had been completely covered by a liquid nitrogen film before the spray was allowed to come into the chamber, a small opening of one eighth of an inch was made on the wall. It was connected to the outside by a small tubing. When the wall surface was covered by the liquid nitrogen film, we could see a stream of liquid nitrogen flowing out of the tubing. The opening was plugged with a round head screw, leaving a very small clearance for liquid nitrogen to flow through. Using one liquid nitrogen tank at the maximum flow rate, the stream began to flow out of the tubing in about

two and a half minutes. By this time enough liquid nitrogen had flowed into the lower chamber and the whole collecting unit had arrived at a very low temperature. The solenoid switch was then turned on and the sample liquid began to spray into the cut-off drawer. After the pressure gauge had assumed a steady reading, the cut-off drawer was pulled so that the sample liquid could be sprayed into the cold chamber for a predetermined time. The drawer was then pushed back quickly to cut off the spray. The particles sprayed into the chamber soon became solidified and were washed down to the sieves by the flowing liquid nitrogen. One minute of flushing time was found to be enough to clean off all the spray particles from the wall surface.

During the test runs the heat transfer rate in the chamber was found to be of critical importance. The freezing of spray particles formed by water or aqueous solutions required the removal of a large amount of latent as well as sensible heat in a very short time. Hence, we decided to increase the liquid nitrogen flow rate by adding another liquid nitrogen tank. When two tanks were being used, the maximum flow rate was about seven to eighth liters per minute which were found to be sufficient for a flow rate of spray fluid up to sixty grams per second. It was also found that sometimes partially frozen particles were collected in the sieves, resulting in cake formation or particle agglomeration. To eliminate this happening, the exit opening of the cold chamber was reduced from an original dimension of four inches to two inches in order that the opening could be closed by the down-flowing liquid nitrogen. Spray particles had to travel through this closing film to arrive at the sieves, and were thereby completely solidified.

The frozen particles in the cold chamber flowed with liquid nitrogen

through a guiding trough into the lower chamber and were collected in a set of nine sieves. A high and removable weir was used with the top sieve to prevent fine particles from flying outside the sieve. Some very fine particles were wet screened by liquid nitrogen all the way down to the bottom of the lower chamber. The bottom of the chamber was lined with a large sheet of aluminum foil so that the fine particles can be recovered by careful decantation.

After sufficient flushing of the cold chamber with liquid nitrogen, the lower chamber was removed from it and the sieves were quickly transferred to the sieve container for screening. The sieves had been wrapped with a sheet of asbestos cloth to prevent moisture condensations from the atmosphere, and the sieve container had been precooled with one and a half liters of liquid nitrogen. Then the container was clamped to the shaker and screened for thirty minutes during which time two liters of liquid nitrogen were poured intermittently over the container to keep a low temperature. Due to the added weight of the sieve container and the damping of vibrations exercised by the insulation material, the present giant shaker was constructed to achieve satisfactory screening.

When the screening was done the sieves were transferred inside the weighing box which contains a couple blocks of dry ice. The sieves were allowed one hour of time to come up to the same temperature as in the box before the asbestos cloth was taken off and the sieves weighed. The box was always saturated with water vapor and the loss of the sample weight due to evaporation was found to be negligible, as checked by repeated weighing of the same sample over several hours.

The percentage material recovery was found to range from about 80 to 110. The loss of material was chiefly due to some particles being left on

the inside surface of the chamber, while the gain of material was due to the incorrect spray time recorded by the timer. When large nozzles were in operation, the suitable spray time was of the order of half a second. In these cases, the electric timer which was triggered by the manually operated drawer could have recorded incorrect spray time.

The liquid nitrogen consumption on the average was twenty-four liters per run including the storage loss from both tanks. Each run required about four and a half hours of work including the necessary washing and cleaning of the equipment due to the use of polymer solutions.

SECTION VI - SELECTION OF NON-NEWTONIAN FLUIDS AND THEIR RHEOLOGICAL MEASUREMENTS

A Newtonian fluid exhibits a linear relationship between the shear stress and shear rate which, when plotted, give a straight line through the origin. Hence, the viscosity of a Newtonian fluid is a constant for all shear rates. A fluid whose relationship between shear stress and shear rate deviates from this simple law is classified as a non-Newtonian fluid. Polymer solutions and melts, emulsions, slurries, and biological fluids such as blood all fall into this category. The branch of science which studies the flow behaviors of non-Newtonian fluids, commonly termed as the rheology of non-Newtonian fluids, is of great importance.

Polymer solutions are generally chosen as the working materials for rheological studies. The polymers which have been used in rheological research can be loosely divided into two groups. The first group contains those polymers whose dilute solutions exhibit basically a non-linear relationship between shear stress and shear rate, or simply a non-Newtonian viscosity. To the second group belong those polymers whose dilute solutions exhibit pronounced elastic effects in addition to the non-Newtonian viscosities, and hence they are commonly called viscoelastic materials. The elastic effect can be revealed in several ways by experiments. It causes the materials to exhibit stress relaxation, the Weissenberg effect, friction drag reduction, die swelling or thinning, and other phenomena. While a rheological diagram of apparent viscosity versus shear rate is sufficient to characterize the flow behavior of a simple non-Newtonian fluid, information from normal stress or relaxation measurements is necessary for characterizing viscoelastic materials. Some of the simple non-Newtonian polymers which are soluble in water are given in Table III.

TABLE III - WATER SOLUBLE POLYMERS

Trade Name	Chemical Structure	Manufacturer
CMC	Sodium carboxymethyl cellulose	Hercules
Natrosol	Hydroxyethyl cellulose	Hercules
Carbopol	Polycarboxyvinyls	B.F. Goodrich
Elvanol	Polyvinyl alcohol	Du Pont

From the foregoing list of polymers we have selected CMC and Carbopol as the working materials. Natrosols are very similar to CMC in rheological and physical properties, but they are surface active which makes them less satisfactory for our purpose. Elvanols are much less frequently used in research work. The specific grade of CMC we have chosen was CMC-7L. This substance was chosen because of its low consistency at relatively high concentrations.

In order to eliminate the variations in the concentrations of sample solutions, only one batch of powder was used for each polymer material. The moisture content of the powder had been corrected for each preparation of the solutions. The solutions of Carbopol-934 were acidic and the viscosities exhibited a strong dependence on the acidities of the solutions. However, the viscosities were essentially constant over the pH range from 6 to 10. For best results, the Carbopol solutions were neutralized with sodium hydroxide to a pH of 7.5 corresponding to the most stable condition.

Since the apparent viscosities depend upon shear rates as well as on concentrations, it is necessary to determine the rheological behaviors before deciding what concentration of the solution is suitable for a certain purpose. In this work, the rheological diagrams of apparent viscosity versus shear rate have been determined with a Weissenberg Rheogoniometer (Model R-16) manufactured by the Farol Research

Engineers, Ltd., England. This Rheogoniometer is driven by a 1,800 RPM motor with speed reducing gears. The highest shear rate obtainable with a pair of 10 cm cone-and-plate of a 2 degree gap is about 1,000 per second. Above this limit, the liquid contained in gap is spinned out due to centrifugal force. When the normal force diaphragm assembly and the normal force spring are installed, the total normal force exerted on the plate by the fluid can be measured in the same time with tangential stress. The instrument is equipped with a two channel ultraviolet light recorder which is fast in response and convenient in use.

The measurements of tangential stresses were straightforward. The experimental results of apparent viscosities versus shear rate up to 1,000 per second obtained for Carbopol-934 and CMC-7L for several concentrations are shown in Figures 12 and 13, respectively.

SECTION VII - EXPERIMENTAL RESULTS

Following the experimental method described in Section V we have performed 113 accepted runs, of which 15 were made on water, 6 on 76% glycerine solution, 17 on 0.11% Carbopol-934, 45 on 0.15% Carbopol-934, and 29 on 4.5% CMC-7L. Another 45 runs were rejected because of the reasons stated in Section VIII.

Thirteen nozzles were used. The orifice diameter ranged from 343 to 2066 microns. The pressure was varied from 125 to 1,700 psi and the flow rate from 2.65 to 68 grams/sec. The average recovery of the sprayed particles was 90.4%.

1. Drop Size Distribution

The drop size distributions were measured by using a set of nine sieves in the sieve analysis. These nine sieves were properly selected each time from a total number of 18 sieves whose designation number ran from 25 to 400 in the U.S. sieve series. The selection of the nine sieves depended upon the mean drop diameters which varied from 40 to 370 microns. The drop sizes determined by the sieve analysis were in good agreement with the square-root normal distribution. When plotted versus the square-root of drop diameters on a probability paper, the cumulative weight percentage based on square-root normal distribution would give a straight line from which the mean drop diameter and the standard deviation can be readily obtained. Three sets of experimental data plotted on probability papers are shown in Figures 14 to 16. It can be seen from these figures that the square-root normal distribution is a reasonable description of the drop size distributions over a wide range of drop sizes. The complete data of mean drop diameters and standard deviations are given in Tables V and VI of Appendix I.

In Section IV we have shown by dimensional analysis that the mean drop diameters could be correlated with the physical variables by Equation (IV-34).

$$\frac{\bar{x}}{D_2} = f\left(\frac{D_2\sqrt{P\rho}}{\mu_{app}}, \frac{D_2 P}{\sigma}, A\right) = f(Re, We, A) \qquad \text{(IV-34)}$$

In this equation, μ_{app} is the apparent viscosity of the non-Newtonian fluid. Since it is a function of shear rate, it is necessary to estimate the representative shear rate of the atomization process. From a practical point of view, the liquid disintegration by a pressure nozzle can be considered taking place right at the nozzle orifice provided that the operating pressure is sufficiently high. If this is the case, the proper shear rate can be taken as the ratio of V_{ax}/h, where V_{ax} is the axial velocity of the liquid at the orifice based on the liquid film thickness (h). Using the values of liquid film thickness calculated from the quantity, Z_m, in Table VIII of Appendix II, the proper shear rates at the nozzle orifice have been calculated for each nozzle and each extreme pressure. These values are given in Table XI of Appendix II. The calculated proper shear rate ranges from 0.59×10^5 to 7.5×10^5 per second. An average value of 2.0×10^5 (i.e. the mid-point between the two extremes on logarithmic scale) was arbitrarily chosen to be the characteristic shear rate of the atomization process.

This characteristic shear rate is well above the limit of Weissenberg Rheogoniometer. The experimental results obtained with this instrument have to be extrapolated to give the apparent viscosity at the characteristic shear rate. Since the extrapolation has to go across two logarithmic cycles, it was made to follow the general trend of the rheological curve rather than linear extrapolation. The extrapolations are

shown by the dashed lines in Figures 12 and 13. For the 4.5% CMC-7L solution, the extrapolation gave a value of 25 centipoises for apparent viscosity at the characteristic shear rate. For the 0.11% and 0.15% Carbopol-934 solutions, it gave 4.0 and 5.5 centipoises, respectively. These three solutions were used in determining drop size distributions.

In order to obtain a more general correlation, the mean drop diameters obtained from the 113 runs were combined with the 97 runs obtained by Nelson [N-1] for organic fluids. By so doing, a wide range of Reynolds and Weber numbers could be covered. The reason that we could pool these data together is because they were obtained in very similar conditions. The water data obtained in 13 runs by Nelson were not included because they were not in agreement with the bulk of the organic data. By a careful searching for the best fit line on a log-log plot, we were able to correlate the mean drop diameters for the totality of 210 runs by the following simple equation,

$$Y = 0.60X + 1.40 \qquad \text{(VII-1)}$$

where

$$Y = \log_{10}\left[\frac{\bar{x}}{D_2}\right]$$

$$X = \log_{10}\left[Re^{0.40}\, We^{0.52}\, A^{0.30}\right]$$

The correlation is shown in Figure 17. The average deviation of the drop diameters about the straight line was 12.76%. Considering the wide ranges covered by the physical variables and the simple method of estimating the apparent viscosities of non-Newtonian fluids, this correlation could be considered as rather satisfactory. The numerical calculations are summarized in Tables V and VI of Appendix I.

The correlation given by Equation (VII-1) had been checked by using a

regression program on an IBM-360 computer. The regression analysis gave a slightly different equation with the sum of the squares of residuals being equal to 0.0609 and the standard error of estimates being equal to 0.0172. For Equation (VII-1), the sum of the residuals was 0.0768 and the standard error of estimate was 0.0194. The differences were not significant. Equation (VII-1) was preferred because the experimental points were more uniformly distributed about the equation line.

The physical properties of the eleven fluids included in the correlation are given in Table IV.

TABLE IV - PHYSICAL PROPERTIES OF FLUIDS AT 75°F

Fluid		Viscosity (cp)	Density (g/cm^3)	Surface Tension (dynes/cm)
Carbopol-934	0.11% Sol.	4.0*	0.997	72.0
Carbopol-934	0.15% Sol.	5.5*	0.997	72.0
CMC-7L	4.5% Sol.	25.0*	1.013	72.0
Water		0.89	0.997	72.0
Glycerine	76% Sol.	31.0	1.200	67.5
Aniline		3.70	1.017	42.3
Nitrobenzene		1.84	1.198	43.3
Cyclohexane		0.88	0.774	24.5
N-Octyl alcohol		7.83	0.820	27.0
Carbon tetrachloride		0.90	1.585	26.2
1,1,2,2-Tetrabromoethane		8.29	2.950	49.0

*Estimated apparent viscosity at $\sigma = 2 \times 10^5$ sec.$^{-1}$

In Table IV the surface tension of each polymer solution has been checked by using a capillary glass tubing of 0.33 mm in capillary diameter. The elevation of each polymer solution was found to be the same as that of water, which was 8.9 cm at 75°F. However, the time rate for the polymer solutions to reach the equilibrium elevation was quite slow due to the high viscosities at low shear rates.

2. Correlation of Mean Drop Sizes With Boundary Layer Thickness

From Equation (IV-28) we can see that the mean drop diameter obtained from the fan-spray nozzles is a function of the parameter, k_o, which is related to the thickness of the liquid sheet. In other words, the mean drop diameter is a function of the liquid sheet thickness. In our case of swirl-type pressure nozzles, the liquid sheet thickness is the film thickness at the nozzle orifice since the central portion of the orifice is occupied by the air core. The film thickness is determined by the flow behavior inside the swirl chamber.

Taylor [T-6] suggested that the fluid flow inside the swirl chamber could be represented by a free vortex and that the transport of the fluid toward the orifice was by way of a boundary layer along the wall surface of the swirl chamber. Based upon this model he performed an analysis for the laminar boundary layer growth of a Newtonian fluid by solving the boundary-layer equations of motion using momentum integral method. Numerical calculations for the boundary layer thickness were tabulated. In Appendix III, we have extended Taylor's analysis to include the simple non-Newtonian fluids whose constitutive equations could be represented by the Power Law Model.

By assuming that the mean drop size was a function of the boundary layer thickness, we have attempted to seek a correlation between these two quantities. The correlation could be represented satisfactorily by the following equation for both Newtonian and non-Newtonian fluids,

$$Y = 0.671X - 0.433 \qquad \text{(VII-2)}$$

where

$$Y = \log_{10}(\delta)$$

$$X = \log_{10} \left[(\bar{x}) \, (Re)^{-0.436} \, (We)^{0.258} \, (A)^{-0.339} \right]$$

δ = boundary layer thickness (microns)

$\bar{x}$ = volumetric mean drop diameter (microns)

The correlation is shown in Figure 18. The average deviation of the experimental points about the equation line was 11.87%. The numerical calculations are summarized in Tables XIII and XIV of Appendix III.

3. Standard Deviation Correlation

The standard deviation measured from the straight line of cumulative weight percentage on a probability paper has the dimension of square-root of a micron. Therefore, it is more convenient to use $s/\sqrt{D_2}$ in the correlation. Since the experimental values of $s/\sqrt{D_2}$ covered only a small range, it would be better to stretch the ratio of $s/\sqrt{D_2}$ in order to get a more meaningful correlation. This could be accomplished by multiplying $s/\sqrt{D_2}$ by another dimensionless group, say the Weber number as was used by Nelson [N-1]. Then the correlation for standard deviations could be represented by the following equation,

$$Y = 0.071 \, X^2 - 0.211 \, X + 1.062 \qquad \text{(VII-3)}$$

where

$$Y = \log_{10} \left[\frac{s}{\sqrt{D_2}} \, We^{0.5} \right]$$

$$X = \log_{10} \left[Re^{-0.671} \, We^{1.296} \right]$$

The correlation is shown in Figure 19. The average deviation from the equation line was 10.84%.

The experimental results indicated a relation between $\bar{x}$ and s. A plot of s versus $\bar{x}$ is shown in Figure 20. The standard deviations were approximately correlated with the mean drop sizes by the following equation.

$$s = 0.076\ (\bar{x})^{0.72} \qquad \text{(VII-4)}$$

where

s = square-root standard deviation $(\text{microns})^{1/2}$

$\bar{x}$ = volumetric mean drop diameter (microns)

A similar equation for pneumatic atomizers was reported by Gretzinger and Marshall [G-2].

SECTION VIII - DISCUSSION

1. Comparison of the Experimental Results with Previous Works on Grooved-Core Swirl Nozzles

For the purpose of comparing the experimental results with previous works described in Section II, we write the correlation for mean drop size (Equation VII-1) and its equivalent forms in the following:

$$Y = -0.60Z + 1.40 \qquad \text{(VII-1)}$$

$$\frac{\bar{x}}{D_2} = 25.1\ Re^{-0.24}\ We^{-0.312}\ A^{-0.18} \qquad \text{(VII-1a)}$$

$$\bar{x} = 25.1\ D_2^{-0.552}\ P^{-0.432}\ \mu^{0.24}\ \rho^{-0.12}\ \sigma^{0.312}\ A^{-0.18} \qquad \text{(VII-1b)}$$

where

$$Y = \log_{10}\left[\frac{\bar{x}}{D_2}\right]$$

$$X = \log_{10}\left[Re^{0.40}\ We^{0.52}\ A^{0.30}\right]$$

$$Re = \frac{D_2\sqrt{P\rho}}{\mu}$$

$$We = \frac{D_2 P}{\sigma}$$

First, we notice that the experimental results are in agreement with those obtained by Nelson [N-1] for organic fluids, since we have seen in Section VII that the results of the two independent studies can be correlated by the same equations. In Nelson's correlations the average axial velocity based upon the liquid film thickness and the spray cone angle are chosen as the dynamic and the nozzle size parameters. In this work, the total pressure and the area factor A are chosen as the corresponding parameters. The fact that we are able to obtain the drop size correlations indicates that the use of pressure and the parameter A in correlation

is as valid as the use of axial velocity and spray cone angle. The mean deviation for the mean drop size correlation (Equation VII-1) is 12.85% as compared to 8.25% for Equation (II-7) obtained by Nelson. An inspection on Nelson's plot of mean drop size for organic fluids indicates that the main portion of the data can be represented by the following equation:

$$Y = -0.54Z + 1.2 \qquad \text{(VIII-1)}$$

where

$$Y = \log_{10}\left[\frac{\bar{x}}{D_2}\right]$$

$$X = \log_{10}\left[Re^{0.45}\, We^{0.55}\, (\tan\frac{\theta}{2})^{1.2}\right]$$

$$Re = \frac{D_2 V_{ax} \rho}{\mu}$$

$$We = \frac{D_2 V_{ax}^2 \rho}{\sigma}$$

The values for Y calculated from Equation (VII-1) and Equation (VIII-1) for a given value of Z are within 9% of each other. Therefore, it can be stated that the two different sets of the dynamic and nozzle size parameters lead to essentially the same numerical equation. A comparison between the correlations for standard deviations (Equations VII-3 and II-9) reveals that they are within 12% of each other. The mean deviation for Equation (VII-3) is 10.84% as compared to 13.0% for Equation (II-9).

In order to compare the experimental results obtained by Turner and Moulton [T-8], we transformed their correlation (Equation II-1) into the following form by using Equations (III-1) and (III-2) on the assumption that Equation (III-2) is valid for the spray nozzles that were used.

$$\bar{x} = 30.8\, D_2^{-0.36}\, P^{-0.11}\, \mu^{0.16}\, \rho^{-0.11}\, \sigma^{0.71}\, A^{0.20} \qquad \text{(II-1a)}$$

Comparing Equation (II-1a) with Equation (VII-1b), we see that the constant coefficient and the exponential indexes for μ and ρ are close, while the indexes for D_2, σ, and A are quite different. The discrepancies are mostly due to the narrow ranges covered by the physical variables in Equation (II-1). We should also notice that the difference in experimental conditions could be an important factor in causing the discrepancies.

It is difficult to compare with the correlation of Tate and Marshall [T-3] as represented by Equation (II-3). Since only water was used and only twelve experimental observations were made in obtaining the correlation, its reliability is certainly less than Equation (VII-2) from a statistical viewpoint.

Darnell's data of mean drop size for water are represented by either Equation (II-4) or Equation (II-7). The latter was obtained by Nelson as we have described in Section II. Since the mean drop sizes obtained by Darnell have been found to be larger than those obtained by Nelson for organic fluids, it is certain that either Equation (II-4) or Equation (II-7) will predict a larger mean drop size than Equation (VII-1). However, Darnell's data were based on the samples taken at a distance of ten inches below the orifice. His observation that the samples taken at the ten inch distance were coarser than at the five inch distance probably explains the discrepancies between the water and organic data. The cause of the difference in mean drop size at the two distances below the orifice is most likely due to the coalescence of the initially formed drops. In the freezing method, the coalescence is essentially suppressed, and, therefore, the mean drop size should be smaller than those observed by Darnell.

2. Comparison with Theoretical Analyses

In Section IV we have reviewed the theoretical analyses for liquid

disintegrations. Both Equation (IV-23) and Equation (IV-26) indicate that the mean drop diameter is proportional to $\sigma^{1/3}$ or $We^{1/3}$. Other theoretical considerations made by Holdroyd [H-11] for liquid jet and by Keller and Kolodner [K-1] for liquid sheet under unbalanced pressures also yielded the same dependence of mean drop size on a properly defined Weber number. In this respect, the correlation represented by Equation (VII-1a) is in good agreement with the theoretical results.

3. Comparison with Correlations for Fan-Spray Nozzles

In both fan-spray and swirl-type nozzles, the spray drops are produced from the breakup of a liquid sheet. Therefore, there should exist some similarities between the correlations for the two types of nozzles.

According to Equation (IV-28), $\bar{x} \sim P^{-1/3} \sigma^{1/3} \rho^{1/6}$, while Equation (VII-1b) shows that $\bar{x} \sim P^{-0.432} \sigma^{0.312} \rho^{-0.12}$. The faster decrease of $\bar{x}$ with increasing pressures is obviously due to the more efficient use of pressure in the swirl-type nozzles. The existence of the air core generated by the tangential component of the velocity in the orifice constitutes the difference. The dependence of $\bar{x}$ on σ is almost the same. The reason for the different effect of density on $\bar{x}$ is not clear.

The effect of viscosity on $\bar{x}$ for fan-spray nozzles has been studied experimentally by Hasson and Mizrahi [H-4] using molten wax. According to their results, $\bar{x} \sim \mu^{1/6}$. This is also comparable with Equation (VII-1b).

4. Justification of Using the Extrapolated Apparent Viscosities

In order to test the extrapolated values of apparent viscosities at the characteristic shear rates, the spray cone angles of the 4.5% CMC-7L and 0.15% Carbopol-934 solutions were measured by photographic method. They are plotted versus the Reynolds number in Figure 11. The experimental points lie close to the curve determined from the glycerin solution which has a constant viscosity of 24 centipoises. This seems to indicate that the

apparent viscosities obtained by extrapolation of the rheological measurements are reasonable.

5. Alternative Methods of Correlating the Drop Size Distributions

Instead of using pressure as the dynamic variable in the drop size correlation, it should be equally possible to use the average axial velocity at the orifice based on liquid film thickness, as was done by the previous workers. However, this would necessitate the measuring of the liquid film thickness as a function of Reynolds number since the film thickness is not constant at the low Reynolds number region. If a superficial velocity based on either orifice area or the inlet flow area is used, we have found that the correlation cannot be achieved for low Reynolds numbers unless one additional factor of nozzle characteristics is included. This factor can be the spray cone angle or the discharge coefficient. While at high Reynolds numbers the axial and the tangential velocities should bear a definite ratio and hence the spray cone angle is constant, at low Reynolds numbers the spray cone is gradually diminishing with decreasing pressures. The fact that the correlation based on the pressure is able to hold for both high and low Reynolds numbers seems to indicate that it is the total energy of the fluid that is responsible for atomization. It also indicates that the breakup mechanism of the liquid sheet in both high and low Reynolds number region is probably the same, although at low Reynolds numbers the spray cone angle is not fully developed and hence the liquid film is much thicker.

6. Discussion on Experiments

(1) Reasons for Rejecting Unaccepted Runs - Forty-five unaccepted runs were rejected because of the following reasons:

(a) Recovery was below 60% because some spray drops stuck to

the wall surface of the cold chamber. This was mainly caused by an insufficient liquid nitrogen flow rate.

(b) Some spray drops flew outside the collecting sieves. They were recovered together with the fine drops that were wet-screened through all the sieves. As a result, abnormal distributions were obtained.

(c) Caking or agglomeration of the spray drops happened, usually in the top sieve.

(d) Drop sizes obtained from a run at a higher pressure were larger than those at a lower pressure. This could be due to either a corroded nozzle orifice or insufficient flow rate of liquid nitrogen.

(e) Mistakes in experimental procedures occurred.

(2) Dependability of Sieve Analysis - The dependability of sieve analysis relies upon the accuracy of the individual sieves and upon the sufficiency of the sieve shaker. The three finest sieves numbered 270, 325 and 400 were not so reliable in accuracy as the other sieves because the delicate sieve cloth became much less tightly stretched after several times of use. However, the mean drop diameters were not so sensitive to the sieve accuracies as the standard deviations.

In order to know the sufficiency of the sieve shaker, several pictures were taken of the spray drops in a few sieves. Enlarged photographs (Figure 6) clearly revealed that the spray drops in a given sieve were quite uniform in size and spherical in shape and that no drops smaller than the sieve openings were remaining in the sieve.

(3) Shattering or Coalescence of Spray Drops - The shattering or secondary atomization of the very initial drops by air friction is very difficult to control. In view of what we have discussed in the disintegration mechanism of a liquid drop, it appears that secondary atomization is not an important factor in drop size distribution for pressure nozzles, since the initially formed drops are de-accelerated instead of being accelerated by the ambient gas. However, the shatter of the frozen drops due to their collision with the wall surface of the collecting chamber should be eliminated. Enlarged photo pictures revealed no existence of fractured drops. The coalescence of the spray drops can be minimized by using a high flow rate of liquid nitrogen. When the liquid nitrogen flow rate is not sufficient, the mean drop size and the standard deviation could be larger than those obtained at a lower pressure. This clearly shows that if the heat transfer rate is not high enough, coalescence of the drops definitely happens. This is in agreement with Darnell's observation that the spray drops collected at ten inches below the orifice are larger than those collected at five inches below.

(4) Effect of Ambient Pressure - It has been observed in many studies on fan-spray nozzles that the mean drop size is inversely proportional to the 1/6 power of the ambient gas pressure in agreement with Equation (IV-23). When the ambient pressure is two atmospheres, the mean drop size would be 12% less. Since the collecting system used in the present work is virtually a closed one, it is necessary to release the pressure built up by the

vaporization of liquid nitrogen prior to the introduction of the sprays into the cold chamber. The pressure is released through a vent hole near the bottom of the lower chamber so that the pressure inside the collecting chambers is atmospheric when the spray is injected in. The effect of ambient pressure on mean drop size has been discussed extensively by Dombrowski and Hooper [D-5].

SECTION IX - CONCLUSIONS

The results of the present study can be summarized as follows:

1. The performance characteristics of grooved-core swirl nozzles, namely, the discharge coefficient, the air core diameter, and the spray cone angle, are solely determined by the parameter A at high Reynolds numbers. The parameter A is defined as the ratio of the orifice area to the total flow area of the grooved slots.

2. The drop size distributions for grooved-core swirl nozzles can be correlated by using the total pressure and the parameter A as the dynamic and the nozzle size variables, respectively. The use of these two variables in correlation is adequate for drop size distributions obtained at both high and low Reynolds numbers.

3. The drop size distributions for the dilute aqueous polymer solutions which are simple non-Newtonian fluids can be correlated together with Newtonian fluids by choosing proper values for the apparent viscosities at the characteristic shear rate of 2.0×10^5 per second.

4. The drop size distributions of both non-Newtonian and Newtonian fluids for grooved-core swirl nozzles can be adequately described by the square-root normal distribution over the wide range of 40 to 370 microns in mean drop diameters.

5. The drop size distributions obtained in the present study are in agreement with those previously obtained by Nelson [N-1] for organic fluids. The experimental results of the two independent studies covering eleven fluids of widely varying physical properties can be correlated by the same Equations (VII-1, VII-3, and VII-4).

6. The present experimental study has invaded considerably into the low Reynolds number region where the spray cone is not fully developed and the

liquid film thickness is much thicker. The fact that the correlation based on pressure is able to hold for both high and low Reynolds numbers strongly suggests that it is the total energy of the fluid that is responsible for atomization and that the breakup mechanism is basically the same irrespective of the spray cone angle and the liquid film thickness.

7. The correlation of mean drop size for grooved-core swirl nozzles is in fair agreement with the correlation for fan-spray nozzles. This indicates that the breakup mechanism for both types of nozzles are similar. The instabilities of the liquid sheets are most likely due to the amplitude growths of the initial disturbances.

8. The mean drop size can be correlated satisfactorily with the boundary layer thickness of the fluid at the nozzle orifice. In most cases, the ratio of the boundary layer thickness to the mean drop size is close to unity. This perhaps furnishes some evidences to the original concept of Taylor [T-6] that the transport of the fluid in the swirl chamber toward the orifice is by means of the boundary layer.

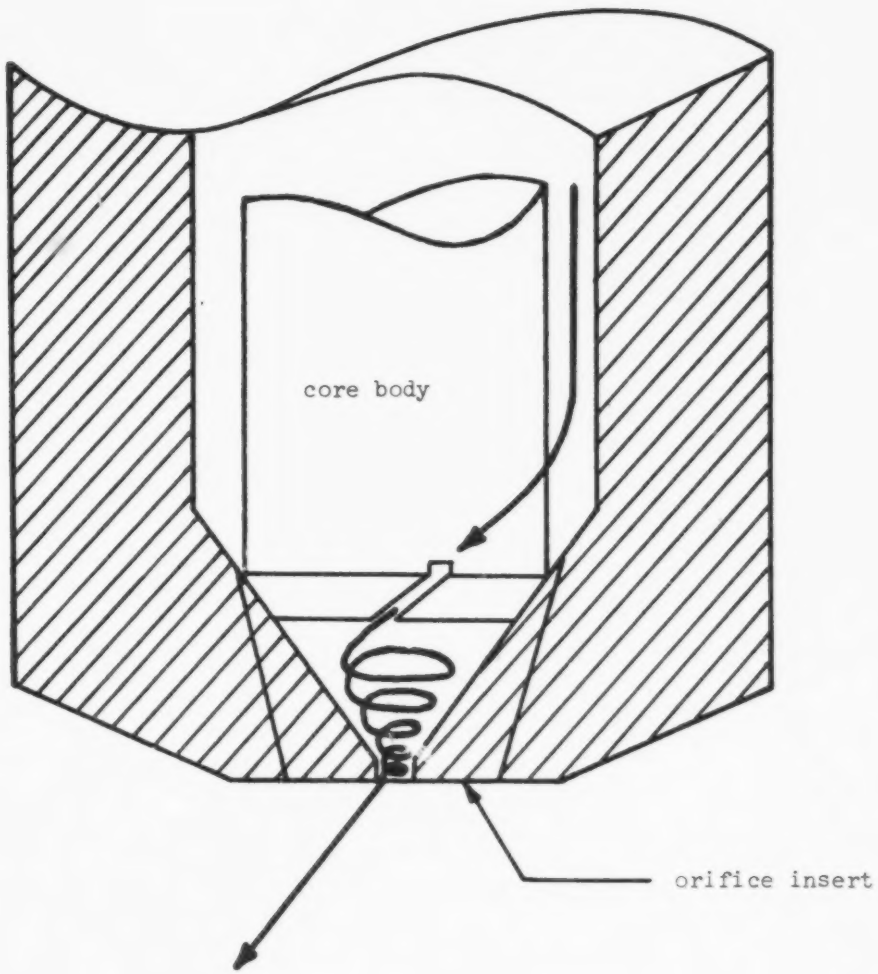

Figure 1 - Diagram of the Grooved-Core Swirl Nozzle

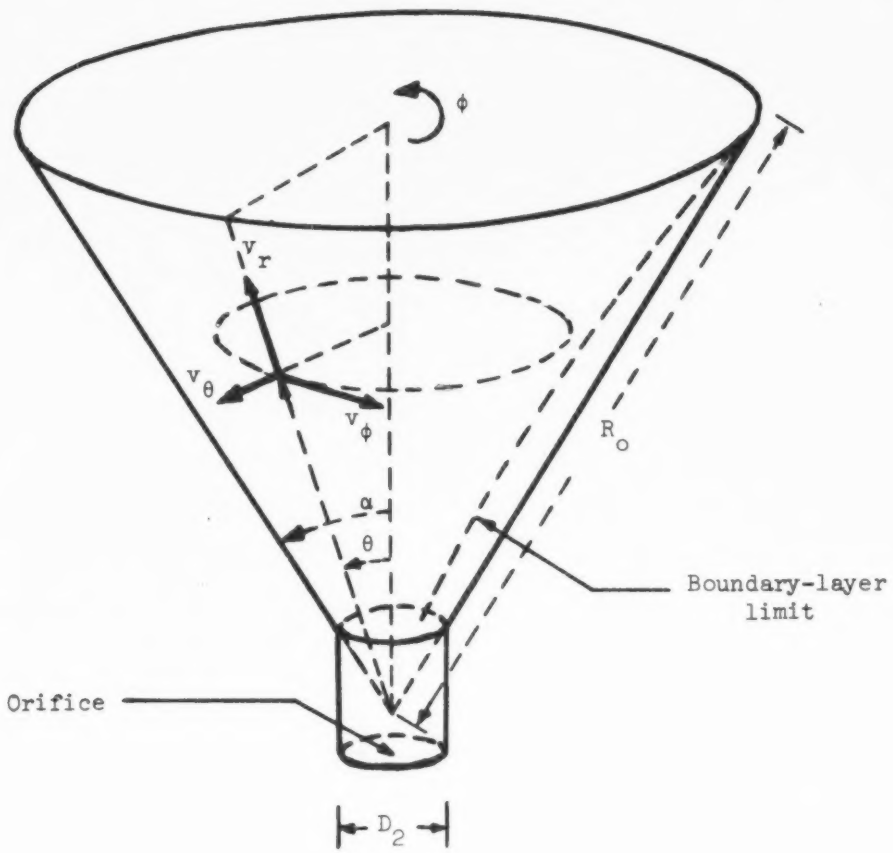

Figure 2 - Coordinate System for Boundary-Layer Analysis

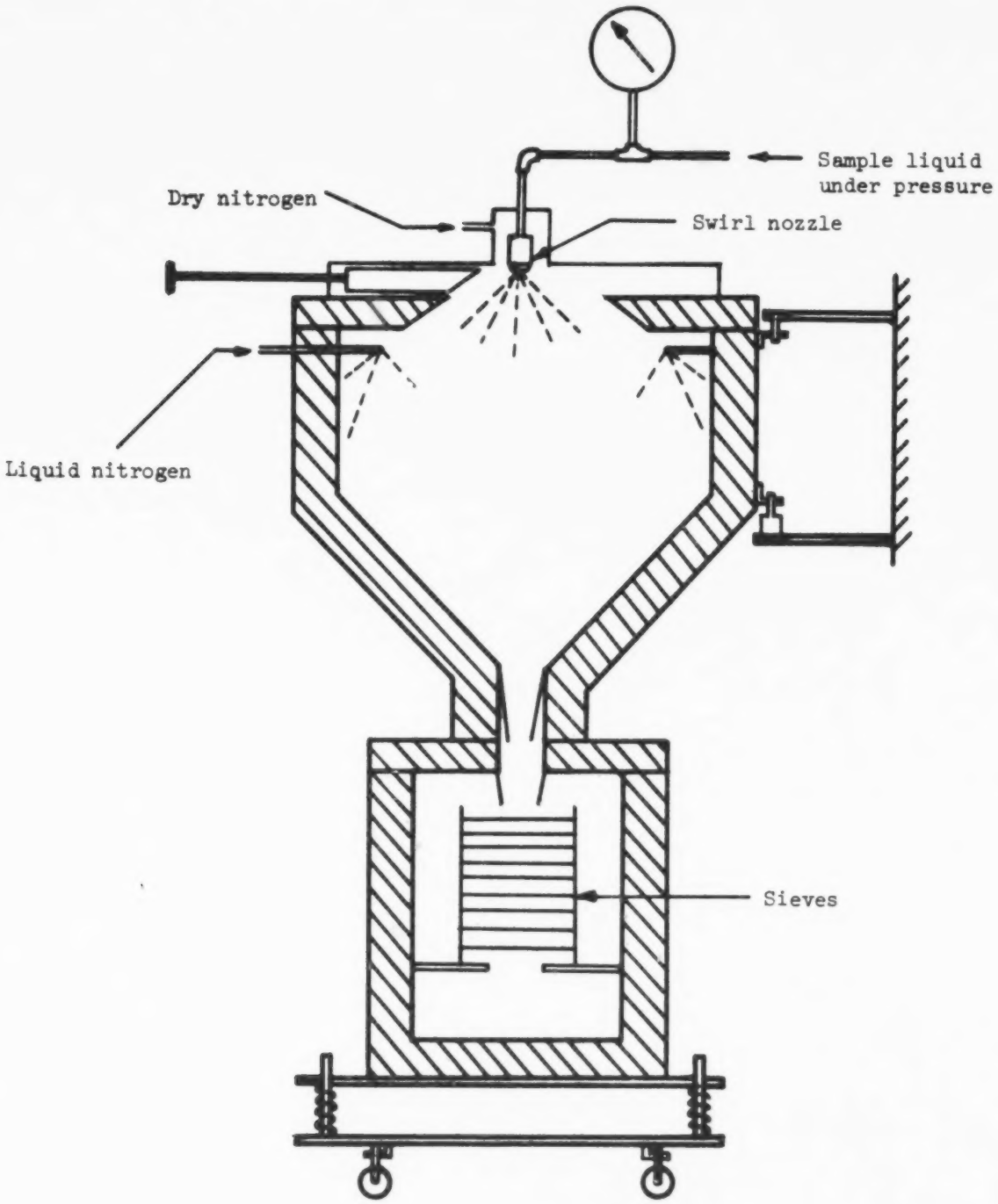

Figure 3 - Diagram of the Spray Collector

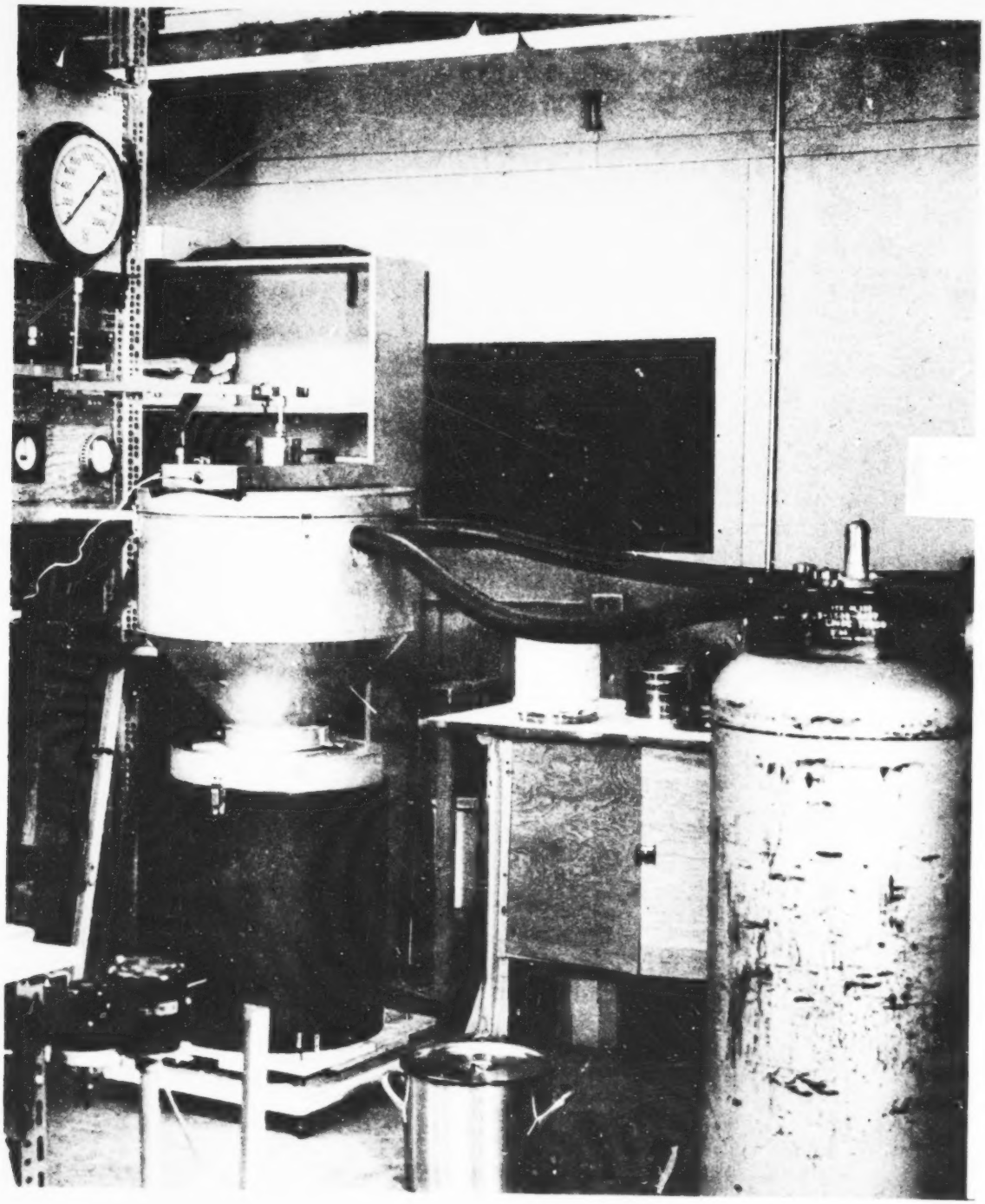

Figure 4 - Photograph of the Equipment

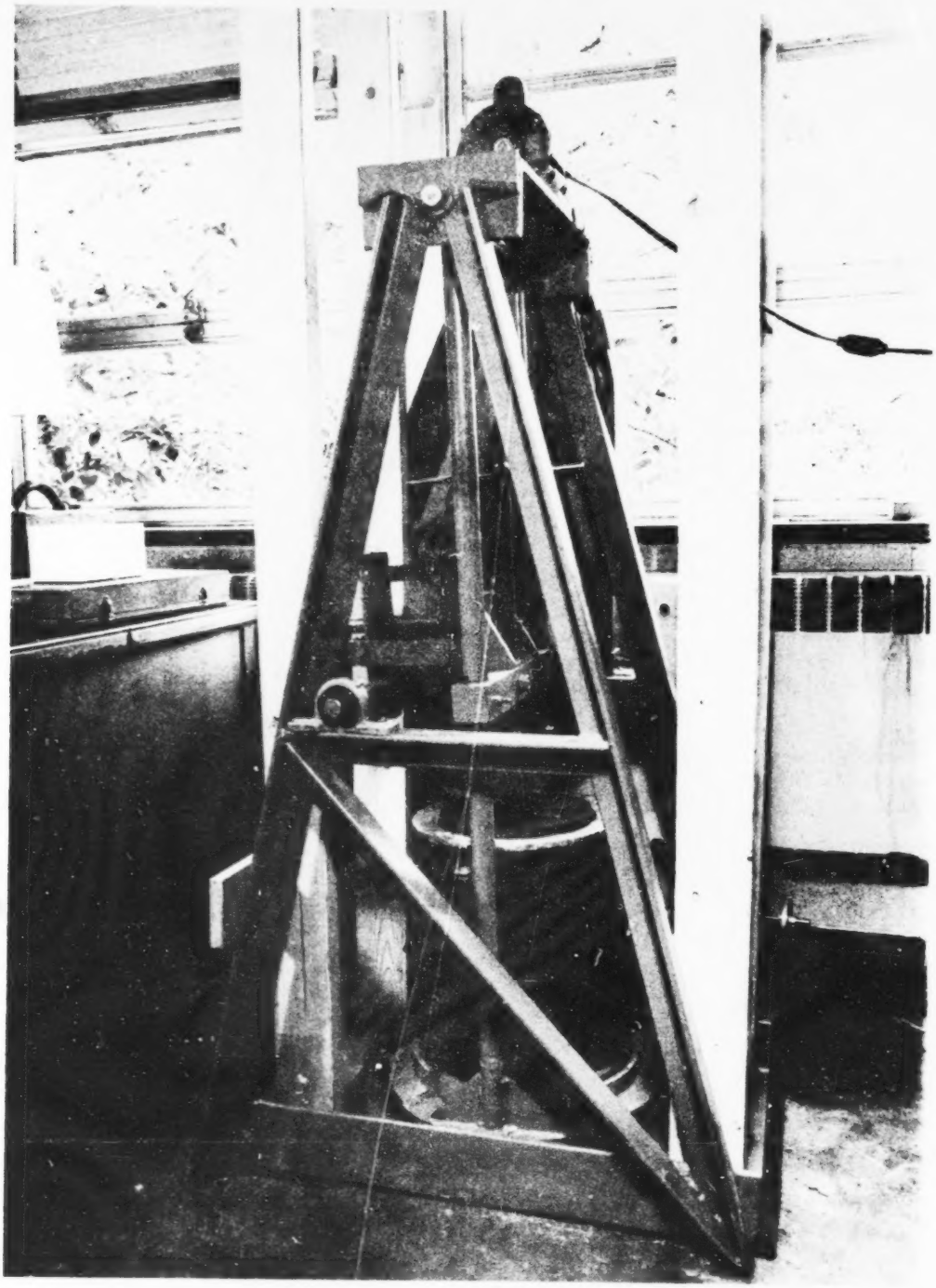

Figure 5 - Photograph of the Sieve Shaker

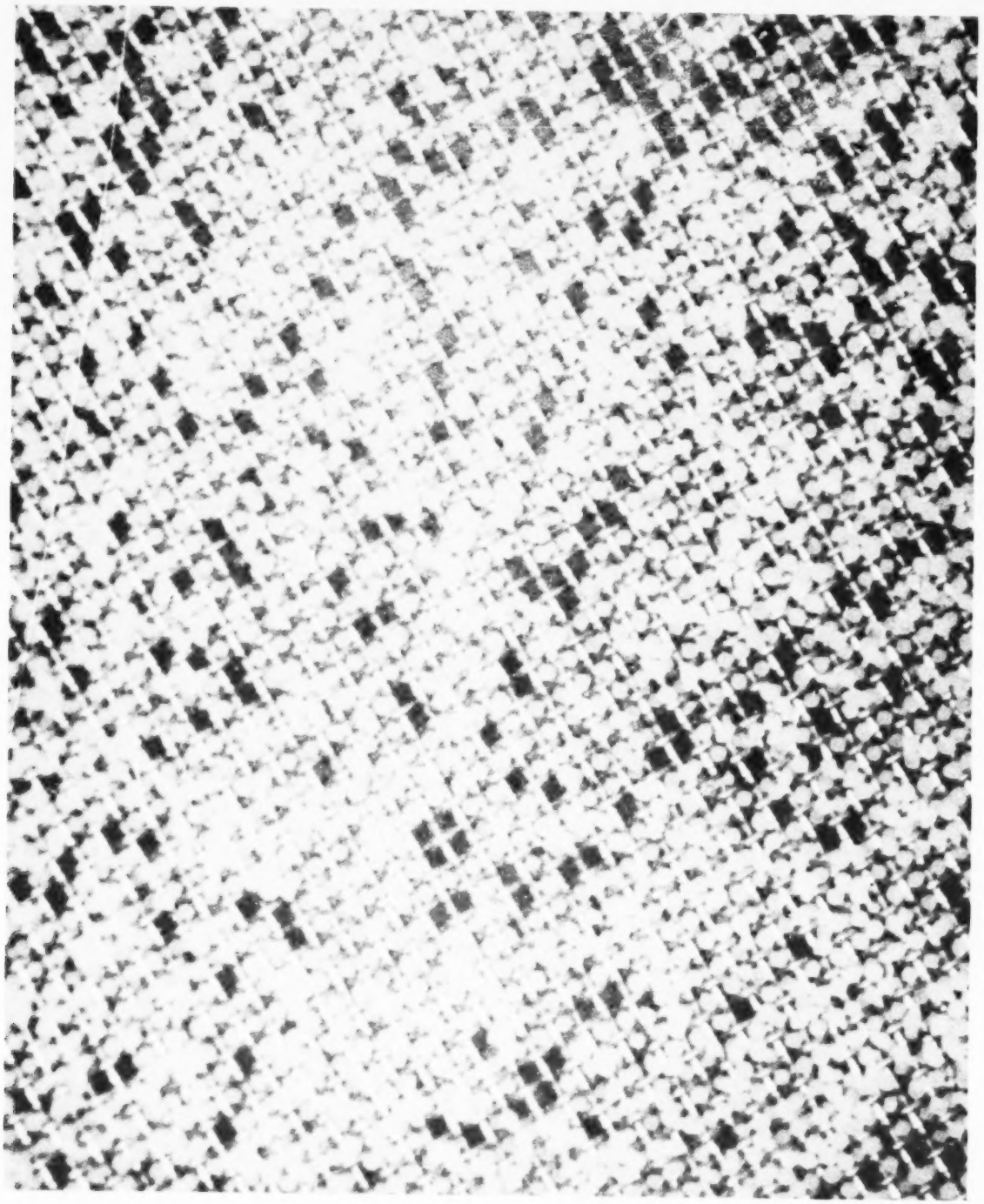

Figure 6 - Photograph of the Spray Drops

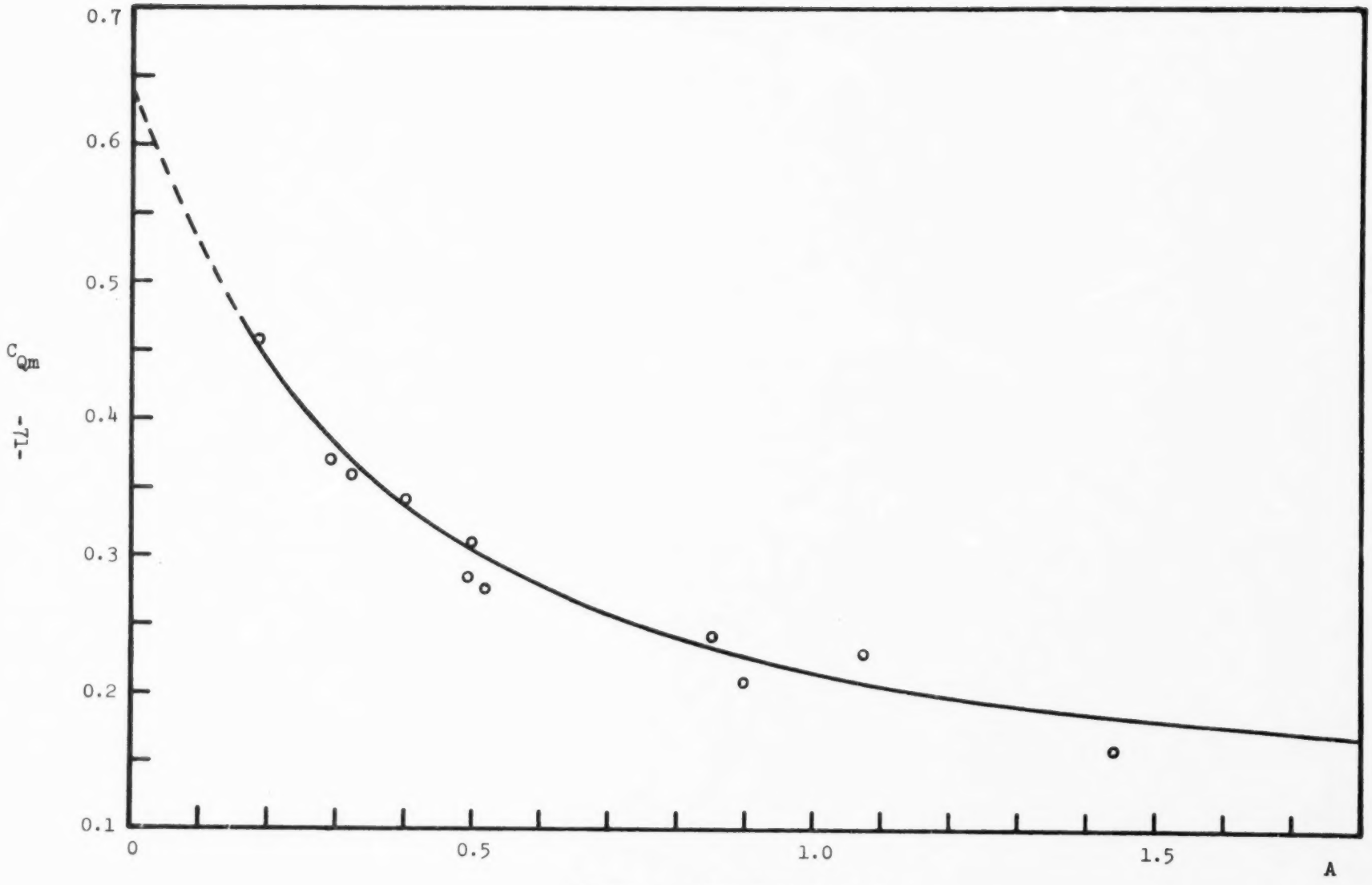

Figure 7 - Correlation of C_{Qm}

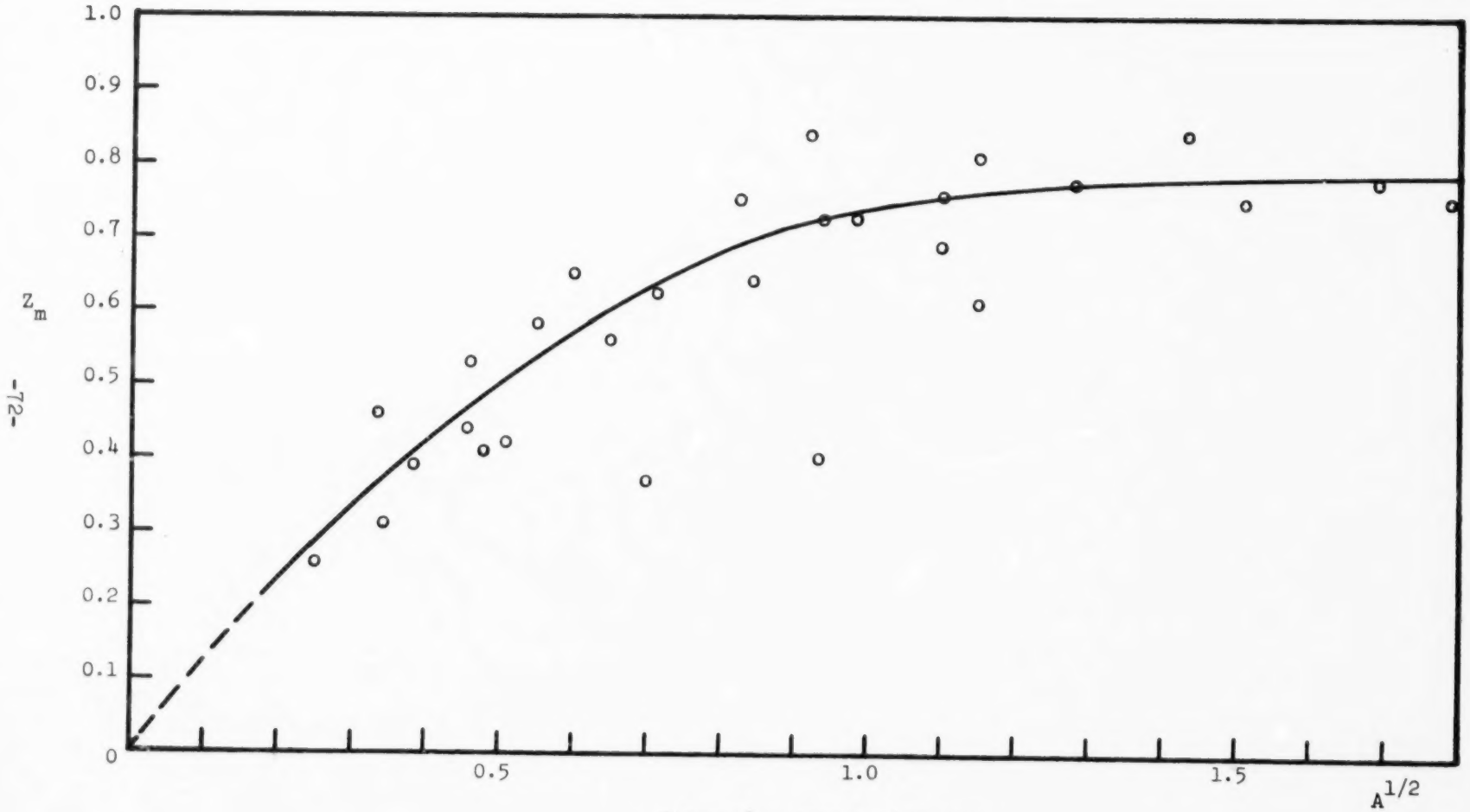

Figure 8 - Correlation of Z_m

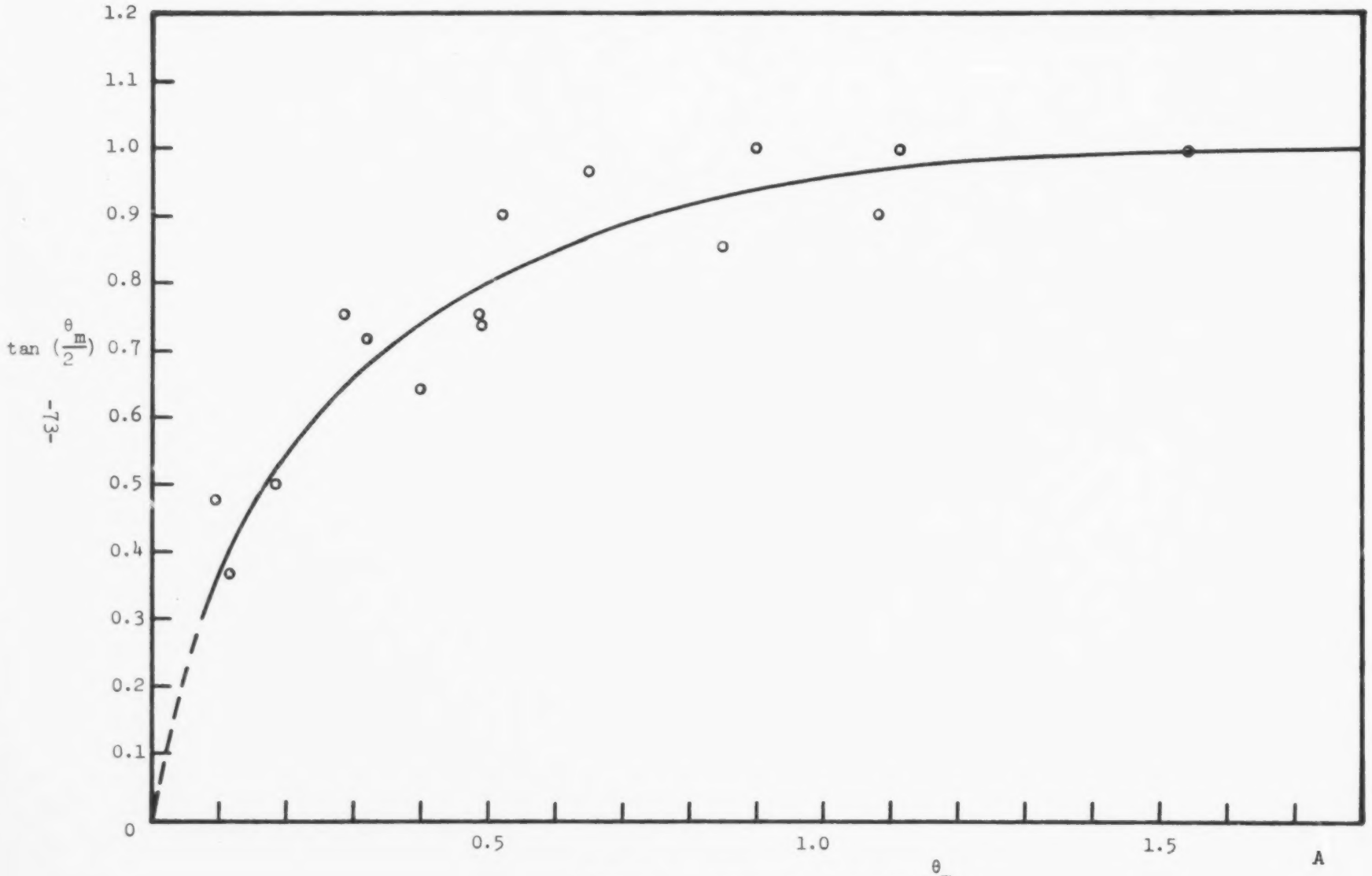

Figure 9 - Correlation of tan $(\frac{\theta_m}{2})$

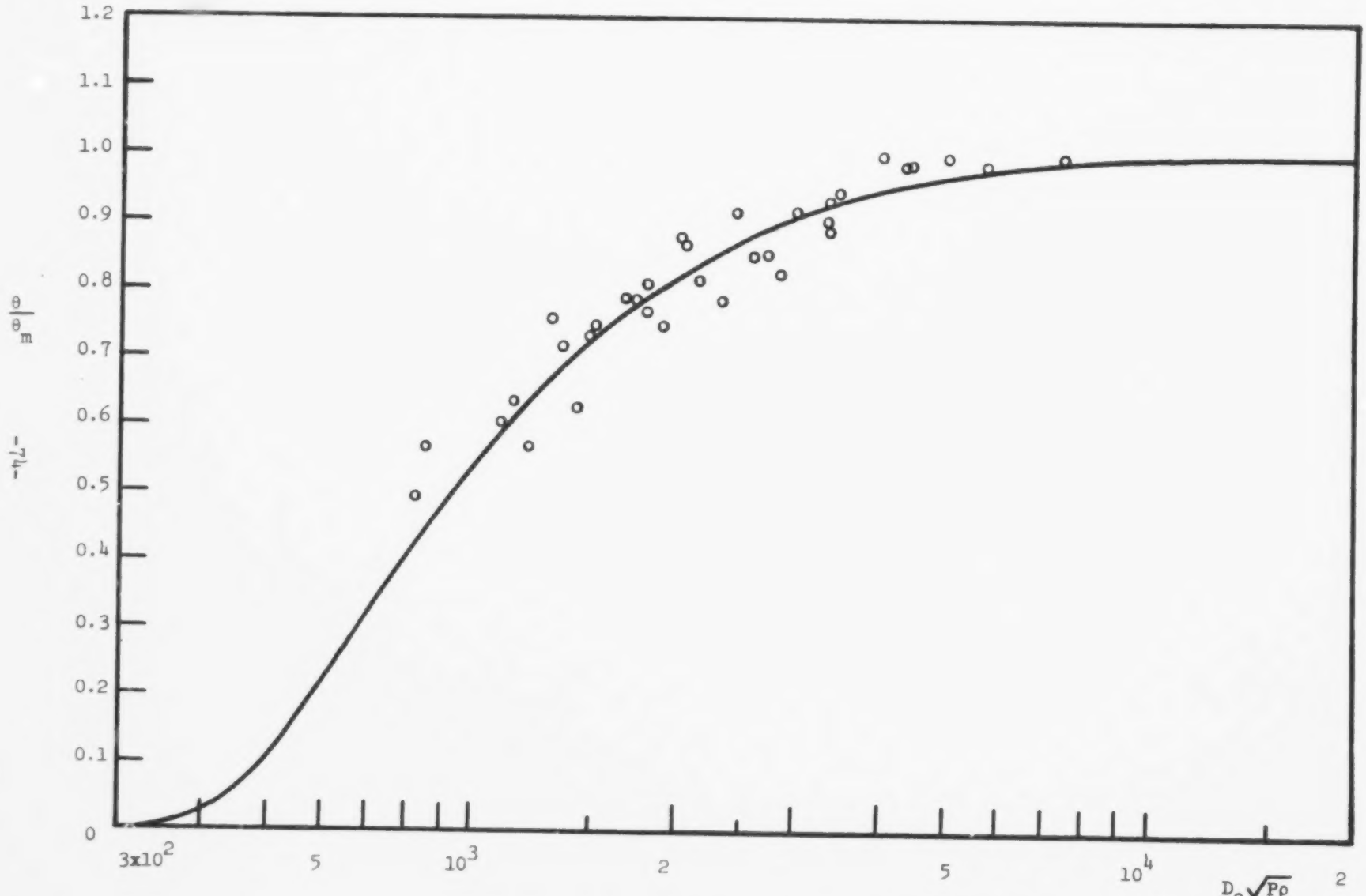

Figure 10 - Correlation of θ/θ_m for Glycerine Solution

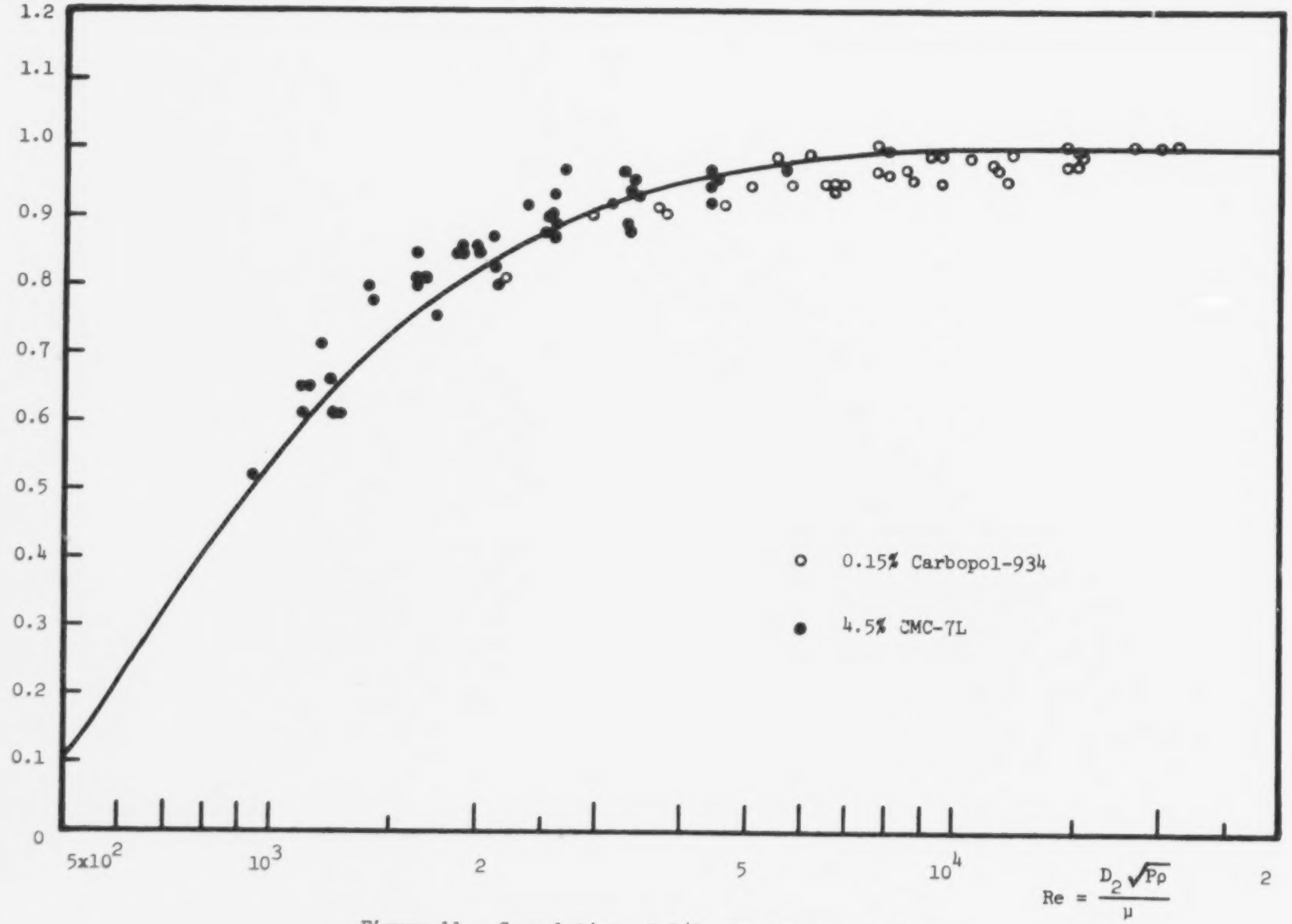

Figure 11 - Correlation of θ/θ_m for Polymer Solution

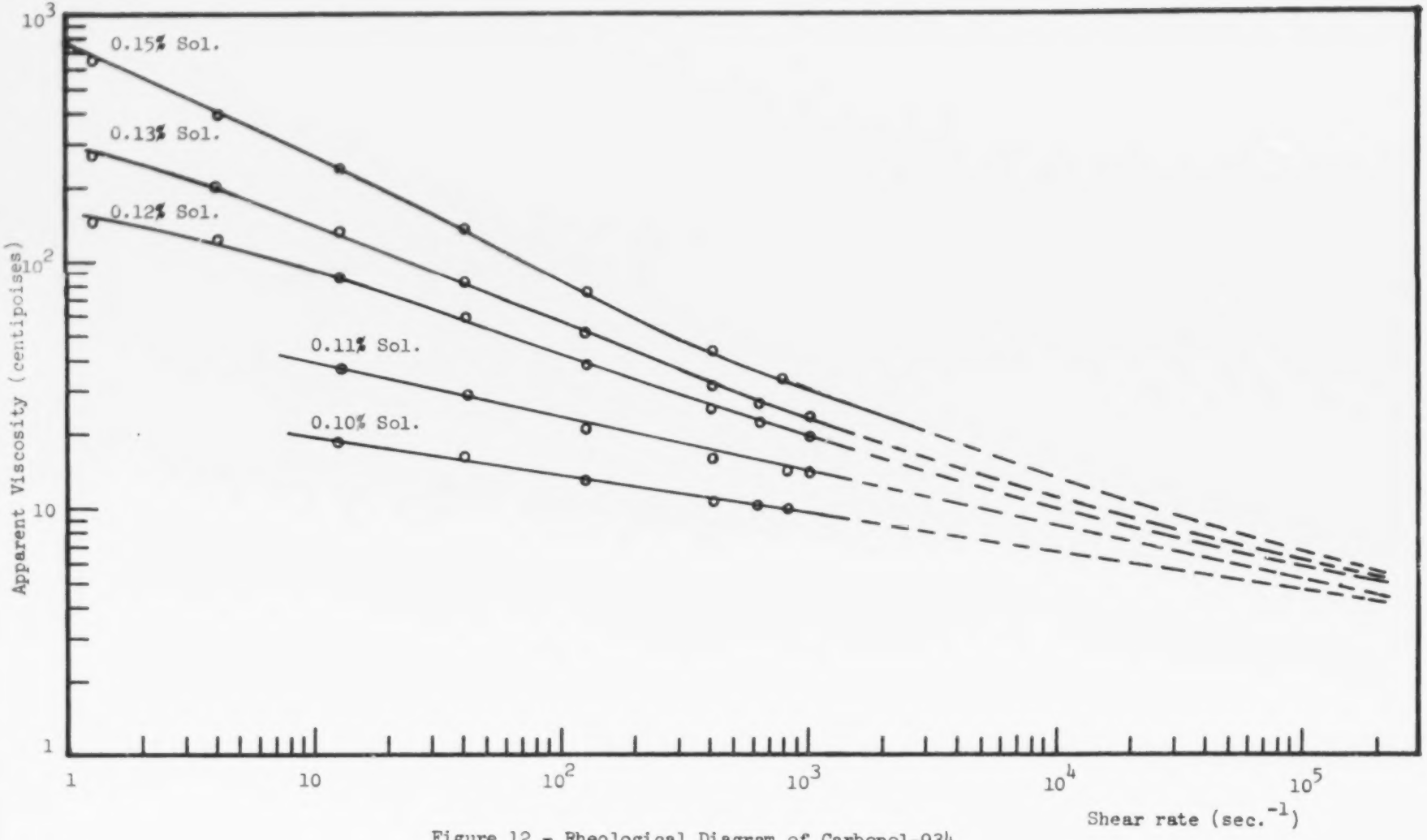

Figure 12 - Rheological Diagram of Carbopol-934

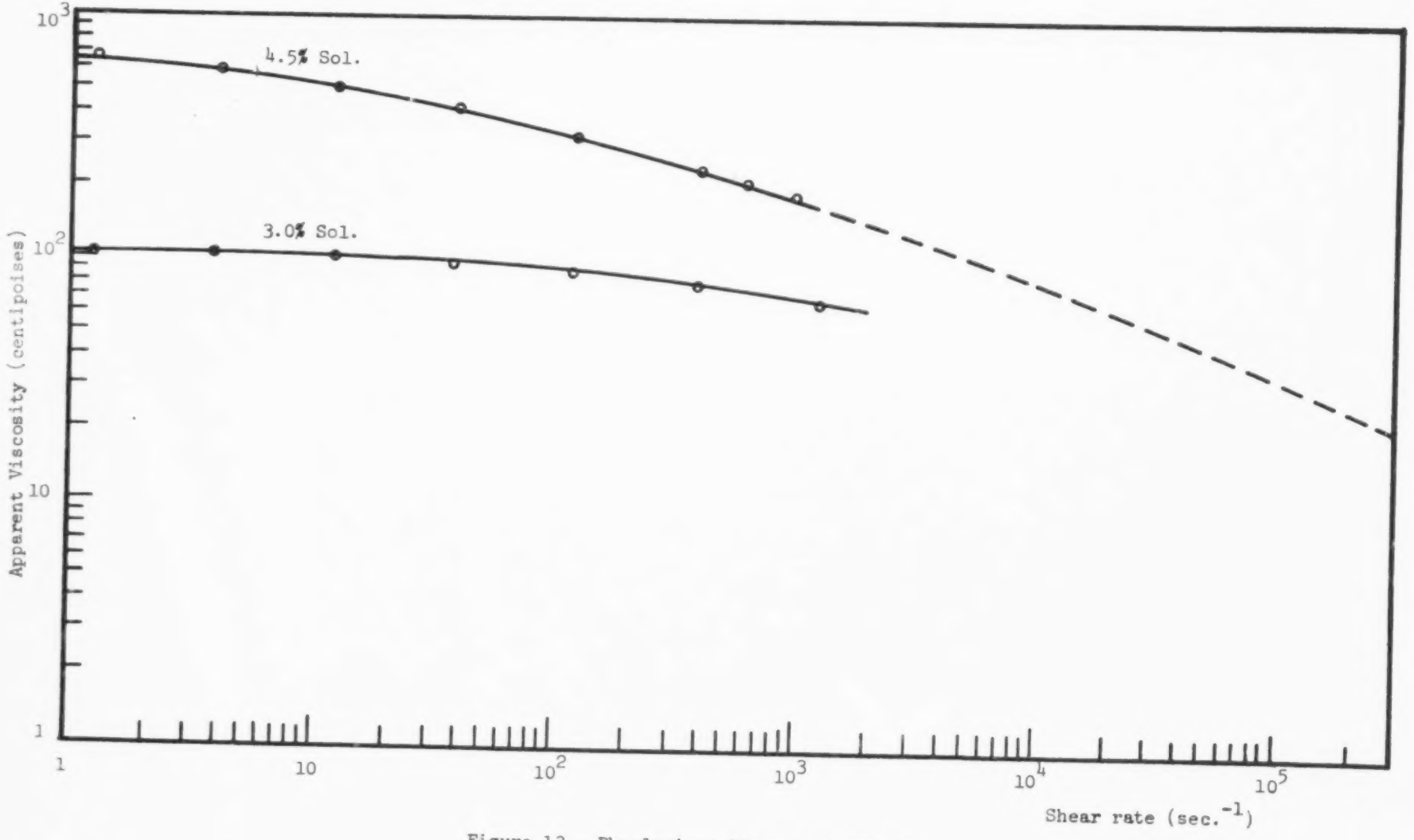

Figure 13 - Rheological Diagram of CMC-7L

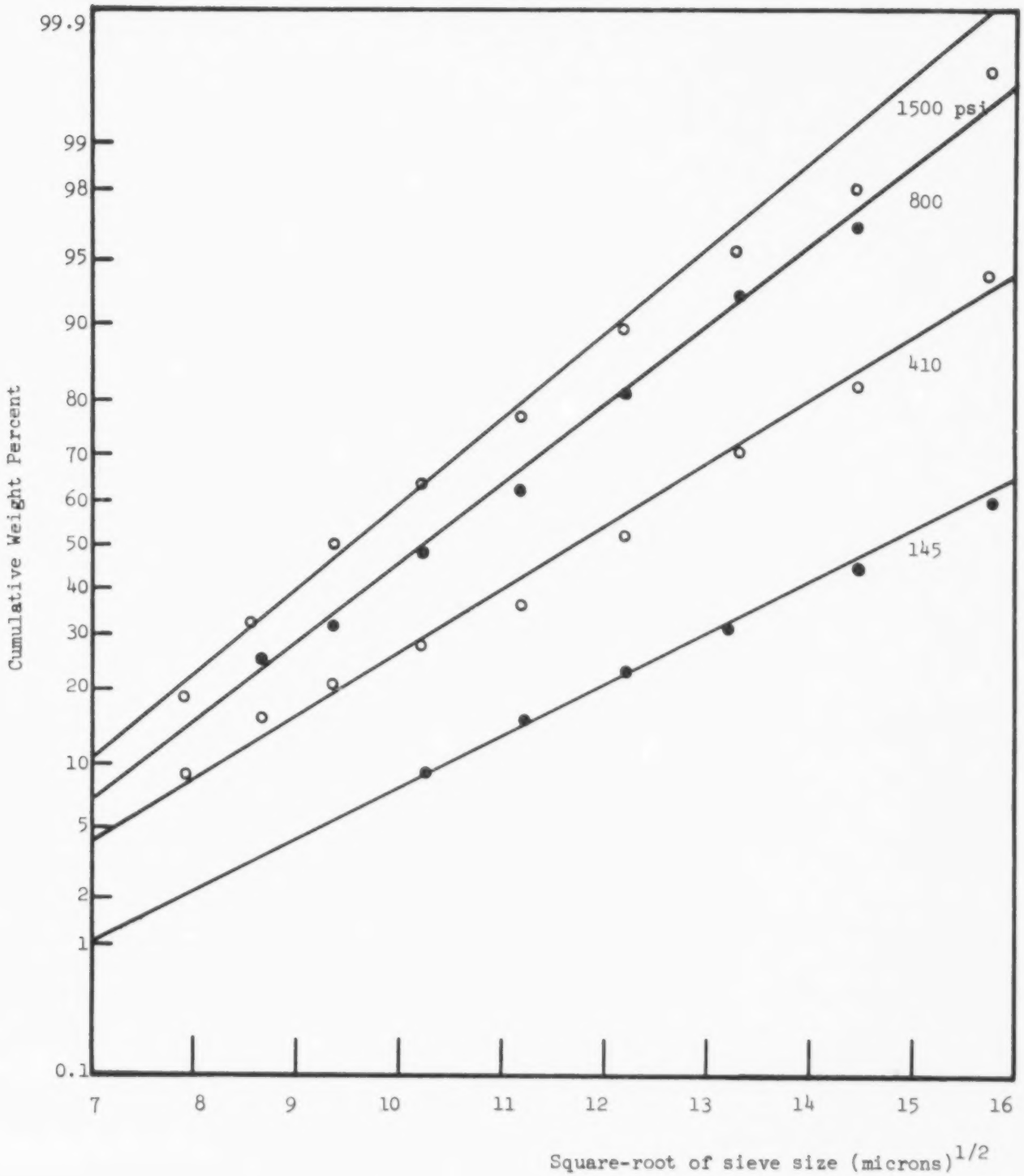

Figure 14 - Drop Size Distribution of CMC-7L, Nozzle 74-20

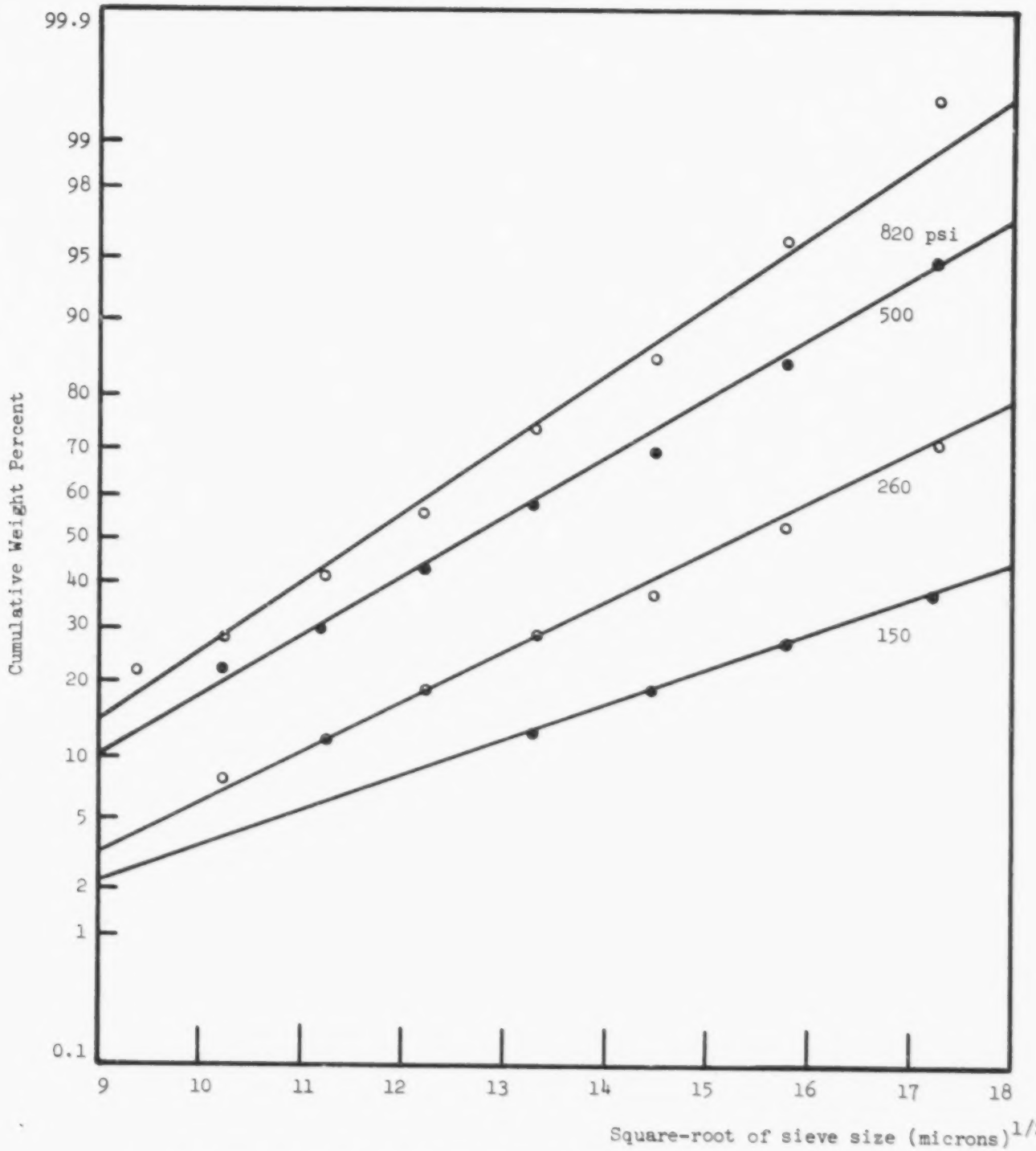

Figure 15 - Drop Size Distribution of CMC-7L, Nozzle 58-21

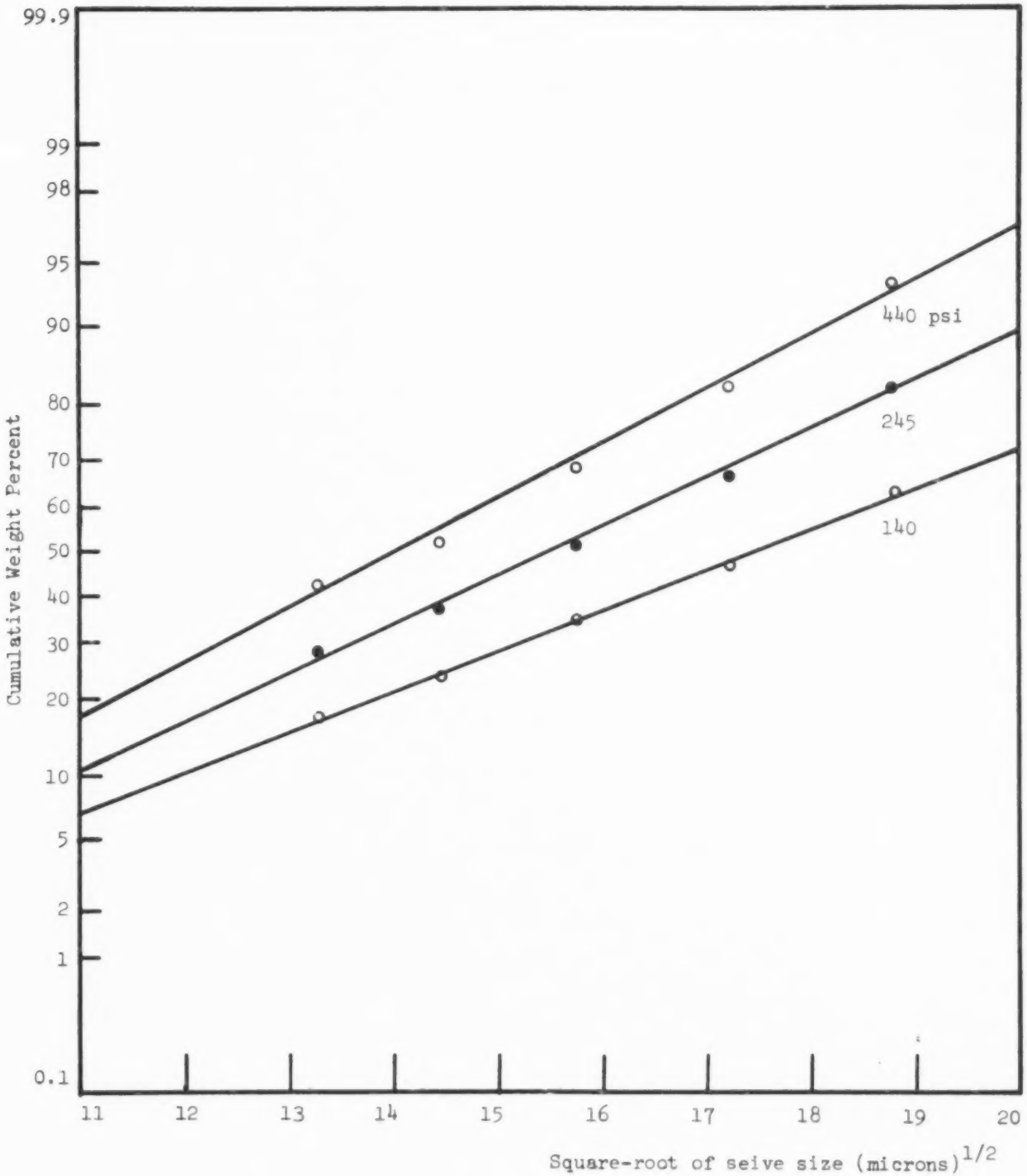

Figure 16 - Drop Size Distribution of CMC-7L, Nozzle 54-27

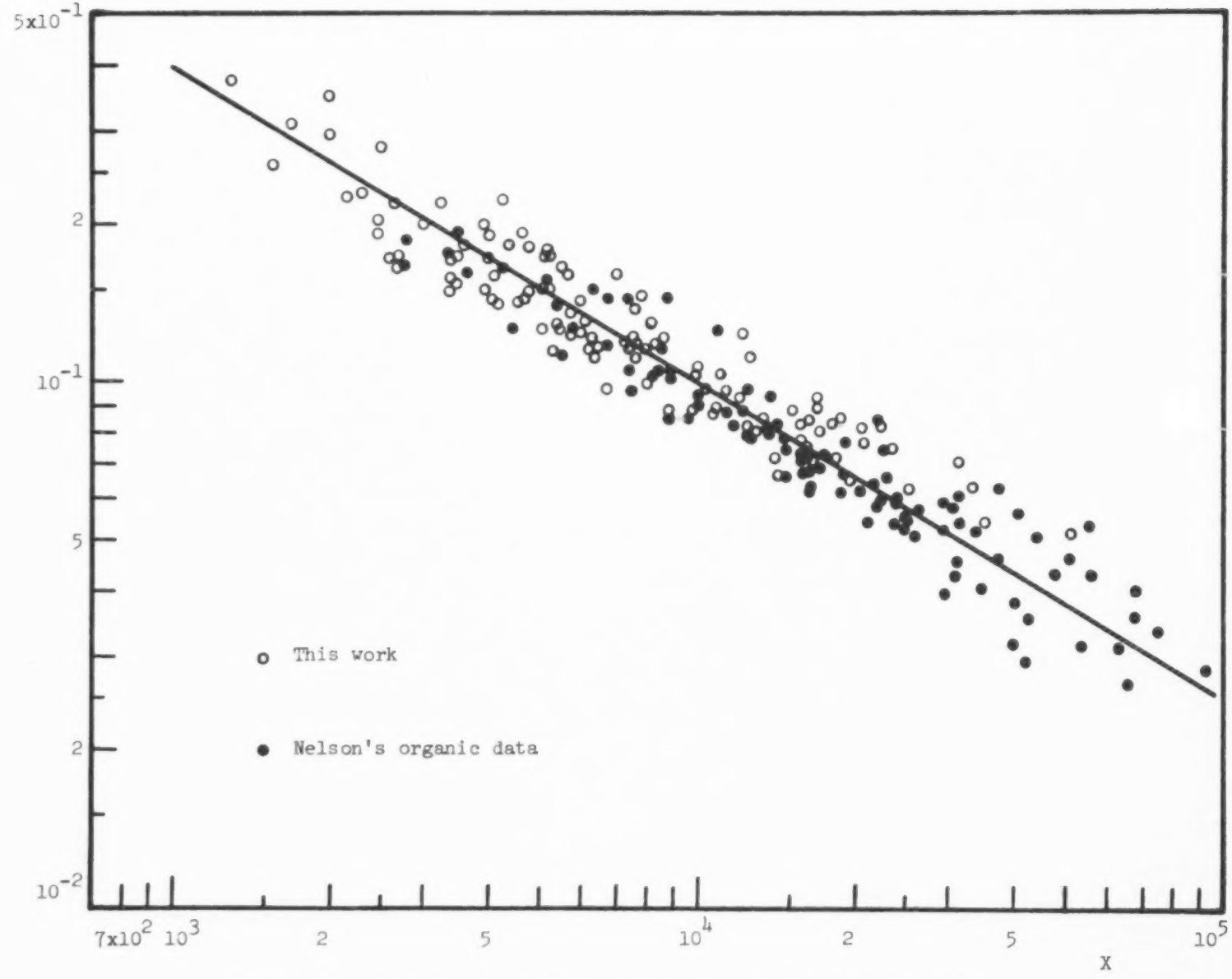

Figure 17 - Correlation of Mean Drop Size with Physical Variables

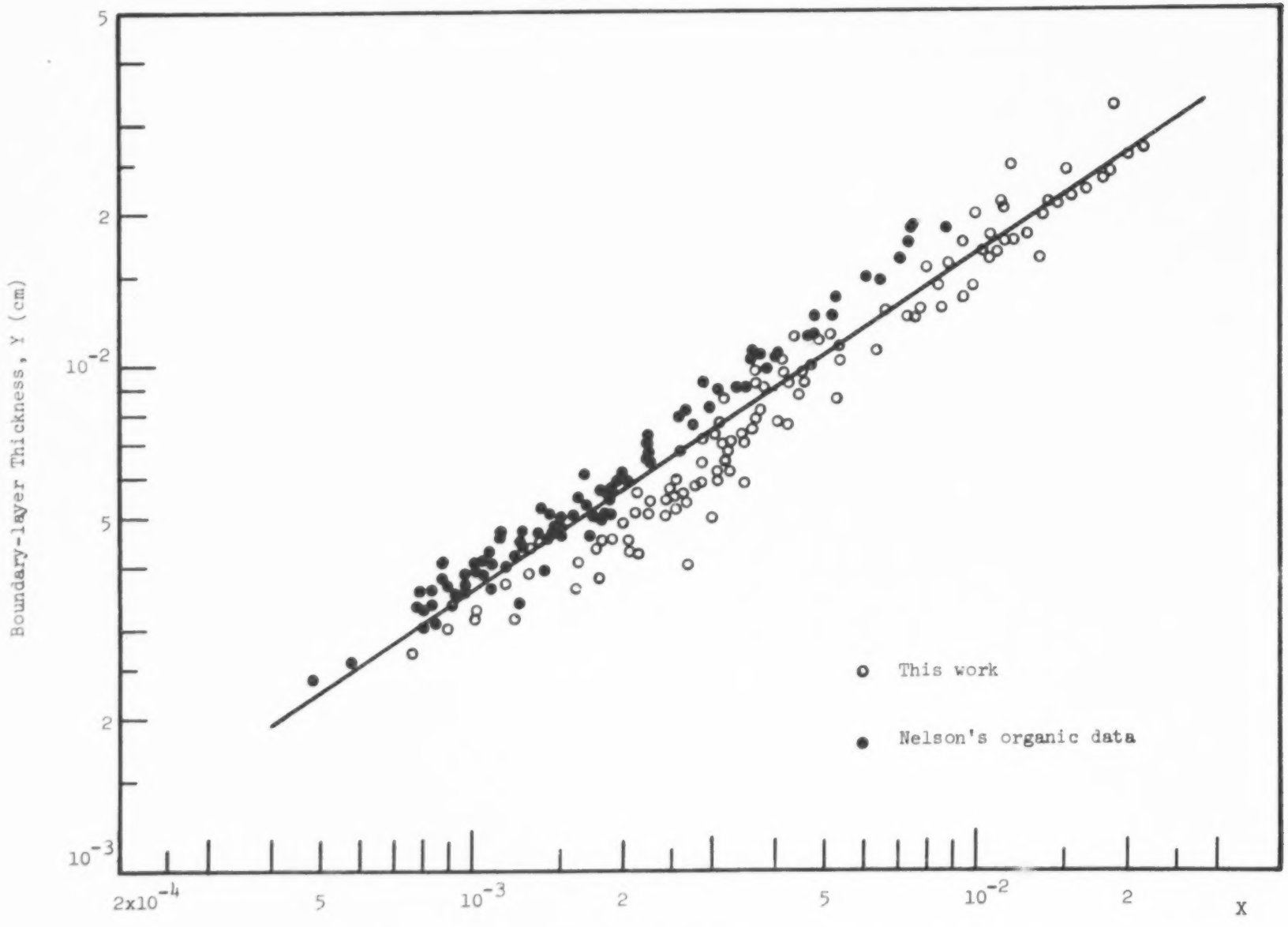

Figure 18 - Correlation of Mean Drop Size with Boundary-layer Thickness

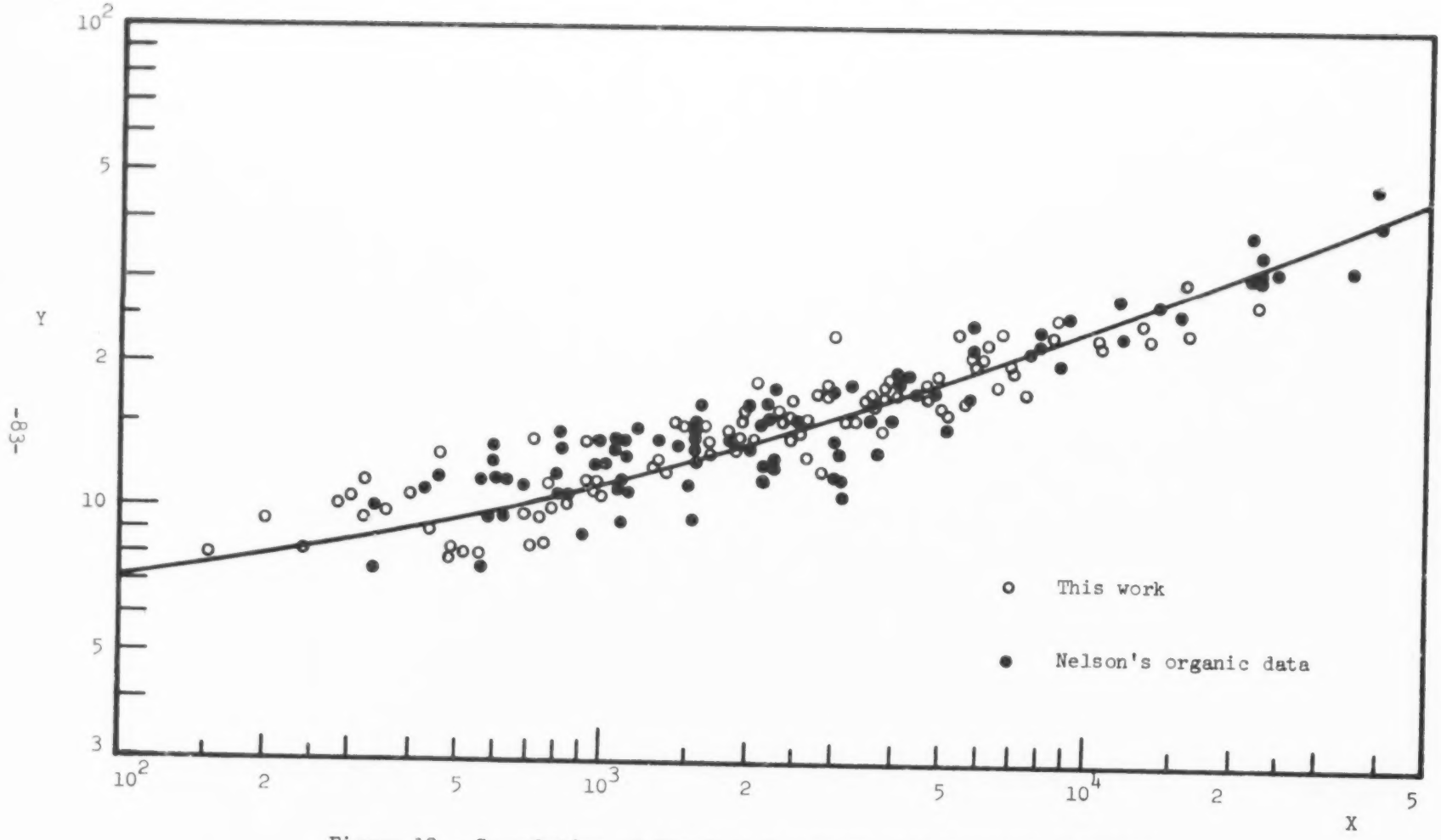

Figure 19 - Correlation of Standard Deviation with Physical Variables

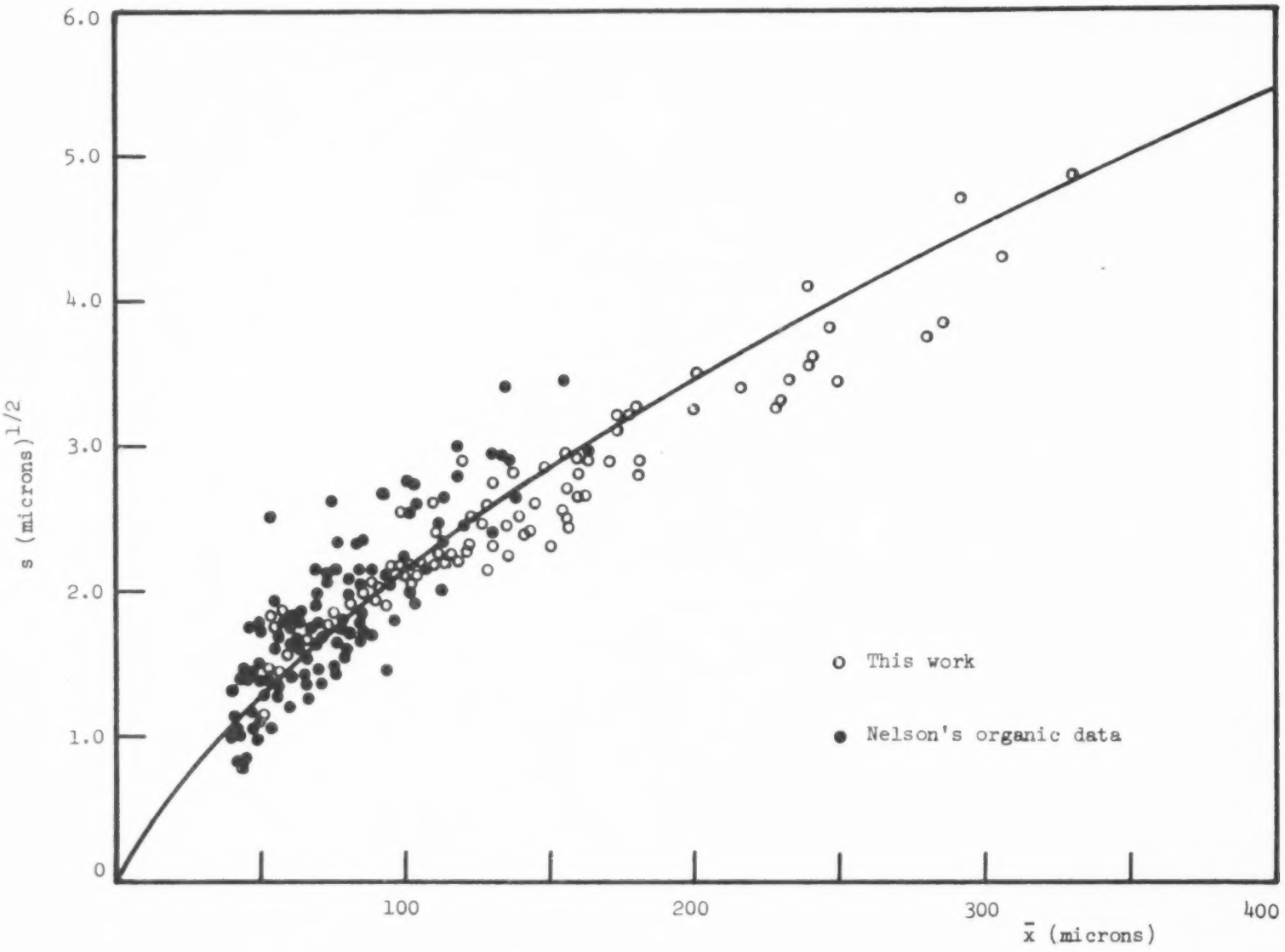

Figure 20 - Correlation of Standard Deviation with Mean Drop Size

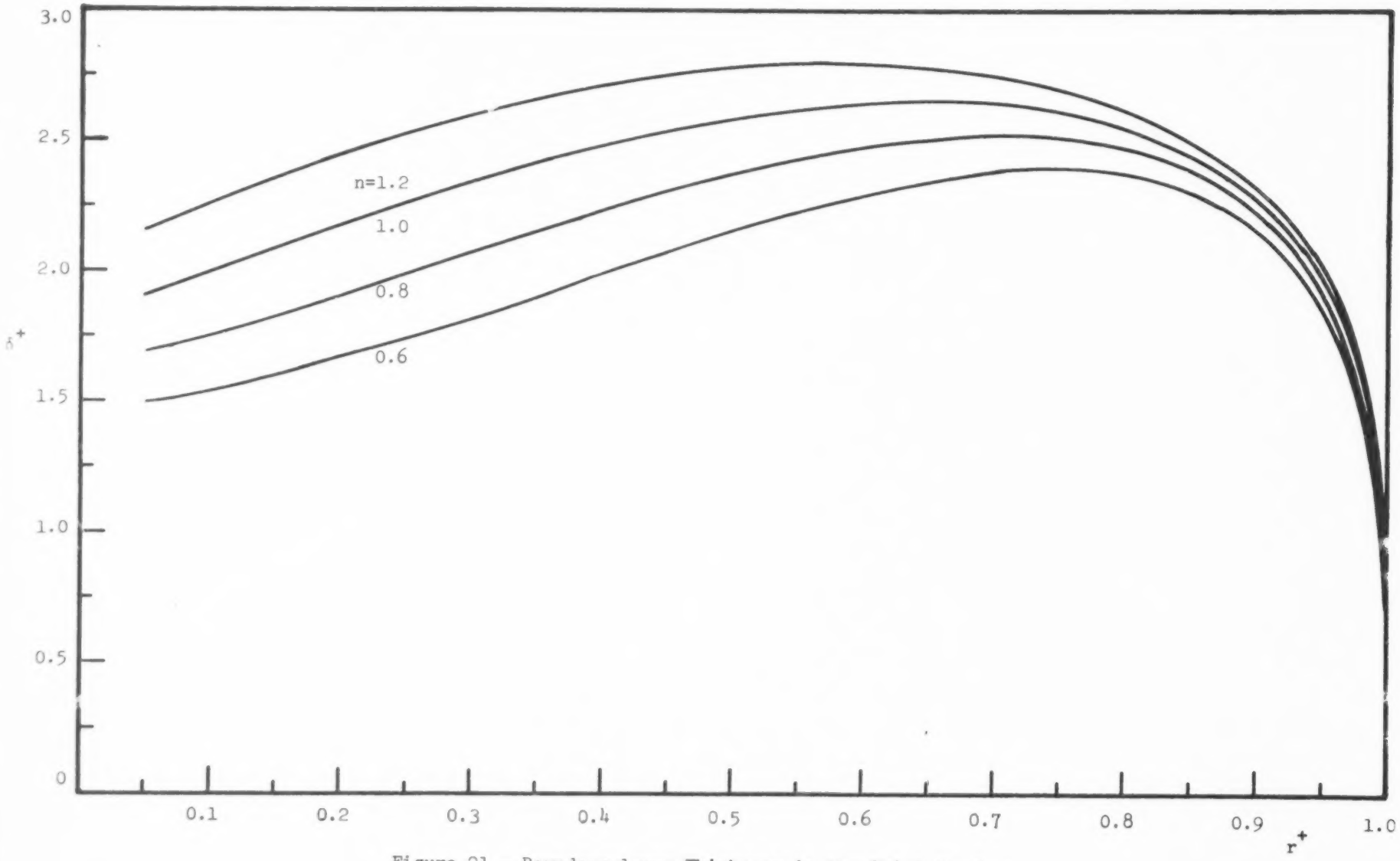

Figure 21 - Boundary-layer Thickness in the Swirl Chamber

LITERATURE CITED

A-1 Adler, C.R., Mark, A.M., Marshall, W.R., Jr., and Parent, R.J., Chem. Eng. Progr., 50, 14 (1954).

B-1 Batchelor, G.K., and Davies, R.M., "Survey in Mechanics", Cambridge University Press (1956).

B-2 Binnie, A.M., and Harris, D.P., Quart. J. Mech. Appl. Math., 3, Part 1, 89 (1950).

B-3 Bitron, M.D., Ind. Eng. Chem., 47, 23 (1955).

C-1 Castleman, R.A., Jr., J. Research Nat. Bur. Standards, 6, 281, 369 (1931).

C-2 Choudhury, A.P.R., Ph.D. Thesis, Northwestern Univ. (1955).

C-3 Christiansen, R.M., and Hixson, A.N., Ind. Eng. Chem., 49, 1017 (1957).

C-4 Cohen, N., U.S. AFOSR TR-2525 (1962).

C-5 Cooke, J.C., J. Aeronautical Sci., 19, 486 (1952).

D-1 Darnell, W.H., Ph.D. Thesis, University of Wisconsin (1953).

D-2 Dityakin, I.F., and Yagodkin, V.I., NACA TN F-63 (1961).

D-3 Dombrowski, N., and Fraser, R.P., Phil. Trans. Roy. Soc. (London), A-247, 101 (1954).

D-4 Dombrowski, N., Hasson, D., and Ward, D.E., Chem. Eng. Sci., 12, 35 (1960).

D-5 Dombrowski, N., and Hooper, P.C., Chem. Eng. Sci., 17, 291 (1962).

D-6 Dombrowski, N., and Johns, W.R., Chem. Eng. Sci., 18, 203 (1963).

D-7 Dorman, R.G., Brit. J. Appl. Phys., 3, 189 (1952).

D-8 Doumas, M., and Laster, R., Chem. Eng. Progr. 49, 518 (1953).

E-1 Epstein, B., Ind. Eng. Chem., 40, 2289 (1948).

F-1 Fraser, R.P., Eisenkalm, E.P., and Dombrowski, N., Brit. Chem. Eng., 1, 496 (1957).

F-2 Fraser, R.P., Eisenkalm, P., Dombrowski, N., and Hasson, D., AIChE. J. 8, 672 (1962).

F-3 Friedman, S.J., Gluckert, F.A., and Marshall, W.R., Jr., Chem. Eng. Progr., 48, 181 (1952).

LITERATURE CITED (Cont'd.)

G-1 Golitzine, N., Sharp, C.R., and Radham, L.C., Nat. Aeronautical Estab., Canada, R-14, ME-186 (1951).

G-2 Gretzinger, J., and Marshall, W.R., Jr., AIChE J., 7, 312, 1961.

H-1 Haenlein, A., NACA TM-659 (1932).

H-2 Hagerty, W.W., and Shea, J.F., Trans. Am. Soc. Mech. Engrs., 77, 509 (1955).

H-3 Hanson, A.R., Domick, E.G., and Adams, H.S., Report 125, University of Minnesota, Rosemont Aero. Lab.

H-4 Hasson, D., and Mizrahi, J., Trans. Inst. Chem. Engr., 39, 415 (1961).

H-5 Hatch, T., and Choate, S.P., J. Franklin Inst., 207, 309 (1929).

H-6 Herdan, G., "Small Particle Statistics", Elsevies Publishing Co., New York (1953).

H-7 Hinze, J.O., Appl. Sci. Res., A1, 263, 273 (1949).

H-8 Hinze, J.O., AIChE J., 1, 289 (1955).

H-9 Hinze, J.O., and Milborn, H., J. Appl. Mech., 17, 145 (1950).

H-10 Hodgkinson, T.G., Proton Tech. Report No. 191, British Ministry of Supply (1950).

H-11 Holdroyd, H.B., J. Franklin Inst., 215, 93 (1933).

J-1 Jeffreys, H., Proc. Roy. Soc. (London), A107, 189 (1925).

J-2 Joyce, J.R., J. Inst. Fuel, 22, 150 (1949).

K-1 Keller, J.B., and Kolodner, I., J. Appl. Phys., 25, 918 (1954).

K-2 Klinter, R.C., "Advances in Chem. Eng.", Vol. 4, Academic Press, New York (1953).

K-3 Kottler, F., J. Franklin Inst., 250, 339, 419 (1950).

L-1 Lal, K., Trans. Am. Soc. Mech. Engrs., 34, 497 (1967).

L-2 Lamb, Sir H., "Hydrodynamics", pp. 472, 625, Dover Publications, New York (1945).

L-3 Lane, W.R., Ind. Eng. Chem., 43, 1312 (1951).

L-4 Levich, V.G., "Physicochemical Hydrodynamics", Prentice-Hall, Inc. (1962).

LITERATURE CITED (Cont'd.)

L-5 Lewis, H.C., Edwards, D.G., Golia, M.J., Rice, R.I., and Smith, L.W., Ind. Eng. Chem., 40, 67 (1948).

L-6 Longwell, J.P., Ph.D. Thesis, Mass. Inst. Techn. (1934).

L-7 Lyshersky, A., Nanchr. Tr. Novocherkassky Politekhn. In-ta 39, 53, 81 (1957).

M-1 Magarvey, R.H., and Taylor, B.W., J. Applied Physics, 27, 1129 (1956).

M-2 Marshall, W.R., Jr., "Atomization and Spray Drying", Am. Inst. Chem. Engrs., New York (1954).

M-3 Masters, K., and Mohtadi, M.F., Brit. Chem. Eng., 12, 1890 (1967).

M-4 Masugi, N.J., American Rocket Society Preprint, pp. 355-256 (1956).

M-5 Mayer, E., ARS J., 31, 1783 (1961).

M-6 Merrington, A.C., and Richardson, E.G., Proc. Phys. Soc., 59, 1 (1947).

M-7 McIrvine, J.D., M.S. Thesis, University of Wisconsin (1953).

M-8 Metzner, A.B., and Park, M.G., J. Fluid Mech., 20, 291 (1964).

M-9 Miesse, C.C., Ind. Eng. Chem., 47, 1690 (1955).

M-10 Miesse, C.C., Jet Prop., 25, 525 (1955).

M-11 Mugele, R.A., and Evans, H.D., Ind. Eng. Chem., 43, 1317 (1951).

N-1 Nelson, P.A., Ph.D. Thesis, Northwestern University (1958).

N-2 Nelson, P.A., and Stevens, W.F., AIChE J., 7, 80 (1961).

N-3 Nukiyama, S., and Tanasawa, Y., Trans. Soc. Mech. Engrs. (Japan), 4, Nos. 14, 86, and Nos. 15, 138 (1938); 5, Nos. 18, 63 and 68 (1939); 6, Nos. 22, II-7 and Nos. 23, II-8 (1940).

O-1 Ohnesorge, W. von, Z. angew. Math. Mech., 16, 355 (1936).

O-2 Orr, C., Jr., and Dallavalle, J.M., "Fine Particle Measurement", MacMillan Co., New York (1959).

P-1 Pigford, R.L., and Pyle, C., Ind. Eng. Chem., 43, 1649 (1951).

P-2 Ponstein, J., Appl. Sci. Res., A-8, 425 (1959).

R-1 Rayleigh, Lord, "Theory of Sound", Vol. 2, pp. 360, 376, Dover Publications, New York (1945).

LITERATURE CITED (Cont'd.)

R-2 Rayleigh, Lord, Phil. Mag., 34, 153 (1892).

R-3 Ranz, W.E., and Hofelt, C., Jr., Ind. Eng. Chem., 49, 288 (1957).

S-1 Scheubel, F.N., NACA TM-644 (1937).

S-2 Sinbel, M.A., Trans. Am. Soc. Mech. Engrs., 81, 477 (1959).

S-3 Spraying System Co., Catalog No. 25 (1963).

S-4 Squire, H.B., Brit. J. Appl. Phys., 4, 167 (1953).

T-1 Tanasawa, Y., and Kobayasi, K., Tech. Rep. Tohoku Univ., 20, 27 (1955).

T-2 Tanasawa, Y., Sasaki, S., and Nagai, N., Tech. Rep. Tohoku Univ., 22, 73 (1957).

T-3 Tate, R.W., and Marshall, W.R., Jr., Chem. Eng. Progr., 49, 169, 226 (1953).

T-4 Taylor, G.I., Proc. Roy. Soc. (London) 146, 501 (1934).

T-5 Taylor, G.I., 7th Proc. Int. Congr. Appl. Mech., 2, 280 (1948).

T-6 Taylor, G.I., Quart. J. Mech. Appl. Math., 3, Part 2, 129 (1950).

T-7 Tomotika, S., Proc. Roy. Soc. (London), A150, 322; A153, 302 (1935).

T-8 Turner, G.M., and Moulton, R.W., Chem. Eng. Progr., 49, 185 (1953).

T-9 Tyler, E., Phil. Mag., 16, 504 (1933).

V-1 Vereshchagin, L.F., Semerchan, A.A., and Sekoyan, S.S., Soviet Phys. - Tech. Phys., 4, 38 (1959).

V-2 Volinsky, M.S., C.R. Acad. Sci. U.S.S.R., 62, 301 (1948).

W-1 Watson, E.A., Proc. Inst. Mech. Engrs. (London), 158, 187 (1948).

W-2 Weber, C., Z. angew. Math. Mech., 11, 136 (1931).

W-3 Weber, H.E., Trans. Am. Soc. Mech. Engrs., 78, 587 (1956).

W-4 Weiss, M.A., and Worsham, C.H., ARS J., 29, 252 (1959).

W-5 Wetzel, R.H., Ph.D. Thesis, University of Wisconsin (1951).

W-6 Wetzel, R.H., and Marshall, W.R., Jr., paper presented at Washington, D.C., National Meeting, AIChE (1954).

Y-1 York, J.L., Stubbs, H.E., and Tek, M.R., Trans. Am. Soc. Mech. Engrs., 74, 1157 (1952).

NOMENCLATURE

a = radius of a cylindrical jet or a sphere; half thickness of a liquid sheet

A = (orifice area)/(total flow area of grooved slots)

A_2 = orifice area

A_i = total flow area of grooved slots

B = a numerical coefficient

c = velocity of disturbance wave on the surface of a liquid

C_Q = discharge coefficient of a pressure nozzle

d = drop diameter

D = a characteristic length

D_2 = orifice diameter

f_n = density function based on the number of particles

f_v = density function based on the volume of particles

F_v = distribution function based on the volume of particles

h = liquid film thickness at orifice

k = wave number

k_o = thickness parameter of a liquid sheet produced by a fan-spray nozzle

m = maximum drop diameter; coefficient in the Power Law Model for shear stress and shear rate relation

n = number of particles; index in the Power Law Model for shear stress and shear rate relation

N = total number of particles

P = total pressure of the liquid

Q = volumetric flow rate

R_o = length of the generator of the conic swirl chamber in a nozzle

Re = Reynolds number defined as $\frac{D_2\sqrt{P\rho}}{\mu}$ or $\frac{D_2 V_{ax}\rho}{\mu}$

Re' = Reynolds number used in calculation of boundary thickness, defined in Appendix III

s = standard deviation

v = volume of particles

V = velocity; velocity of the liquid; total volume of particles

V_i = inlet velocity of the liquid

V_{ax} = axial velocity of liquid at orifice

V_t = tangential velocity of liquid

W = mass flow rate of liquid

We = Weber number defined variously as $\frac{D_2 P}{\sigma}$, $\frac{\rho D_2 V_{ax}^2}{\sigma}$, $\frac{a\rho V_t^2}{\sigma}$, $\frac{\rho \beta^2 a^2}{\sigma k}$, $\frac{a\rho_a V^2}{\sigma}$, or $\frac{D\rho V_a^2}{\sigma}$.

We' = Weber number defined as $\frac{a\rho V^2}{\sigma}$

x = drop size

$\bar{x}$ = mean drop size or diameter

X,Y = coordinates of the logarithmic plot of correlation

Z = (air core diameter)/(orifice diameter)

Greek Symbols

α = amplitude of disturbance wave

β = amplitude growth rate of disturbance wave

γ = sheltering coefficient

δ = displacement of a liquid particle in a volume of liquid; boundary-layer thickness; parameter in drop size distribution

δ^+ = dimensionless boundary-layer thickness defined in Appendix III

λ = wave length

ρ = density

σ = surface tension

μ = viscosity

μ' = viscosity of ambient liquid

Ω = circulation constant

General Subscripts

m	=	asymptotic value at high Reynolds number
max	=	value at the maximum growth rate of disturbance wave
a	=	properties of ambient gas

APPENDICES

APPENDIX I - DROP SIZE DISTRIBUTION DATA

TABLE V - DROP SIZE DISTRIBUTION FOR NON-NEWTONIAN FLUIDS

Nozzle	Press. (psi)	Recovery (grams)	Recovery %	$\bar{x}$ (microns)	$\frac{1}{2}$ (microns)^2	$\frac{\bar{x}}{D_2}$	Re	We
Carbopol-934		0.11%	Solution					
80-16	220	21.70	----	89.5	1.95	0.261	3340	7226
"	410	17.50	86.5	70.5	1.72	0.205	4559	13467
"	830	21.20	102.0	54.8	1.40	0.160	6487	27262
"	1520	18.40	96.4	41.2	1.00	0.120	8779	49925
74-20	230	19.40	95.5	95.0	2.15	0.166	4132	12576
"	830	22.50	92.0	55.5	1.45	0.0972	7850	45384
67-17	140	21.35	98.5	121.0	2.25	0.149	6307	10886
"	140	25.45	101.5	129.0	2.15	0.159	6307	10886
"	410	23.25	89.7	93.0	1.90	0.115	10790	31880
"	1440	25.85	84.1	53.0	1.42	0.0653	14700	111970
58-17	135	23.45	104.2	135.5	2.25	0.127	8130	13781
"	420	22.05	81.4	102.0	2.02	0.0957	14340	42874
54-17	140	22.90	110.5	160.0	2.65	0.115	10840	18715
"	410	25.10	97.5	113.5	2.25	0.0813	18560	54810
"	420	44.90	102.0	124.5	2.53	0.0892	18780	56146
46-27	210	28.05	104.9	174.0	3.20	0.0842	19600	41426
Carbopol-934		0.15%	Solution					
80-10	800	36.90	90.6	62.7	1.60	0.183	4632	26276
"	1540	41.15	84.0	54.8	1.35	0.160	6152	50582
80-16	400	21.30	91.5	77.5	1.82	0.226	3275	13138
"	800	22.25	90.8	59.3	1.55	0.173	4632	26276
"	1680	25.20	92.3	49.0	1.15	0.143	6712	55181
74-16	410	30.30	92.7	82.0	1.92	0.144	5518	22418
"	800	29.35	87.4	64.0	1.64	0.112	7710	43743
"	1520	27.30	85.5	53.0	1.45	0.0928	10628	83112
74-20	220	16.55	93.1	99.0	2.10	0.173	4043	12029
"	420	27.45	88.0	81.0	1.93	0.142	5587	22965
"	760	31.60	85.5	67.0	1.65	0.117	7515	41556
67-20	810	38.25	84.3	72.2	2.00	0.0889	7758	62983
"	1700	23.90	70.0	53.3	1.85	0.0656	15984	132187
67-17	120	26.85	95.5	143.0	2.40	0.1760	4247	9931
"	200	29.30	98.0	122.0	2.33	0.1500	5482	15551
"	400	32.30	90.0	96.0	2.10	0.1180	7753	31103
"	830	27.35	91.0	72.2	1.73	0.0889	11169	64538
"	1480	28.20	76.8	54.8	1.75	0.0675	14914	115081
67-21	135	24.35	94.5	156.0	2.70	0.1920	4504	10497
"	220	42.75	92.0	125.5	2.45	0.1550	5750	17107
"	410	41.60	90.5	102.0	2.20	0.1260	7849	31880
"	810	37.85	85.0	72.2	1.75	0.0889	11033	62983
"	1520	23.00	---	57.0	1.70	0.0702	15114	118191
"	1580	29.45	88.5	54.0	1.80	0.0665	15409	122856
58-17	140	33.65	101.0	151.0	2.30	0.1420	6022	14291
"	200	39.00	111.0	135.0	2.43	0.1270	7198	20416
"	200	38.10	107.0	134.5	2.40	0.1260	7198	20416
"	410	32.95	88.8	113.0	2.20	0.1040	10305	41853
"	420	41.20	96.0	114.0	2.20	0.1070	10430	42874

APPENDIX I - DROP SIZE DISTRIBUTION DATA (Cont'd.)

TABLE V - DROP SIZE DISTRIBUTION FOR NON-NEWTONIAN FLUIDS (Cont'd.)

Nozzle	Press. (psi)	Recovery (grams)	Recovery %	$\bar{x}$ (microns)	$\frac{1}{2}$ (microns)^2	$\frac{\bar{x}}{D_2}$	Re	We
58-17	800	28.70	92.4	83.5	1.95	0.0783	14395	81664
"	800	37.90	81.9	88.0	2.07	0.0826	14395	81664
"	830	31.55	81.0	90.0	2.13	0.0844	14660	84727
"	1530	30.30	73.0	67.3	1.65	0.0631	19907	156183
54-17	125	36.25	100.7	156.0	2.45	0.1120	7451	16710
"	420	38.90	102.2	123.0	2.48	0.0881	13660	56146
"	650	34.10	90.5	107.0	2.15	0.0766	16992	86893
"	1380	17.55	75.0	74.8	1.85	0.0536	24758	184480
54-21	130	36.15	107.0	177.0	3.20	0.1270	7595	17379
"	140	28.95	98.4	172.0	2.90	0.1230	7882	18715
"	220	28.65	92.5	138.0	2.80	0.0989	9880	29410
"	420	28.00	98.9	114.5	2.40	0.0820	13652	56146
"	430	35.10	94.5	110.0	2.62	0.0789	13810	57483
54-27	230	21.95	104.9	160.0	2.80	0.1150	8426	21389
"	410	27.35	95.2	121.0	2.45	0.0867	13490	54809
46-27	120	17.70	109.3	237.0	4.10	0.1150	10770	23672
"	220	22.90	95.5	181.0	3.25	0.0876	14580	43400
"	390	32.05	76.1	147.5	2.85	0.0714	19410	76934
CMC-7L		4.5%	Solution					
74-20	195	16.50	99.1	216.0	3.40	0.3780	838	10662
"	410	16.80	113.0	131.0	2.75	0.2290	1316	22418
"	800	14.70	106.0	105.0	2.20	0.1840	1696	43743
"	1510	15.30	109.5	91.5	2.03	0.1600	2330	82565
67-20	165	23.05	113.0	287.0	3.85	0.3530	1096	12830
"	230	24.25	103.0	228.0	3.25	0.2810	1293	17884
"	440	19.90	98.5	156.0	2.50	0.1920	1789	34213
"	1070	14.75	86.0	112.0	2.25	0.1380	2790	83200
67-21	240	30.70	---	239.0	3.60	0.2940	1321	18662
"	410	16.55	92.0	162.5	2.90	0.2000	1727	31880
"	790	20.30	94.4	121.0	2.90	0.1490	2400	61428
"	1480	8.65	108.0	98.0	2.55	0.1210	3281	115081
58-17	380	19.40	109.0	161.0	2.65	0.1510	2183	38790
"	800	24.55	94.3	128.0	2.60	0.1200	3167	81664
58-21	150	25.85	---	329.0	4.85	0.3090	1371	15312
"	260	77.95	---	233.0	3.45	0.2190	1805	26541
"	500	16.50	87.3	160.0	2.90	0.1500	2504	51040
"	800	10.95	96.2	136.0	2.50	0.1280	3206	83706
54-17	220	17.90	105.2	250.0	3.45	0.1790	2175	29410
"	870	17.40	94.8	140.5	2.50	0.1010	4325	116302
"	1480	11.50	89.0	114.5	2.25	0.0820	5641	197848
54-21	150	21.50	110.0	279.0	3.75	0.2000	1796	20052
"	240	18.90	107.0	231.0	3.30	0.1660	2271	32083
"	410	19.60	102.0	182.0	2.90	0.1300	2969	54809
54-27	140	21.30	111.0	306.0	4.35	0.2190	1735	18715
"	245	18.55	103.0	240.0	3.60	0.1720	2295	32752
"	440	19.75	94.0	197.5	3.25	0.1290	3076	58820
46-27	140	14.35	93.3	373.0	6.30	0.1810	2560	27617
"	260	24.55	94.9	292.0	4.70	0.1420	3489	51290

APPENDIX I - DROP SIZE DISTRIBUTION DATA (Cont'd.)

TABLE VI - DROP SIZE DISTRIBUTION FOR NEWTONIAN FLUIDS

Nozzle	Press. (psi)	Recovery (grams)	Recovery %	$\bar{x}$ (microns)	$s^{\frac{1}{2}}$ (microns)	$\frac{\bar{x}}{D_2}$	Re	We
Water								
80-16	430	36.30	94.9	65.5	1.65	0.1910	20890	14120
"	1640	26.20	92.1	42.5	1.05	0.1240	40800	53870
74-20	150	26.15	91.9	82.2	2.10	0.1440	20540	8200
"	410	28.70	91.0	66.9	1.70	0.1170	33960	22420
"	1600	28.25	80.2	47.0	1.20	0.0823	67080	87490
67-21	160	21.50	90.1	110.0	2.40	0.1360	30170	12440
58-17	160	29.35	88.6	104.0	2.10	0.0976	39600	16330
"	820	16.15	80.7	67.3	1.65	0.0631	89650	83710
54-17	180	28.90	105.0	130.0	2.30	0.0931	55000	24060
"	205	17.45	88.0	117.5	2.20	0.0842	58700	27410
"	420	17.60	91.2	98.0	2.20	0.0702	84030	56150
"	850	12.60	86.5	72.2	1.70	0.0516	119540	113630
54-27	160	18.85	108.5	145.0	2.60	0.1039	51860	21390
46-27	140	33.30	90.6	173.0	3.10	0.0840	71590	27620
"	200	16.10	112.0	155.0	2.95	0.0753	85560	39450
Glycerine		76%	Solution					
67-21	410	18.90	95.0	182.0	2.80	0.2240	1393	34000
"	530	17.90	95.6	141.5	2.40	0.1740	1583	43960
54-17	230	27.75	98.7	240.0	3.80	0.1720	1793	32800
"	240	20.00	96.5	247.0	3.55	0.1770	1832	34220
"	420	33.20	100.0	202.0	3.50	0.1450	2423	59890
"	830	13.95	100.0	155.0	2.55	0.1110	3407	118350
Nelson's data on Organic Fluids [N-1]								
Aniline								
54-17	104	44.7	89.5	162.3	2.96	0.1163	10100	23660
"	203	42.1	85.1	130.5	2.42	0.0935	14110	46180
"	405	51.2	85.5	103.5	1.88	0.0741	19940	92140
"	810	48.8	93.4	88.3	1.72	0.0633	28200	184280
"	1395	40.9	69.7	74.7	1.52	0.0535	37000	317590
Nitrobenzene								
54-17	105	49.1	92.0	115.5	2.79	0.0827	22410	23340
"	208	45.9	89.4	94.3	2.44	0.0676	31540	46240
"	400	45.8	88.0	81.2	2.08	0.0581	43730	88920
"	1200	34.5	79.6	50.0	1.38	0.0358	75740	266760
Cyclohexane								
54-17	104	53.3	86.5	107.0	2.16	0.0766	37400	40860
"	205	45.2	88.5	84.7	1.84	0.0607	52530	80540
"	300	44.8	94.6	78.1	1.82	0.0560	63550	117860
"	405	42.1	83.3	64.0	1.41	0.0459	73010	159110
"	604	45.2	98.7	55.5	1.34	0.0398	90170	237290
80-16	103	44.2	94.9	64.1	1.87	0.1870	9150	9940
"	186	37.3	83.0	56.1	1.71	0.1640	12300	17960
"	323	43.4	91.6	51.0	1.29	0.1490	16200	31180
"	355	36.4	83.6	40.2	1.02	0.1170	16990	34270

APPENDIX I - DROP SIZE DISTRIBUTION DATA (Cont'd.)

TABLE IV - DROP SIZE DISTRIBUTION FOR NEWTONIAN FLUIDS (Cont'd.)

Nozzle	Press. (psi)	Recovery (grams)	Recovery %	$\bar{x}$ (microns)	$s^{\frac{1}{2}}$ (microns)	$\frac{\bar{x}}{D_2}$	Re	We
80-16	356	40.8	93.5	49.0	1.13	0.1430	17010	34370
"	508	37.0	91.2	40.2	1.02	0.1170	20320	49040
46-27	107	47.3	92.5	112.0	2.47	0.0544	56000	62030
"	145	47.9	99.2	93.9	2.11	0.0456	65190	84060
"	205	44.1	108.0	78.5	1.74	0.0381	77520	118840
"	307	48.7	99.0	65.0	1.68	0.0316	94860	177970
"	410	52.8	107.5	55.2	1.43	0.0268	109620	237680
54-21	102	45.1	95.1	102.0	1.99	0.0731	37050	40070
"	204	41.7	85.9	71.0	1.68	0.0510	52400	80140
"	300	44.8	97.3	56.8	1.34	0.0407	63550	117850
"	400	39.9	87.2	49.8	1.10	0.0357	73380	157130
"	695	28.2	85.9	44.0	1.04	0.0315	96720	27302
80-10	104	40.8	104.0	65.6	1.37	0.1920	9190	10040
"	176	30.6	90.9	53.6	1.07	0.1560	11960	16990
"	290	27.4	91.0	49.1	0.97	0.1430	15350	27990
"	500	27.3	92.5	43.0	0.80	0.1250	20160	48260
54-27	103	41.3	88.0	100.0	2.21	0.0716	37230	40460
"	205	44.3	91.5	67.5	1.74	0.0481	52530	80530
"	302	31.4	90.6	55.2	1.38	0.0396	63760	118640
"	500	29.5	92.3	41.3	1.11	0.0296	82040	196420
"	104	42.2	91.6	85.0	1.78	0.1050	21760	23760
"	201	33.5	91.4	65.0	1.42	0.0800	30630	47070
"	280	30.7	90.1	55.5	1.28	0.0684	35710	63980
"	400	33.4	93.2	48.0	1.08	0.0591	42680	91400
"	590	24.0	86.8	42.0	0.83	0.0519	51840	134810
"	103	43.8	103.3	81.0	1.96	0.0997	21660	23540
"	199	32.3	87.3	67.3	1.53	0.0829	30100	45470
"	405	26.5	87.8	48.0	1.14	0.0591	42950	92540
"	595	28.6	100.5	43.4	1.01	0.0534	52060	135960
67-21	111	41.4	90.2	84.6	1.71	0.1040	22480	25360
"	202	33.4	85.7	70.5	1.46	0.0868	30330	46160
"	605	19.8	81.3	45.2	0.82	0.0556	52500	138240
n-Octyl Alcohol								
54-17	202	43.4	86.2	134.5	3.42	0.0964	6030	72020
"	325	53.7	96.5	101.0	2.76	0.0724	7640	115870
"	505	52.8	94.6	84.0	2.36	0.0602	9520	180050
"	805	36.4	87.8	72.5	2.12	0.0520	12100	287000
"	1310	28.2	79.3	60.4	1.74	0.0433	15340	467070
54-27	104	41.7	86.3	155.0	3.44	0.1110	4320	37080
"	202	41.2	94.5	199.0	3.00	0.0853	6010	72020
"	412	46.6	91.6	91.7	2.68	0.0657	8600	146900
"	800	36.7	92.0	75.2	2.62	0.0538	11990	285230
"	1490	32.4	82.3	64.0	2.50	0.0458	16360	531240
67-20	106	40.0	93.5	130.0	2.96	0.1600	2540	21980
"	199	34.6	83.1	102.0	2.74	0.1257	3480	41270
"	404	33.0	83.2	68.5	2.16	0.0844	4960	83780
"	805	37.4	---	57.7	1.80	0.0710	6990	166950
"	1280	26.4	84.2	47.0	1.74	0.0579	8870	265450

APPENDIX I - DROP SIZE DISTRIBUTION DATA (Cont'd.)

TABLE IV - DROP SIZE DISTRIBUTION FOR NEWTONIAN FLUIDS (Cont'd.)

Nozzle	Press. (psi)	Recovery (grams)	Recovery %	$\bar{x}$ (microns)	$s^{\frac{1}{2}}$ (microns)	$\frac{\bar{x}}{D_2}$	Re	We
67-21	102	34.7	85.1	134.0	2.94	0.1650	2490	21150
"	202	42.4	89.9	102.5	2.56	0.1260	3500	41890
"	405	38.7	93.3	76.8	2.32	0.0945	4960	83990
"	1200	29.5	85.0	50.3	1.78	0.0619	8540	248860
"	1200	29.4	85.9	51.3	1.74	0.0632	8540	248860
"	1200	33.9	94.7	54.8	1.96	0.0675	8540	248860
Carbon Tetrachloride								
54-17	109	47.3	93.5	89.2	2.13	0.0639	53340	40050
"	169	54.0	103.4	82.7	2.08	0.0592	64130	62100
"	290	40.3	98.6	70.7	1.89	0.0507	87020	106550
"	400	47.5	97.8	61.6	1.64	0.0431	101980	146970
"	605	36.4	104.2	46.6	1.45	0.0336	125690	222300
"	805	29.2	80.6	39.6	1.31	0.0284	144990	215780
54-27	102	41.8	90.1	104.0	2.61	0.0745	51610	37480
"	143	47.4	95.1	85.7	2.34	0.0614	61110	52540
"	209	41.6	97.0	70.1	1.99	0.0520	73880	76790
"	280	35.3	94.9	59.8	1.77	0.0428	85510	102880
"	405	34.3	97.7	44.2	1.47	0.0317	102840	148810
67-20	106	41.1	104.2	73.4	2.07	0.0904	30610	22650
"	149	36.2	97.3	63.2	1.85	0.0778	36260	31840
"	202	25.2	90.0	58.7	1.61	0.0723	42250	43170
"	283	33.1	95.3	50.3	1.50	0.0619	50000	60480
"	405	39.9	103.8	46.2	1.41	0.0569	59820	86560
67-21	112	39.3	84.5	83.0	2.13	0.1022	31460	23940
"	147	32.0	86.0	75.8	2.14	0.0834	36040	31420
"	206	32.0	87.4	63.5	1.79	0.0781	42660	44030
"	283	31.4	85.1	54.7	1.60	0.0674	50000	60480
"	415	33.7	92.0	44.0	1.42	0.0542	60560	88730
1,1,2,2-Tetrabromoethane								
67-20	105	47.4	107.5	144.0	2.92	0.1770	4530	12000
"	204	45.1	106.5	114.0	2.60	0.1400	6310	23310
"	407	---	---	85.0	2.20	0.1047	8910	46500
"	805	38.0	93.7	63.5	1.64	0.0782	12530	91970
"	1500	39.1	88.0	53.2	1.38	0.0655	17110	171370

APPENDIX II - DETERMINATION OF NOZZLE PERFORMANCES

1. Determination of C_{Qm}

C_{Qm} is the asymptotic value of the discharge coefficient (C_Q) at high Reynolds numbers (Re). The value of C_{Qm} for each nozzle is calculated from the measured flow rate of water at a pressure level of 1,000 psi. In the following tables, the parameter A is the ratio of the orifice area (A_2) to the inlet flow area (A_i) of the nozzle. The values of C_{Qm} are plotted against A in Figure 7.

TABLE VII - EXPERIMENTAL VALUES OF C_{Qm}

Nozzle	$A_2(cm^2)$	$A_i(cm^2)$	A	$Q(\frac{cm^3}{sec.})$	Re	C_{Qm}
80-10	0.924×10^{-3}	2.32×10^{-3}	0.398	3.70	2.78×10^{4}	0.342
80-16	0.924	4.96	0.186	5.00	2.78	0.457
74-16	2.561	4.96	0.516	7.40	4.63	0.246
74-20	2.561	8.00	0.320	9.60	4.63	0.357
67-20	5.179	8.00	0.647	13.85	6.58	0.228
67-17	5.179	9.93	0.522	16.75	6.58	0.276
67-21	5.179	18.08	0.286	22.50	6.58	0.370
58-17	8.925	9.93	0.899	21.75	8.64	0.208
58-21	8.925	18.08	0.494	31.00	8.64	0.284
54-17	15.306	9.93	1.541	28.50	11.30	0.159
54-21	15.306	18.08	0.847	43.50	11.30	0.240
54-27	15.306	31.00	0.494	56.00	11.30	0.312
46-27	33.329	31.00	1.075	90.00	16.70	0.230

2. Determination of Z_m

Z_m is the asymptotic value of Z at high Reynolds numbers, where Z is the ratio of the air-core diameter to the orifice diameter. The values of Z_m in Table VIII were determined by Darnell [D-1] using water. Each value of Z_m was averaged from six observations at pressures of 100, 400, 700, 1,000, 1,300 and 1,600 psi. Since water is only slightly viscous, the air-core diameter for a given nozzle at a pressure level of 100 psi is essentially the same as those at high pressure levels. The value of Z_m are plotted against $(A)^{1/2}$ in Figure 8. From this figure, the predicted values

of Z_m for the nozzles used in the present work are read off and are compared in Table IX with those values obtained by Nelson [N-1] by correlating Darnell's data with the spray cone angle.

TABLE VIII - EXPERIMENTAL VALUES OF Z_m

D_2(in)	A_i(cm^2)	A	$A^{1/2}$	Z_m
0.015	0.36×10^{-3}	0.490	0.701	0.369
"	0.77	0.229	0.479	0.410
"	1.20	0.147	0.384	0.388
"	1.50	0.118	0.343	0.311
"	2.80	0.063	0.251	0.256
0.020	0.36	0.872	0.934	0.400
"	0.77	0.424	0.602	0.563
"	1.20	0.216	0.511	0.420
"	1.50	0.212	0.457	0.440
"	2.80	0.112	0.335	0.460
0.036	0.77	1.320	1.150	0.611
"	0.77	1.320	1.150	0.810
"	1.20	0.840	0.921	0.838
"	1.50	0.677	0.824	0.750
"	2.80	0.353	0.602	0.650
"	4.80	0.212	0.461	0.528
0.043	1.20	1.210	1.100	0.688
"	1.50	0.967	0.983	0.725
"	2.80	0.518	0.719	0.650
"	4.80	0.302	0.550	0.581
0.056	0.77	3.190	1.788	0.750
"	1.20	2.045	1.433	0.838
"	1.50	1.640	1.281	0.775
"	2.80	0.879	0.938	0.725
"	4.80	0.511	0.716	0.650
"	4.80	1.511	0.710	0.625
0.066	1.20	2.845	1.688	0.775
"	1.50	2.280	1.510	0.750
"	2.80	1.220	1.105	0.763
"	4.80	0.712	0.844	0.638

TABLE IX - COMPARISON BETWEEN PREDICTED VALUES OF Z_m

Nozzle	A	$A^{1/2}$	Z_m	
			This Work	Nelson
80-10	0.398	0.631	0.590	0.360
80-16	0.186	0.431	0.430	0.320
74-16	0.516	0.718	0.640	-----
74-20	0.320	0.566	0.550	0.580
67-20	0.647	0.804	0.683	0.750
67-17	0.522	0.722	0.642	0.700
67-21	0.286	0.535	0.524	0.620
58-17	0.899	0.948	0.730	0.750
58-21	0.494	0.703	0.630	-----
54-17	1.541	1.241	0.770	0.760
54-21	0.847	0.920	0.720	0.720
54-27	0.494	0.703	0.630	0.640
46-27	1.075	1.037	0.745	0.680

3. Determination of θ_m

θ_m is the asymptotic value of the spray cone angle (θ) at high Reynolds numbers. The spray cone angles were measured from photographs taken at different levels of pressures up to 1,600 psi. The values of θ_m of each nozzle determined from several fluids are given in Table X. The values of $\tan(\frac{\theta_m}{2})$ based on water are plotted versus the nozzle size parameter (A) in Figure 9. Using the values of θ_m based on the measured water data, two plots of θ/θ_m versus Reynolds number are shown in Figure 10 for glycerine (24 cp) and in Figure 11 for 0.15% Carbopol-934 and 4.5% CMC-7L solutions. These plots are made in order to test the extrapolated values of apparent viscosities for the 0.15% Carbopol-934 and 4.5% CMC-7L solutions.

TABLE X - SPRAY CONE ANGLE (IN DEGREES) AT HIGH REYNOLDS NUMBERS

Nozzle	A	Manufacturer's Data	Water	Glycerine (24 cp)	Carbopol-934 0.12%	Carbopol-934 0.15%	CMC-7L 3.0%	CMC-7L 4.5%	$\tan[\frac{\theta_m}{2}]$ **
80-10	0.398	65	63						0.636
80-16	0.186	54	53		50	48	44		0.499
80-20	0.116		40		48				0.364
80-17	0.093		50						0.476
74-16	0.516	71	71*	70					0.714
74-20	0.320	68	71	65	76	69	72	65	0.714
67-20	0.647		88		92	87	83	85	0.965
67-17	0.522	74	84			78	81	81	0.900
67-21	0.286	63	74	66	83	71	76	71	0.753
58-20	1.112		90						1.000
58-17	0.899	83	90		93	90	90	84	1.000
58-21	0.494	73	74	73	77	73	77	72	0.753
54-17	1.541		91	90	93		92	95	1.000
54-21	0.847	81	81*						0.854
54-27	0.494	73	73*						0.740
46-27	1.075	84	84*	83					0.900

* Use manufacturer's data [S-3] based on water

** $\tan[\theta_m/2]$ is based on the measured water data in column 4

4. Determination of the Characteristic Shear Rate

The average shear rate of the liquid at the nozzle orifice is taken as the ratio of V_{ax}/h, where V_{ax} is the axial velocity of the liquid based on the liquid film thickness (h). The values of axial velocities (V_{ax}) are based on the water flow rates at the two pressure levels of 100 and 1,500 psi. The values of the liquid film thickness (h) are calculated from the quantity Z_m given in Table IX. The computed shear rates at the two pressure levels are listed in Table XI. The lowest and the highest shear rates are 0.59×10^5 and 7.5×10^5 per second, respectively. The characteristic shear rate is taken to be 2.0×10^5 per second, which is the midpoint between the lowest and the highest shear rates in logarithmic scale.

TABLE XI - SHEAR RATE OF LIQUID AT ORIFICE BASED ON WATER FLOW RATE

Nozzle	h (cm)	Pressure at 100 psi			Pressure at 1,500 psi		
		$Q(\frac{cm^3}{sec.})$	$V_{ax}(\frac{cm}{sec.})$	$\frac{V_{ax}}{h}(sec.^{-1})$	$Q(\frac{cm^3}{sec.})$	$V_{ax}(\frac{cm}{sec.})$	$\frac{V_{ax}}{h}(sec.^{-1})$
80-10	1.01×10^{-2}	1.25	2.08×10^{3}	2.05×10^{5}	4.50	7.48×10^{3}	7.40×10^{5}
80-16	1.37	1.65	2.20	1.61	6.00	8.00	5.84
74-16	1.03	2.50	1.66	1.61	9.00	5.96	5.79
74-20	1.29	3.20	1.79	1.39	11.50	6.44	4.99
67-20	1.62	4.60	1.67	1.03	16.00	5.80	3.58
67-17	1.99	5.70	1.87	0.94	20.30	6.67	3.35
67-21	2.84	7.60	2.02	0.71	27.00	8.87	3.12
58-17	1.44	7.25	1.74	1.21	26.30	6.30	4.38
58-21	1.97	10.75	2.00	1.02	37.00	6.88	3.49
54-17	1.54	10.00	1.61	1.05	34.50	5.55	3.60
54-21	2.09	15.00	2.04	0.98	39.20	5.33	2.55
54-27	3.65	19.25	2.09	0.59	50.00	5.42	1.52
46-27	2.52	31.00	2.09	0.84	80.00	5.41	2.15

APPENDIX III - BOUNDARY LAYER ANALYSIS

The flow of an incompressible fluid through a swirl-type pressure nozzle is an interesting but complicated problem. Many authors including Doumas and Laster [D-8], Tanasawa and Kobayasi [T-1], and Taylor [T-5] have attempted to describe the fluid behavior in the nozzles as an inviscid flow, neglecting the viscous and the boundary-layer effect. The sufficiency of the inviscid model can be tested by comparing with experimental results of spray cone angle, discharge coefficient and liquid film thickness. At high Reynolds numbers, the agreement between the theoretical and the experimental results are fair. Tanasawa and Kobayasi [T-1] have also considered the importance of the viscous dissipation due to the radial gradient of the tangential velocity.

Taylor [T-6] suggested that the boundary layer of the fluid on the wall surface of the swirl chamber could be an important factor in determining the nozzle performances, especially at relatively low Reynolds numbers. He proposed that the main body of the fluid in the swirl chamber could be considered as a free vortex, while the boundary layer was responsible for the transport of the fluid toward the orifice. The result of his theoretical analysis indicated that, even with a slightly viscous fluid such as water, a large portion of the fluid arrived at the orifice by way of the boundary-layer. Extensions and applications of his analysis to other problems have been made by Binnie and Harris [B-2], Cooke [C-5], Lal [L-1], Sinbel [S-2], and Weber [W-3].

Hodgkinson [H-10] has made use of Taylor's analysis to determine the design features of a swirl nozzle and to predict the mean drop size. He showed that the boundary layer thickness (δ) was related to the pressure (P) by

$$\delta \sim \left[\frac{Q\mu}{P}\right]^{1/3} \tag{1}$$

Since $Q = C_Q\,(\pi D_2^2/4)(\sqrt{2P/\rho})$ and assuming that $\bar{x}_{32} \sim \delta$, we get from Equation (1) the following result:

$$\frac{\bar{x}_{32}}{D_2} \sim \left[\frac{\mu}{D_2\sqrt{P\rho}}\right]^{-1/3} (C_Q)^{1/3} \tag{2}$$

Using Equation (III-2), we obtain

$$\frac{\bar{x}_{32}}{D_2} \sim (Re)^{-1/3}\,(A)^{-0.152} \tag{3}$$

Comparing Equation (3) with Equation (VII-1a), we see that the agreement is reasonable as far as the functional forms of the equations are concerned. However, no direct comparison of the boundary-layer thickness with experimental mean drop size has been made by previous authors.

We have intended to make a quantitative comparison between the calculated boundary-layer thickness and the experimental mean drop size for both Newtonian and non-Newtonian fluids. For this purpose, we have extended Taylor's analysis to cover those simple non-Newtonian fluids whose relations between shear stress and shear rate can be represented by the Power Law Model.

Referring to the coordinate system shown in Figure 2 and using the formulation of Taylor, we can state that our problem is to seek a solution for the following Equations (4), (5), and (6).

Boundary-Layer Equations of Motion

$$\rho\left[v_r\frac{\partial v_r}{\partial r} + \frac{v_\theta}{r}\frac{\partial v_r}{\partial \theta} - \frac{v_\phi^2}{r}\right] = -\frac{\partial p}{\partial r} - \frac{1}{r}\frac{\partial \tau_{r\theta}}{\partial \theta} \tag{4}$$

$$\rho \left[v_r \frac{\partial v_\phi}{\partial r} + \frac{v_\theta}{r} \frac{\partial v_\phi}{\partial \theta} \frac{v_\phi v_r}{r} \right] = \frac{-1}{r} \frac{\partial \tau_{\theta\phi}}{\partial \theta} \tag{5}$$

Equation of Continuity

$$\frac{\partial v_r}{\partial r} + \frac{2v_r}{r} + \frac{1}{r} \frac{\partial v_\theta}{\partial \theta} = 0 \tag{6}$$

Boundary Conditions

(i) $v_r = v_\phi = 0$ at $\theta = \alpha$

(ii) $v_r = 0$ and $v_\phi = \frac{\Omega}{r \sin \alpha}$ at $\theta = \alpha - \frac{\delta}{r}$

where

α = half apex angle of the conical swirl chamber

δ = boundary-layer thickness

Ω = circulation constant of the free vortex outside the boundary layer

Assumptions Involved

(i) $\delta << R_o$

(ii) $\frac{\partial p}{\partial \theta} = 0$ inside boundary layer

(iii) $v_r = 0$ and $v_\phi = \frac{\Omega}{r \sin \theta}$ outside boundary layer

(iv) $v_r = 0$ at $r = R_o$

Shear Stress-Shear Rate Relation

$$\underset{\sim}{\tau} = -m \left| \frac{1}{2} (\underset{\sim}{\Delta} : \underset{\sim}{\Delta}) \right|^{\frac{n-1}{2}} \underset{\sim}{\Delta} \tag{7}$$

where

$\underset{\sim}{\tau}$ - viscous stress tensor

$\underset{\sim}{\Delta}$ - rate of strain tensor

$\underset{\sim}{\Delta} : \underset{\sim}{\Delta}$ = second invariant of $\underset{\sim}{\Delta}$

Using an order-of-magnitude consideration based on the equation of continuity, Equation (7) can be reduced to the simple form:

$$\underset{\sim}{\tau} = -m \left| \frac{1}{r^2} \left[\left(\frac{\partial v_r}{\partial \theta}\right)^2 + \left(\frac{\partial v_\phi}{\partial \theta}\right)^2 \right] \right|^{\frac{n-1}{2}} \underset{\sim}{A} \tag{8}$$

Integrating the equations of motion over the boundary-layer thickness and eliminating v_θ by means of the equation of continuity, we obtain

$$2 \int_\alpha^{\alpha-\delta/r} v_r \frac{\partial v_r}{\partial r} \, d\theta + 2 \int_\alpha^{\alpha-\delta/r} \frac{v_r^2}{r} \, d\theta + \int_\alpha^{\alpha-\delta/r} \left(\frac{\Omega}{r^3 \sin^2} - \frac{v_\phi^2}{r}\right) d\theta$$

$$= \frac{1}{\rho r} \tau_{r\theta} \text{ (wall)} \tag{9}$$

$$\frac{-\Omega}{r^2 \sin} \int_\alpha^{\alpha-\delta/r} \left(r \frac{\partial v_r}{\partial r} + 2v_r\right) d\theta \int_\alpha^{\alpha-\delta/r} \frac{\partial}{\partial r} (v_r v_\phi) \, d\theta + 3 \int_\alpha^{\alpha-\delta/r} \frac{v_r v_\phi}{r} \, d\theta$$

$$= \frac{1}{\rho r} \tau_{\theta\phi} \text{ (wall)} \tag{10}$$

We define the following velocity profiles and the dimensionless quantities:

$$v_r = \frac{\Omega E(r)}{r \sin \alpha} f(\xi) = \frac{\Omega E(r)}{r \sin \alpha} (\xi - 2\xi^2 + \xi^3) \tag{11}$$

$$v_\phi = \frac{\Omega}{r \sin \alpha} g(\xi) = \frac{\Omega}{r \sin \alpha} (2\xi - \xi^2) \tag{12}$$

$$\xi = \frac{r(\alpha-\theta)}{\delta} \tag{13}$$

$$\mathrm{Re} = \frac{\rho (R_o)^n (\Omega/R_o)^{2-n}}{m} \tag{14}$$

$$r^+ = \frac{r}{R_o}$$

$$\delta^+ = (\mathrm{Re})^{\frac{1}{n+1}} (\sin \alpha)^{\frac{n-2}{n+1}} \left(\frac{\delta}{R_o}\right) \tag{16}$$

Then Equations (9) and (10) can be evaluated to give

$$\frac{\delta^{+2}}{r^{+2}}\left[(r^{+}\frac{dE^2}{dr^{+}} - E^2 + \frac{r^{+}E^2}{2\delta^{+2}}\frac{d\delta^{+2}}{dr^{+}}) + 49\right] = -105E\left(\frac{E^2+4}{r^{+2}\delta^{+2}}\right)^{\frac{n-1}{2}} \tag{17}$$

and

$$\frac{\delta^{+2}}{r^{+2}}\left[r^{+}\frac{dE^2}{dr^{+}} + \frac{r^{+}E^2}{\delta^{+2}}\left(\frac{d\delta^{+2}}{dr^{+}}\right)\right] = 120E\left(\frac{E^2+4}{r^{+2}\delta^{+2}}\right)^{\frac{n-1}{2}} \tag{18}$$

For the purpose of numerical calculations, Equations (17) and (18) can be maneuvered to yield:

$$\frac{dE^2}{dr^{+}} = \frac{-98}{r^{+}} + \frac{2E^2}{r^{+}} - \frac{330(r^{+})^{2-n}E^2}{E(\delta^{+})^{1+n}}\left[E^2+4\right]^{\frac{n-1}{2}} \tag{19}$$

and

$$\frac{dE(\delta^{+})^{1+n}}{dr^{+}} = \frac{49E(\delta^{+})^{1-n}}{r^{+}E^2}(n) - \frac{E(\delta^{+})^{1+n}}{r^{+}}(n) + (225n+60)(r^{+})^{2-n}\left[E^2+4\right]^{\frac{n-1}{2}} \tag{20}$$

When n=1, Equations (19) and (20) reduce to the equation obtained by Taylor for a Newtonian fluid.

Numerical calculations for the last two equations start at $r^{+} = 1$ and are continued to $r^{+} = 0.05$. The starting values of E^2 and $E(\delta^{+})^{1+n}$ can be obtained by assuming $E^2 = E(\delta^{+})^{1+n} = 0$ at $r^{+} = 1$. Then the last two equations become

$$\left(\frac{dE^2}{dr^{+}}\right)_{r^{+}=1} \simeq \frac{E^2-0}{r^{+}-1} = -98 - 330\frac{E^2}{E\delta^{+2}}(\delta^{+})^{1-n}(4)^{\frac{n-1}{2}} \tag{21}$$

and

$$\left[\frac{d(E(\delta^{+})^{1+n})}{dr^{+}}\right]_{r^{+}=1} \simeq \frac{E(\delta^{+})^{1+n}-0}{r^{+}-1} = \frac{49E(\delta^{+})^{1+n}}{E^2}(n) + (225n-60)(4)^{\frac{n-1}{2}} \tag{22}$$

whence

$$E^2 = \frac{-49(120)(1+n)}{(225n+390)}(r^+-1) \tag{23}$$

and

$$E(\delta^+)^{1+n} = \frac{(120n+120)(225n+60)(4)^{\frac{n-1}{2}}}{(120n+120)+n(225n+390)}(r^+-1) \tag{24}$$

The calculated values of δ^+ for several values of n are shown in Figure 21. The effect of the rheological parameter m is included in the Reynolds number (Re) which influences δ^+ according to Equation (15). The pressure affects δ^+ through the circulation constant Ω in Equation (14). For a given nozzle and a given pressure, the circulation constant (Ω) is calculated from the inlet velocity (V_i) at the grooved slots according to the relation

$$\Omega = (V_i)(R_o \sin \alpha) \tag{25}$$

and the value of δ^+ can be obtained from Figure 21 at the correct value of r^+ for the given nozzle. For all the nozzles used, the value of R_o is 0.24 cm and α is 45 degrees.

The value of the rheological constants for polymer solutions are obtained from the rheological diagram by extrapolating the tangential line to the curve at the characteristic shear rate of 2.0×10^5 per second. The values so determined are listed in Table XII. For a Newtonian fluid, $m = \mu$ and $n = 1.0$.

TABLE XII - RHEOLOGICAL PARAMETERS OF POLYMER SOLUTIONS

Polymer Solution	m(g sec.$^{n-2}$ cm^{-1}) (at shear rate of 1.0 sec.$^{-1}$)	n
0.11% Carbopol-934	29	0.838
0.15% Carbopol-934	220	0.704
4.5% CMC-7L	2800	0.624

The summarized calculations of the boundary-layer thickness (δ) for the 210 runs of non-Newtonian and Newtonian fluids as well as the comparisons

between δ and $\bar{x}$ are shown in Tables XIII and XIV. The result shows that in most of the 210 runs, the ratio of $\delta/\bar{x}$ is close to unity, indicating a close relation between the two quantities.

TABLE XIII - BOUNDARY LAYER CALCULATIONS FOR NON-NEWTONIAN FLUIDS

Nozzle	Press. (psi)	$\bar{x}$ (microns)	Q (cm^3/sec)	V_i (cm/sec)	Re'	δ^+	δ (microns)	$\frac{\delta}{\bar{x}}$
Carbopol-934	0.11% solution							
80-16	220	89.5	2.65	534	1433	1.71	93.8	1.048
"	410	70.5	3.50	705	1979	1.71	78.7	1.116
"	830	54.8	4.80	966	2854	1.71	64.5	1.176
"	1520	41.2	6.35	1284	3972	1.71	53.9	1.307
74-20	230	95.0	4.75	600	1641	1.91	97.3	1.024
"	830	55.5	8.45	1057	3169	1.91	68.0	1.226
67-17	140	121.0	6.25	635	1753	2.02	99.3	0.821
"	140	129.0	6.25	635	1753	2.02	99.3	0.770
"	410	93.0	10.50	1058	3172	2.02	71.9	0.773
"	1440	53.0	19.25	1934	6380	2.02	49.1	0.926
58-17	135	135.5	8.60	865	2510	2.13	86.1	0.635
"	420	102.0	15.50	1560	4981	2.13	59.3	0.581
54-17	140	160.0	12.40	1250	3850	2.28	73.0	0.456
"	410	113.5	21.75	2200	7427	2.28	51.1	0.450
"	420	124.5	22.00	2220	7505	2.28	50.8	0.408
46-27	210	174.0	47.00	1517	4822	2.51	71.1	0.409
Carbopol-934	0.15% solution							
80.10	800	62.7	3.85	1660	2090	1.64	50.5	0.806
"	1540	54.8	5.20	2220	3046	1.64	40.5	0.739
80-16	400	77.5	3.70	745	740	1.64	92.9	1.199
"	800	59.3	4.86	980	1055	1.64	75.4	1.272
"	1680	49.0	6.70	1350	1599	1.64	59.1	1.207
74-16	410	82.0	6.30	1270	1477	1.73	65.3	0.797
"	800	64.3	8.40	1693	2144	1.73	52.5	0.820
"	1520	53.0	11.00	2216	3039	1.73	42.8	0.807
74-20	220	99.0	4.80	600	559	1.73	115.6	1.167
"	420	81.0	6.35	800	8111	1.73	92.9	1.146
"	760	67.0	8.20	1012	1100	1.73	77.7	1.159
67-20	810	72.2	12.50	1560	1928	1.83	59.1	0.819
"	1700	53.3	17.50	2190	2992	1.83	45.7	0.857
67-17	120	143.0	6.70	675	651	1.83	111.8	0.782
"	200	122.0	8.50	865	898	1.83	92.6	0.759
"	400	96.0	11.90	1210	1387	1.83	71.7	0.747
"	830	72.2	16.80	1700	2155	1.83	55.4	0.767
"	1480	54.8	22.00	2218	3042	1.83	45.2	0.825
67-21	135	156.0	10.40	560	511	1.83	128.8	0.826
"	220	125.5	12.60	691	671	1.83	109.8	0.875
"	410	120.0	16.60	925	979	1.83	88.0	0.862
"	810	72.2	22.50	1240	1432	1.83	70.4	0.975
"	1520	57.0	29.70	1655	2081	1.83	56.5	0.991
"	1580	54.0	30.00	1660	2090	1.83	56.4	1.044

TABLE XIII - BOUNDARY LAYER CALCULATIONS FOR NON-NEWTONIAN FLUIDS (Cont'd.)

Nozzle	Press. (psi)	$\bar{x}$ (microns)	Q (cm^3/sec)	V_i (cm/sec)	Re'	δ^+	δ (microns)	$\frac{\delta}{\bar{x}}$
58-17	140	151.0	8.10	815	831	1.95	103.2	0.683
"	200	135.0	9.60	967	1037	1.95	90.6	0.671
"	200	134.5	9.60	967	1037	1.95	90.6	0.674
"	410	113.0	13.50	1360	1614	1.95	69.9	0.628
"	420	114.0	13.75	1385	1652	1.95	68.9	0.605
"	800	83.5	18.50	1875	2447	1.95	54.8	0.656
"	800	88.0	18.50	1875	2447	1.95	54.8	0.622
"	830	90.0	19.00	1913	2511	1.95	53.9	0.599
"	1530	67.3	25.35	2550	3645	1.95	43.3	0.644
54-17	125	156.0	10.50	1058	1166	2.10	91.1	0.584
"	420	123.0	18.75	1890	2472	2.10	58.6	0.477
"	650	107.0	23.00	2320	2628	2.10	56.6	0.529
"	1380	74.8	33.00	3320	5131	2.10	38.2	0.510
54-21	130	177.0	16.50	920	972	2.10	101.3	0.573
"	140	172.0	17.20	946	1008	2.10	99.2	0.577
"	220	138.0	22.00	1220	1402	2.10	81.8	0.592
"	420	114.5	31.50	1770	2229	2.10	62.3	0.544
"	430	110.0	32.00	1745	2271	2.10	61.6	0.560
54-27	230	160.0	29.50	775	779	2.10	115.5	0.722
"	410	121.0	40.40	1300	1522	2.10	77.9	0.644
46-27	120	237.0	33.00	1065	1176	2.38	102.8	0.434
"	220	181.0	48.00	1550	1912	2.38	77.2	0.427
"	390	147.5	68.00	2200	3010	2.38	59.2	0.401
CMC-7L	4.5% solution							
74-20	195	216.0	6.20	775	111	1.67	243.3	1.126
"	410	131.0	7.30	913	140	1.67	211.7	1.616
"	800	105.0	9.00	1125	206	1.67	177.4	1.690
"	1510	91.5	11.50	1426	258	1.67	145.1	1.586
67-20	165	287.0	6.80	850	127	1.74	234.4	0.817
"	230	228.0	7.70	963	150	1.74	210.9	0.925
"	440	156.0	9.80	1240	213	1.74	170.2	1.091
"	1070	112.0	14.25	1775	349	1.74	125.6	1.121
67-21	240	239.0	13.60	747	106	1.74	261.5	1.094
"	410	162.5	17.40	962	150	1.74	211.1	1.299
"	790	121.0	23.50	1300	227	1.74	163.5	1.351
"	1480	98.0	31.50	1715	333	1.74	129.3	1.320
58-17	380	161.0	14.20	1330	234	1.85	160.4	0.996
"	800	128.0	18.60	1882	378	1.85	127.1	0.993
58-21	150	329.0	14.00	775	111	1.85	269.5	0.819
"	260	233.0	18.00	1000	158	1.85	217.2	0.932
"	500	160.0	24.50	1357	241	1.85	167.7	1.048
"	800	136.0	30.50	1720	334	1.85	137.2	1.008
54-17	220	250.0	13.50	1360	242	2.02	182.7	0.731
"	870	140.5	25.50	2567	579	2.02	106.7	0.759
"	1480	114.5	32.50	3280	812	2.02	86.7	0.756
54-21	150	279.0	17.00	941	146	2.02	249.6	0.895
"	240	231.0	22.00	1220	208	2.02	200.3	0.867
"	410	182.0	29.50	1632	311	2.02	156.6	0.860

TABLE XIII - BOUNDARY LAYER CALCULATIONS FOR NON-NEWTONIAN FLUIDS (Cont'd.)

Nozzle	Press. (psi)	$\bar{x}$ (microns)	Q (cm^3/sec)	V_i (cm/sec)	Re'	δ^+	δ (microns)	$\frac{\delta}{\bar{x}}$
54-27	140	306.0	21.30	685	94	2.02	326.7	1.068
"	245	240.0	29.70	960	150	2.02	245.5	1.023
"	440	197.5	42.00	1375	240	2.02	183.1	0.927
46-27	140	373.0	38.50	1241	213	2.30	224.8	0.603
"	260	292.0	55.50	1775	348	2.30	166.0	0.569

TABLE XIV - BOUNDARY LAYER CALCULATIONS FOR NEWTONIAN FLUIDS

Nozzle	Press. (psi)	$\bar{x}$ (microns)	Q (cm^3/sec)	V_i (cm/sec)	Re'	δ^+	δ (microns)	$\frac{\delta}{\bar{x}}$
Water								
80-16	430	65.5	3.30	665	18728	1.99	43.5	0.665
"	1640	42.5	6.25	1260	35484	1.99	31.6	0.744
74-20	150	82.2	3.90	455	12814	2.10	55.5	0.676
"	410	66.9	6.20	700	19713	2.10	44.8	0.669
"	1600	47.0	11.90	1300	36610	2.10	32.9	0.699
67-21	160	110.0	9.50	503	14165	2.23	56.0	0.509
58-17	160	104.0	9.30	905	25487	2.34	43.9	0.422
"	820	67.3	20.00	1910	53789	2.34	30.2	0.449
54-17	180	130.0	13.00	1310	36892	2.48	38.6	0.297
"	205	117.5	14.00	1410	39708	2.48	37.2	0.316
"	420	98.0	19.25	1932	54409	2.48	31.8	0.324
"	850	72.2	26.50	2720	76600	2.48	26.8	0.371
54-27	160	145.0	23.00	741	20868	2.48	51.3	0.354
46-27	140	173.0	36.00	1112	31316	2.63	44.5	0.257
"	200	155.0	42.50	1320	37174	2.63	40.8	0.263
Glycerine 76% solution								
67-21	410	182.0	15.00	1023	997	2.23	211.0	1.159
"	530	141.5	17.00	1161	1131	2.23	198.0	1.399
54-17	230	240.0	14.50	1740	1696	2.48	179.9	0.750
"	240	247.0	14.80	1790	1745	2.48	177.4	0.718
"	420	202.0	19.50	2660	2592	2.48	145.5	0.720
"	830	155.0	27.50	3320	3236	2.48	130.3	0.840
Nelson's data on organic fluids [N-1] Anilic								
54-17	104	162.3	9.70	977	6761	2.48	90.1	0.555
"	203	130.5	13.55	1365	9446	2.48	76.2	0.584
"	405	103.5	19.10	1929	13349	2.48	64.1	0.620
"	810	88.3	27.05	2722	18837	2.48	54.0	0.611
"	1395	74.7	35.50	3760	26020	2.48	45.9	0.615
Nitrobenzene								
54-17	105	155.5	8.95	903	14843	2.48	60.8	0.527

TABLE XIV - BOUNDARY LAYER CALCULATIONS FOR NEWTONIAN FLUIDS (Cont'd.)

Nozzle	Press. (psi)	$\bar{x}$ (microns)	Q (cm^3/sec)	V_i (cm/sec)	Re'	δ^+	δ (microns)	$\frac{\delta}{\bar{x}}$
Nitrobenzene (Cont'd.)								
54-17	208	94.3	12.60	1270	20875	2.48	51.3	0.544
"	400	81.2	17.50	1761	28945	2.48	43.6	0.536
"	1200	50.0	30.30	3050	50133	2.48	33.1	0.662
Cyclohexane								
54-17	104	107.0	11.20	1130	25051	2.48	46.8	0.438
"	205	84.7	15.75	1585	35138	2.48	39.5	0.467
"	300	78.1	18.90	1900	42122	2.48	36.1	0.462
"	405	64.0	22.10	2210	48994	2.48	33.5	0.523
"	604	55.5	26.80	2700	59857	2.48	30.3	0.546
80-16	103	64.1	1.72	342	7582	1.99	68.4	1.067
"	186	56.1	2.30	464	10287	1.99	58.7	1.047
"	323	51.0	3.04	612	13568	1.99	51.2	1.003
"	355	40.2	3.18	640	14188	1.99	50.0	1.244
"	356	49.0	3.18	640	14188	1.99	50.0	1.020
"	508	40.2	3.81	756	16760	1.99	46.0	1.145
46-27	107	112.0	33.95	1094	24253	2.63	50.6	0.451
"	145	93.9	39.50	1273	28222	2.63	46.9	0.499
"	205	78.5	47.00	1355	30039	2.63	45.4	0.579
"	307	65.0	57.50	1855	41124	2.63	38.8	0.597
"	410	55.2	66.50	2140	47442	2.63	36.2	0.655
54-21	102	102.0	15.65	865	19176	2.48	53.5	0.525
"	204	71.0	22.10	1223	27113	2.48	45.0	0.632
"	300	56.8	26.80	1483	32877	2.48	40.9	0.719
"	400	49.8	31.00	1715	38020	2.48	38.0	0.763
"	695	44.0	40.90	2260	50103	2.48	33.1	0.752
80-10	104	65.6	1.45	646	14321	1.99	49.8	0.759
"	176	53.6	1.89	705	15629	1.99	47.7	0.889
"	290	49.1	2.42	1042	23100	1.99	39.2	0.798
"	500	43.0	3.18	1369	30350	1.99	34.2	0.795
54-27	103	100.0	20.70	667	14787	2.48	60.9	0.609
"	205	67.5	29.20	910	20174	2.48	52.2	0.773
"	302	55.2	35.40	1143	25340	2.48	46.6	0.843
"	500	41.3	45.60	1470	32589	2.48	41.1	0.994
67-17	104	85.0	6.15	620	13745	2.23	56.8	0.668
"	206	65.0	8.70	973	21570	2.23	45.4	0.698
"	280	55.5	10.10	1018	22568	2.23	44.3	0.799
"	400	48.0	12.10	1216	26958	2.23	40.6	0.845
"	590	42.0	14.65	1476	32722	2.23	36.8	0.877
67-20	103	81.0	5.27	660	14632	2.23	55.1	0.680
"	199	67.3	7.33	916	20307	2.23	46.7	0.695
"	405	48.0	10.45	1310	29042	2.23	39.1	0.814
"	595	43.4	12.70	1588	35205	2.23	35.5	0.818
67-21	111	84.6	8.23	455	10087	2.23	66.3	0.784
"	202	70.5	11.10	614	13612	2.23	57.1	0.810
"	605	45.2	19.20	1061	23522	2.23	43.4	0.961

TABLE XIV - BOUNDARY LAYER CALCULATIONS FOR NEWTONIAN FLUIDS (Cont'd.)

Nozzle	Press. (psi)	$\bar{x}$ (microns)	Q (cm^3/sec)	V_i (cm/sec)	Re'	δ^+	δ (microns)	$\frac{\delta}{x}$
n-Octyl Alcohol								
54-17	202	134.5	15.60	1573	4147	2.48	115.1	0.855
"	325	101.0	19.85	2000	5273	2.48	102.0	0.010
"	505	84.0	23.70	2390	6302	2.48	93.3	1.161
"	805	72.5	31.20	3140	8279	2.48	81.4	1.123
"	1310	60.4	39.80	4005	10560	2.48	72.1	1.194
54-27	104	155.0	20.80	670	1767	2.48	176.3	1.137
"	202	199.0	29.00	936	2468	2.48	149.2	1.253
"	412	91.7	41.40	1337	3525	2.48	124.8	1.361
"	800	75.2	57.60	1860	4904	2.48	105.8	1.407
"	1490	64.0	77.70	2540	6697	2.48	90.5	1.415
67-20	106	130.0	6.15	769	2028	2.23	147.9	1.138
"	199	102.0	8.40	1050	2768	2.23	126.6	1.241
"	404	68.5	12.00	1500	3955	2.23	105.9	1.546
"	805	57.7	16.90	2115	5577	2.23	89.2	1.546
"	1280	47.0	21.35	2675	7053	2.23	79.3	1.688
67-21	102	134.0	8.25	475	1252	2.23	188.2	1.405
"	202	102.5	11.60	643	1695	2.23	161.8	1.578
"	405	76.8	16.45	910	2399	2.23	136.0	1.771
"	1200	50.3	28.35	1560	4129	2.23	103.7	2.061
"	1200	51.3	28.35	1560	4113	2.23	103.9	2.025
"	1200	54.8	28.35	1560	4113	2.23	103.9	1.895
Carbon Tetrachloride								
54-17	109	89.2	7.80	785	34690	2.48	39.8	0.446
"	169	82.7	9.70	977	43175	2.48	35.7	0.431
"	290	70.7	12.70	1280	56566	2.48	31.2	0.441
"	400	61.6	14.90	1501	66331	2.48	28.8	0.467
"	605	46.9	18.40	1860	82197	2.48	25.8	0.551
"	805	39.6	21.20	2136	94394	2.48	24.1	0.609
54-27	102	104.0	15.15	489	21610	2.48	50.4	0.485
"	143	85.7	17.95	578	25543	2.48	46.4	0.541
"	209	70.1	21.65	699	30890	2.48	42.2	0.601
"	280	59.8	25.10	810	35795	2.48	39.2	0.655
"	405	44.2	30.20	974	43043	2.48	35.7	0.808
67-20	106	73.4	3.62	451	19931	2.23	47.2	0.643
"	149	63.2	4.29	535	23643	2.23	43.3	0.685
"	202	58.7	4.99	623	27532	2.23	40.2	0.684
"	283	50.3	5.90	725	32039	2.23	37.2	0.740
"	405	46.2	7.06	884	39066	2.23	33.7	0.729
67-21	112	83.0	5.78	320	14141	2.23	56.0	0.675
"	147	75.8	6.62	366	16174	2.23	52.4	0.691
"	206	63.5	7.85	435	19223	2.23	48.0	0.757
"	283	54.7	9.20	509	22494	2.23	44.4	0.812
"	415	44.0	11.10	615	27178	2.23	40.4	0.918
1,1,2,2-Tetrabromoethane								
67-20	105	144.0	2.99	374	3351	2.23	115.1	0.799
"	204	114.0	4.16	521	4668	2.23	97.5	0.855
"	407	85.0	5.89	738	6612	2.23	81.9	0.964
"	805	63.5	8.30	1038	9300	2.23	69.1	0.088
"	1500	53.2	11.30	1415	12677	2.23	59.2	1.112

PART II

APPLICATION OF BRANCHING PROCESS FOR LIQUID ATOMIZATION

by

Yoshisuke Nakano and Chi Tien

I. INTRODUCTION

A number of expressions for drop size distribution in the liquid atomization process have been proposed, most of which are empirical in nature. These expressions, generally speaking, consist of two parts: the first gives the average drop size in terms of physical properties and operating conditions, and the second, the size distribution function. For example, the empirical expression of Nukiyama and Tanasawa (1938, 1939, 1940) for pneumatic atomization is given as:

$$D_{av} = \frac{585\sqrt{\sigma}}{V\sqrt{\rho_\ell}} + 597\left(\frac{\mu}{\sqrt{\sigma\rho_\ell}}\right)^{0.45}\left(\frac{1000\,Q_l}{Q_a}\right)^{1.5} \tag{1a}$$

$$\frac{dN}{dx} = a\,x^p\,e^{-bx^q} \tag{1b}$$

Theoretical studies of this problem have been relatively few, primarily because of the extreme complexity of the atomization process. Mayer's theoretical work (1961, 1963) perhaps represents the first successful attempt in this endeavor. In his model, the drops are formed through wave action along the surface of a liquid jet. More recently, Adelberg (1967) extended Mayer's analysis to more general cases.

Although one can represent the experimental results by a priori assumed distribution function with the proper value of parameters, the basic questions still remain: Why does the distribution function take a certain functional form? What is the physical meaning of each parameter appearing in the distribution function? In the present work, an attempt is made to answer these problems by introducing a statistical model for the atomization process.

The atomization process is considered to consist of two stages: primary and secondary atomization. In the primary stage, the liquid mass is broken up as a result of capillary force. Primary atomization depends on the device of atomization as well as the operating condition. In the secondary stage, the

disintegrated drops further are split into smaller droplets by the dynamic effect of a surrounding medium. Although the device of atomization no longer influences the breakup of the droplets directly, the analytical description of the phenomenon is extremely complex. Since the fluid dynamical state of the surrounding medium is usually turbulent, which is statistical in nature, the secondary atomization caused by the dynamic effect of the surrounding medium can be considered to be a statistical process as a whole. The present analysis considers only the second stage which is interpreted as a statistical branching process.

The roles of the two stages depend on the specific method of atomization. For instance, in the case of pneumatic atomization in a high velocity gas stream, according to the conclusion reached by Weiss and Worsham (1959), the geometry and operation of the injector are least important. Thus, in this case the role of the primary stage is negligible. It is expected that the total process can be explained by the statistical model. Indeed it is shown in a later section that the distribution function of the statistical model could take exactly the same functional form as Equation (1b) under certain conditions.

The class of branching process with which the present work is concerned was first treated by Kolmogorov (1941), who had in mind the grinding of particles. Kolmogorov's work has recently been extended by Fillippov (1961). The applicability of these branching processes for atomization is discussed in the present work.

II. ANALYSIS

Supposing if the size distribution of primary atomization is known, the change of size distribution in time may be determined under the following conditions:

(1) Each drop e is characterized by the mass of the drop; m(e).

(2) At the initial moment, t = 0, there is a finite or countable number

of drops, the sum of whose masses is equal to M_o.

(3) Each drop, e, existing at time, t, can split in the interval of time $(t, t + \Delta t)$ (independent of its past and of the fate of other drops) with probability $P(m)\Delta t + O(\Delta t)$, where the function $P(m)$ depends only on m and is bounded for any interval of the form $\delta < m < N$, where $\delta > 0$, $N < \infty$.

(4) At random moments of time some drops, e, may split into a finite or countable number of smaller drops $e_k (k = 1, 2, ---)$. The number and mass of those small drops, arising from one splitting of drop e, are random variables.

Let

$$\xi = m(e) \qquad \text{for the original drop} \qquad (2)$$

$$\xi_k = m(e_k) \quad k = 1, 2, --- \qquad \text{for the smaller drops formed from splitting of e} \qquad (3)$$

Then

$$\frac{1}{\xi} \sum_{\xi_k < w} \xi_k = \phi(\xi, w) \qquad (4)$$

ϕ represents the mass fraction of drops formed from the split of e with mass less than w and is considered to be a random function (c.f. Yaglom, 1962) with two parameters, ξ, w. We assume that the mathematical expectation of the random function $\phi(\xi, w)$ exists:

$$E\,\phi(\xi, w) = F(\xi, w) \qquad (5a)$$

where E denotes the mathematical expectation.

(5) The sum of the masses of the drops, obtained from one drop through one splitting, is equal to the mass of this drop, i.e.

$$\phi(\xi, \xi) = 1 \qquad (5b)$$

Let conditions (1)-(5) be fulfilled. Introducing the distribution function defined as:

$M(w,t)$ = total mass of drops with size (in terms of their mass) less than w and at time, t,

$M(w,t)$ satisfies the following equation (c.f. Fillippov 1961):

$$\frac{\partial}{\partial t} E\, M(w,t) = \int_w^\infty P(\xi)\, F(\xi,w) d_\xi\, E\, M(\xi,t) \tag{6}$$

where $E\, M(w,t)$ denotes the mathematical expectation of the random function $M(w,t)$ and the right hand side of Equation (6) is the Levesque-Stieltjes Interrelation. It is noted that $E\, M(w,t)$ is generally a function of w and t. The initial condition is given as:

$$E\, M(w,o) = M_o(w) \tag{7}$$

when $M_o(w)$ is the mathematical expectation of the initial drop size distribution function.

The solution of Equation (6), of course, depends upon the specific functional form of P and F. In the present work, we shall limit our attention to the simplest case, by assuming

$$F(\xi,w) = (\frac{w}{\xi})^k \tag{8}$$

and

$$P(w) = w^n \tag{9}$$

where k is a positive constant and n is an arbitrary constant.

These assumptions merit some discussion concerning their physical implications. According to the definition, function $F(\xi,w)$ regulates the rule as to the outcome of the splitting of a drop e with mass ξ. Equation (8) implies that this rule does not depend on the absolute mass of the drop, but on the mass ratio of a newly created droplet to the original drop e. This is a physically acceptable simplification. Also from Equation (8), it is easy to see that the expected number of newly created droplets with a mass of w to w + dw is $k\, w^{k-2}\xi^{-k}\, dw$. The density function $k\, w^{k-2}\xi^{-k}$ represents a variety of monotonic functional relations. This is again

physically acceptable since it is unlikely that the creation of drops of a specific size is particularly favorable or unfavorable. Roughly speaking, P(w) implies the stability of drops. The functional form of Equation (9) represents various monotonic relations and further discussion of this function is made in a later section with reference to the experimental results by Gordon (1959).

Asymptotic solution of Equation (6) with F and P given by Equations (8) and (9) and the assumption that the initial drop size is uniform and is of unit mass, have been given by Fillippov (1961) for $|n| > o$ and by Kolamogorov (1941) if n=0. Their solutions are:

$$q(w,t) = \begin{cases} \dfrac{(k\,t)^{1/4}}{2\sqrt{\pi}\,(-\ln w)^{3/4}\,w^2}\, e^{-(\sqrt{-k \ln w} - \sqrt{t})^2} & \text{for } n=0 \\ \qquad 0 < w < 1 & \qquad (10a) \\ k\,t\, e^{-t}\, w^{k-?}\, \psi(w,t) & \text{for } n \neq 0 \\ \qquad 0 < w < 1 & \qquad (10b) \end{cases}$$

where

$$q(w,t) = \left(\frac{1}{w}\right) \frac{\partial}{\partial w} E\, M(w,t) \qquad (11)$$

$q(w,t)\,dw$ represents the mathematical expectation of the number of drops with mass of w to w+dw at t.

$$\psi(w,t) = F\left[1 + \frac{k}{n},\ 2,\ (1 - w^n)t\right] \qquad (12)$$

and F is the confluent hypergeometric function.

In obtaining Equations (10a) and (10b), it was assumed that the initial drop is of unit mass. For the case where the drop initially is not of unit mass, w can be interpreted as the ratio of the mass of the drop to the mass of the initial drop. For the more general situation in which the initial drop size is not uniform, w should be considered as the

ratio of the mass of the drop to that of the average initial drop. In any event, w becomes a dimensionless quantity. To avoid possible confusion, this quantity is designated as:

$$w^+ = \frac{w}{w^*} = \frac{w}{\int_o^\infty w\, q(w,o)\, dw} \tag{13}$$

The function, q(w,o) gives the frequency function for initial drops. Similarly, one can consider the time variable as dimensionless, or

$$t^+ = \frac{t}{t^*} \tag{14}$$

where t^* represents the characteristic time of the atomization process, although it should be conceded that one does not know how this quantity should be selected. In other words, Equations (10a) and (10b) can be written as

$$q(w^+,t^+) = \begin{cases} \dfrac{(k\,t^+)^{1/4}}{2\sqrt{\pi}\,(-\ell n\, w^+)^{3/4}\,(w^+)^2}\, e^{-(\sqrt{-k\,\ell n\, w^+} - \sqrt{t^+})^2} & \text{for } n=0 \\ \qquad 0 < w^+ < 1 & \qquad (15a) \\ k\,t^+\, e^{-t^+}\,(w^+)^{k-2}\,\psi(w^+,t^+) & \text{for } n\neq 0 \\ \qquad 0 < w^+ < 1 & \qquad (15b) \end{cases}$$

Equation (15b) can be further simplified for the case of large t^+ and $n > 0$. If the asymptotic expression of the confluent hypergeometric function is used, Equation (15b) becomes:

$$q(w^+,t^+) = \frac{k(t^+)^{\frac{k}{n}}}{\Gamma(1+\frac{k}{n})}\,(w^+)^{k-2}\, e^{-t^+(w^+)^n} \left[1 - (w^+)^n\right]^{\frac{k}{n}-1} \tag{16}$$

This expression can be cast into a more convenient form if the particle size is characterized in terms of its dimension rather than mass. Let x be the diameter of the drop,

$$w^+ = \beta x^3 \tag{17}$$

β is a proportionality constant and is inversely proportional to the size of the initial average drop.

Equation (16) can be written as

$$\frac{dN}{dx} = \frac{3k\ \beta^{k-1}(t^+)^{\frac{k}{n}}}{\Gamma(1+\frac{k}{n})}\ x^{3k-4}\ e^{-t^+\beta^n x^{3n}}\ (1-\beta^n x^{3n})^{\frac{k}{n}-1} \tag{18}$$

where dN represents the mathematical expectation of the number of drops with diameter between x and x+dx.

The expression of Equation (18) is a function of two variables, drop size and time. However, for spraying operations with a given type of device and under similar operating conditions, the time interval available for the second atomization step would be essentially constant. Consequently, t^+ can be regarded as constant. If one lets

$$p = 3k - 4 \tag{19}$$

$$b = t^+\beta^n \tag{20}$$

$$q = 3n \tag{21}$$

Equation (18) becomes

$$\frac{dN}{dx} = \frac{(p+4)\ b^{\frac{k}{n}}}{\beta\Gamma(1+\frac{p+4}{q})}\ x^p\ e^{-bx^q}\left[1-(\beta^{\frac{1}{3}}x)^q\right]^{\frac{p+4-q}{q}} \tag{22}$$

which represents the distribution function.

III. DISCUSSION

The validity of Equation (22), of course, can be tested only through comparison with experimental results. However, in the event of small values of β (i.e. the initial average drop size is much greater than the final drop size) or $p+4 \to q$, Equation (22) becomes identical with the empirical expression of

Nukiyama and Tanasawa (Equation 1b) which has been one of the most acceptable drop size distribution functions.

Because of the lack of direct experimental proof, we wish to offer some indirect inferences on the validity of the expression of Equation (22). The experimental results of Nukiyama and Tanasawa (1938, 1939, 1940) indicate that the value p is essentially constant and equal to 2. By Equation (19) one has

$$k = 2 \tag{23}$$

which is consistent with the requirement that the exponent k of Equation (8) should be a positive number in view of the physical requirement that $F(\xi,w)$ should always be less than unity. Similarly, the value of q was found to vary from 0.1 to 1.0. This implies that

$$\frac{0.1}{3} < n < \frac{1}{3} \tag{24}$$

The breakup mechanism of liquid drop has been studied by Gordon (1959). He considered the breakup process as one in which the drop undergoes a series of changes of shape before it splits. The time required for the completion of this process is termed breakup time, which is found to be:

$$\frac{2\,\bar{\eta}^{-2}}{\bar{x}\,(\bar{x}-1)} = \frac{2\,\bar{\eta}\,\bar{t}}{\bar{x}^{2}} - 1 + \exp\left[-\frac{2\,\bar{\eta}\,\bar{t}}{\bar{x}^{2}}\right] \tag{25}$$

where $\bar{x}$ and $\bar{t}$ are the dimensionless size and breakup time, respectively. $\bar{\eta}$ is a dimensionless group consisting of physical properties, as well as operating conditions.

Previously, we stated that the probability of each drop to split within the time interval $[t, t + \Delta t]$ as $P(w)\Delta t + o(\Delta t)$. If the model of breakup proposed by Gordon is correct, one can assume that

$$P(w) = w^{n} = f(\bar{t})$$

The breakup time $\bar{t}$ is found to be almost independent of particle size for large

values of $\bar{n}$ which corresponds to the case of high viscosity ratio of drop liquid to air. This is in agreement with the small value of n as indicated by Equation (24).

Since the solution of Equation (6) is known only for the limited cases, one may not derive any definite conclusion as to the application of the branching process for the atomization process. However, further investigation on the branching process may provide a new method to analyze the atomization process.

ACKNOWLEDGMENT

This work was performed under Grant No. WP-00-867-02, Federal Water Pollution Control Administration, Department of Interior.

NOMENCLATURE

a = constant

b = constant

D_{av} = diameter of a single drop with same ratio of surface to volume as total sum of drop

e, e_k = drop

E = mathematical expectation operator

$F(\xi, w)$ = defined by Equation (5a)

k = constant

$m(e)$ = mass of drop e

$M_o(w)$ = mathematical expectation of the initial distribution

$M(w,t)$ = total mass of drops with mass less than w at time t

N = mathematical expectation of the number of drops with diameters between zero and x in the total sample

n = constant

p = constant

$P(w)$ = defined by condition (3)

q = constant

$q(w,t)$ = defined by Equation (11)

Q_l/Q_a = ratio of volume flow rate of liquid to volume flow rate of air at vena contracta

t = time

t^* = characteristic time

t^+ = dimensionless time defined by Equation (14)

$\bar{t}$ = $\{t\rho_g V^3/(32\sigma)\}\ (\rho_g/\rho_l)^{1/2}$

V = relative velocity between the air stream and liquid stream

w = mass of drop

w^* = average initial drop size

w^+ = dimensionless mass defined by Equation (13)

NOMENCLATURE (Cont'd.)

x = diameter of an individual drop

$\bar{x}$ = $x\rho_g V^2/(16\sigma)$

β = $\pi\rho_\ell/(6w^*)$

Γ = Gamma function

ξ = defined by Equation (2)

ξ_k = defined by Equation (3)

ψ = defined by Equation (12)

$\phi(\xi,w)$ = defined by Equation (4)

μ = liquid viscosity

σ = liquid surface tension

ρ_g = gas density

ρ_ℓ = liquid density

$\bar{\eta}$ = $(\mu V/\sigma)(\rho_g/\rho_\ell)^{1/2}$

LITERATURE CITED

Adelburg, M., "Breakup Rate and Penetration of a Liquid Jet in a Gas Stream", AIAA Journal, Vol. 5, No. 8, Aug. 1967, pp. 1408-1415.

Fillippov, A.F., "On a Size Distribution Law for the Division of Particles", A Theory of Probability and its Application, Vol. 6, No. 3, 1961, pp. 275-294.

Gordon, G.D., "Mechanism and Speed of Breakup of Drops", J. App. Phys., Vol. 30, No. 11, Nov. 1959, pp. 1759-1761.

Kolmogorov, A.H., "Uber das Logarithmisch Normale Verteilungsgesetz der Dimensionen der Teilchen bei Zerstuckelung", Comptes Rendus (Doklady) de l'Academie des Sciences de l'URSS, Vol. 31, No. 2, 1941, pp. 99-101.

Nukiyama, S. and Tanasawa, Y., "Experiments on the Atomization of Liquids in an Air Stream", Trans. Soc. Mech. Eng. (Japan), Vol. 4, No. 14, 1938, pp. 86-93; No. 15, 1938, pp. 138-143; Vol. 5, No. 18, 1939, pp. 62-67, pp. 68-75; Vol. 6, No. 22, 1940, pp. II-7 - II-15, No. 23, 1940, pp. II-18 - II-28.

Mayer, E., "Theory of Liquid Atomization in High Velocity Gas Streams", ARS Journal, Vol. 31, No. 12, Dec. 1961, pp. 1783-1785. Also, "Capillary Mechanism of Liquid Atomization in High Velocity Gas Streams", Proceedings of the 12th International Aeronautical Congress, Academic Press, Vol. 2, 1963, pp. 731-740.

Yaglom, A.M., "An Introduction of the Theory of Stationary Random Function", Prentice-Hall, 1962.